

Materiales compuestos multifuncionales para aplicaciones médicas: Uso de sulfato de bario y nanotubos de carbono con poliésteres bioabsorbibles

Hegoi Amestoy

Supervisores

Jose Ramon Sarasua Oiz

Jone Muñoz Ugartemendia

2021

La presente tesis ha sido realizada dentro del grupo
de investigación:

Grupo de Investigación en Ciencia e Ingeniería de
Biomateriales poliméricos

ZIBIO Group

Departamento de Ingeniería Minero-Metalurgia y
Ciencia de los Materiales

Escuela de Ingeniería de Bilbao

Bilbao

España



BILBOKO
INGENIARITZA
ESKOLA
ESCUELA
DE INGENIERÍA
DE BILBAO

“Para mi familia por todo el apoyo durante esta travesía”

“Per aspera ad astra”

Agradecimientos

Agradecimientos

Esta tesis no habría podido ser posible sin el apoyo de mi familia y mis compañeros de departamento y laboratorio.

Primero me gustaría dar las gracias a mi director de Tesis e Investigador principal del grupo de investigación Jose Ramon Sarasua Oiz por darme la oportunidad de ser parte de su grupo ZIBIO y confiar en mí durante estos años. Aprecio mucho su paciencia durante mi supervisión y su guía constante durante mi investigación.

Segundo a mi co-directora de tesis Jone Muñoz Ugartemendia por introducirme en el mundo de la investigación y no rendirse nunca conmigo. Con ella me llevo una amiga para toda la vida.

También me gustaría agradecer a la Universidad del País Vasco/Euskal Herriko Unibertsitatea (UPV/EHU) por la beca de investigación y al Gobierno Vasco y otras entidades que han proporcionado los medios y la financiación para este proyecto.

No me puedo olvidar de mis compañeros de laboratorio por su apoyo continuo y las buenas ideas que me han proporcionado para sacar esta tesis adelante, incluyendo su tiempo y colaboración activa en muchos de mis resultados.

Finalmente querría agradecer a mi familia el apoyo en esta aventura. A mi madre y a mi padre por creer en que podría conseguirlo y no dudar de mí ni en mis peores momentos.

Estructura de la tesis

Para facilitar la lectura y la comprensión de la presente tesis doctoral se va a presentar una pequeña descripción del contenido de la misma.

La tesis está dividida en una introducción, seguida de cuatro capítulos principales y cerrando con un capítulo de conclusiones generales. La **introducción** contiene información sobre el contexto general de los temas tratados en la tesis como son los materiales compuestos y nano-compuestos y sus posibles aplicaciones en biomedicina, así como los objetivos principales a desarrollar durante la presente tesis.

Los cuatro capítulos que forman el cuerpo principal de la tesis tratan sobre nuevos materiales y el estudio de sus propiedades más relevantes para su aplicación en biomedicina. El **primer capítulo** introduce el material compuesto mezcla de poli(ϵ -caprolactona) (PCL) y partículas de sulfato de bario como material biodegradable y radiopaco, con un estudio de la influencia del refuerzo en la estructura cristalina del polímero y las consecuencias de este en las propiedades mecánicas.

El **segundo capítulo** cambia la matriz polimérica por un material de rápida bioabsorción como es el terpolímeros poli(D,L-L-lactida- ϵ -caprolactona), dando lugar a un compuesto radiopaco para aplicaciones médicas de corta duración. Se estudia en profundidad las consecuencias de introducir un refuerzo en un material biodegradable y como cambia la cinética de degradación del polímero.

El **tercer capítulo** corresponde a los nano-compuestos de matriz poli(ϵ -caprolactona) reforzado con nanotubos de carbono de superficie modificada con un recubrimiento de polidopamina. En este capítulo se estudia el efecto de la cantidad de recubrimiento en las propiedades mecánicas así como el efecto bioactivo que aporta este último a la hora de poder ser utilizado en aplicaciones de regeneración ósea.

Por último el **cuarto capítulo** consta de dos sub-capítulos centrados en el estudio de fatiga del poli(ϵ -caprolactona) simulando las condiciones del cuerpo humano. En el primero se estudia la complejidad de la fatiga de este polímero, dominada por factores visco-elásticos y de mecánica de la fractura. El en segundo sub-capítulo se introduce al refuerzo de nanotubos de carbono y nanotubos de carbono recubiertos de polivinilpirrolidona como medio de aumentar la vida a fatiga del PCL.

Finalmente la tesis doctoral cierra con un capítulo de **conclusiones generales** derivadas de los estudios realizado.

Tabla de contenidos

Agradecimientos.....	1
Estructura de la tesis.....	5
Tabla de contenidos.....	9
Introducción.....	13
Objetivos y metodología	37
Chapter 1: Crystallization behavior and mechanical properties of poly (ϵ -caprolactone) reinforced with barium sulphate sub-micron particles. ...	41
Chapter 2: Formation of a rigid amorphous phase at Poly(D,L-Lactide- ϵ - caprolactone)/barium sub-micro particle interphase and its effect on hydrolytic degradation and mechanical properties	65
Chapter 3: Optimization of Polydopamine coating in Poly(ϵ - caprolactone)/multiwalled carbon nanotubes composites for improvement of mechanical and bioactive properties	97
Chapter 4: Viscoelasticity and fatigue behavior of Poly(ϵ -caprolactone) and Poly(ϵ -caprolactone)/multiwalled carbon nanotube composites.	117
Chapter 4.1: Poly(ϵ -caprolactone)	119
Chapter 4.2: Fatigue analysis of Poly(ϵ -caprolactone) (PCL) and multiwall carbon nanotubes (MWCNT) composites	139
General conclusion.....	155
Appendix	161
A1. List of Figures.....	163
A2. List of Tables	168

A3. Symbols and Abbreviations.....	170
A4. List of Publications and Congresses	173
A5. Curriculum Vitae	174

Introducción

El propósito de esta introducción es presentar el contexto general en el que se ha desarrollado esta tesis a fin de hacer más sencillo al lector entender el objetivo y las necesidades que han llevado a la consecución de este trabajo. El objetivo general de esta tesis es ampliar el conocimiento y mejorar el diseño de materiales para aplicaciones médicas mediante la incorporación de refuerzos que no sólo mejoren las propiedades base sino que además les otorguen nuevas propiedades. De esta manera obtenemos materiales compuestos multifuncionales que pueden ser utilizados en nuevas aplicaciones médicas. Esto queda ejemplificado en la Figura I en el que se muestra un composite multifuncional de matriz Poli(D,L-lactida- ϵ -caprolactona) reforzado con partículas sub-micrométricas de bario sulfato, las cuales le otorgan propiedades nuevas como la radiopacidad que permiten nuevas aplicaciones en medicina.

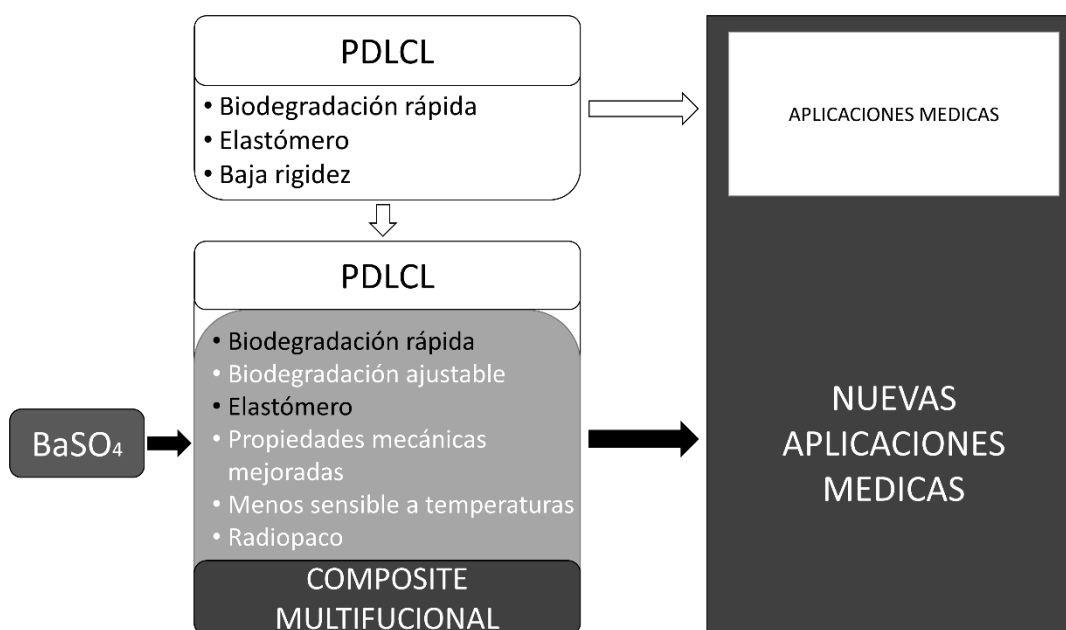


Figura I. Efectos de los refuerzos para obtener materiales médicos multifuncionales.

Esta introducción contiene una aproximación al estado del arte de los materiales bioabsorbibles para aplicaciones médicas. Por una parte introduce las principales aplicaciones de estos materiales en medicina y las propiedades que los materiales deben cumplir en cada caso. A continuación se describe el uso de los poli(ϵ -caprolactona) (PCL) y Poli(L-lactida- ϵ -caprolactona) (PLCL) en aplicaciones médicas, y las limitaciones de estos para su aplicación. Por último, se describe el uso de refuerzos (específicamente

sulfato de bario y nanotubos de carbono) para la mejora en las propiedades de base y la posibilidad de otorgarles nuevas propiedades volviéndolos multifuncionales. Finalmente se introduce el estado del arte de la fatiga de polímeros

Materiales bioabsorbibles para aplicaciones médicas

Los polímeros bioabsorbibles se han establecido como una de las alternativas en el uso de los materiales dentro de la medicina¹⁻⁴. Gracias a sus propiedades se han podido desarrollar variedad de implantes y dispositivos médicos nuevos abriendo campo a nuevas aplicaciones médicas⁵⁻¹⁰. A continuación se describen las tres propiedades claves de estos polímeros:

- **Biodegradación:** Estos polímeros tienen que degradarse dentro del cuerpo humano vía hidrolisis y/o vía enzimática, generando subproductos de degradación solubles en el cuerpo humano¹¹⁻¹⁴. Gracias a esto se pueden diseñar dispositivos médicos temporales que no necesitan de operaciones posteriores para ser eliminados.

La degradación de un polímero en el cuerpo humano ocurre mediante varios mecanismos¹⁵⁻¹⁷, estos deben de ser analizados mediante ensayos *in vitro* (simulando las condiciones del cuerpo humano a 37 °C y pH=7.4) o *in vivo* (en animales) para conocer a fondo su dinámica y poder diseñar implantes temporales ajustados y controlados.

Además, es importante la forma y morfología de degradación de estos materiales, ya que por ejemplo algunos de ellos pueden degradarse en forma de micro- y nano- partículas resistentes que tiendan a acumularse en el cuerpo humano causando inflamación y por lo tanto encapsulación¹⁸⁻²⁰. Lo ideal es que el material se degradase formando subproductos solubles en el cuerpo humano que sean fáciles de liberar por este último.

- **Biocompatibilidad:** Uno de los factores más críticos para un material de aplicación médica es la biocompatibilidad^{21,22}. En el caso de los materiales bioabsorbibles no sólo se requiere que no causen inflamación o respuestas adversas en el cuerpo humano al ser implantados, sino que además los productos procedentes de la degradación del material (monómeros, iniciadores, disolventes y micro-

partículas) sean biocompatibles²¹. Además, debe de tenerse en cuenta la velocidad a la que estos productos son liberados por el implante, mediante mecanismos de difusión y si estos van acumulándose en el organismo provocando problemas médicos²³.

- Propiedades mecánicas: Estos materiales tiene que tener las propiedades mecánicas adecuadas para cada aplicación médica. Esto último incluye el tipo de comportamiento mecánico deseado (Elástico, elastómero, visco-elástico etc.) y su capacidad para soportar una vida útil de diseño (fatiga, fluencia o creep, mecánica de la fractura)^{24,25}.

En el caso de los materiales biodegradables hay que tener en cuenta que estas propiedades cambian en el tiempo debido a los procesos de degradación^{26,27}, los efectos térmicos y cambios estructurales sufridos durante la vida útil en servicio. Por lo tanto es necesario hacer estudios completos a lo largo del tiempo en condiciones *in vitro* o *in vivo* y entender los mecanismos principales que entran en juego a la hora de cambiar las propiedades del material.

Gracias a estas propiedades los polímeros biodegradables pueden utilizarse en múltiples aplicaciones médicas, y ajustarlas a las necesidades de cada una. En esta introducción se va hacer hincapié en tres aplicaciones principales.

- Ingeniería de tejidos: La Ingeniería de tejidos es una rama multidisciplinar de la ingeniería biomédica donde se busca el diseño de dispositivos para la regeneración de tejidos vivos (hueso, cartílago, nervios, etc.). En el contexto de los materiales biodegradables, estos últimos se utilizan principalmente como soportes (normalmente conocidos con el término anglo-sajón de “*Scaffolds*”) como el que se muestra en la Figura II²⁸ para el crecimiento y diferenciación de las células del cuerpo humano²⁸⁻³⁰.

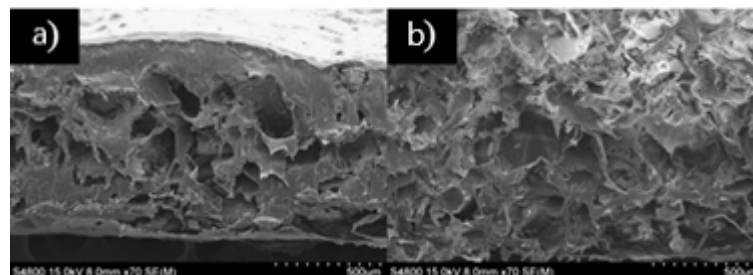


Figura II. Imágenes SEM de *scaffolds* de Poli(Lactida) con porosidades del a) 70 y b) 90%.²⁸

La idea fundamental es crear un soporte con las propiedades mecánicas suficientes para sustituir el tejido original, que además tenga una estructura que ayude a las células para ir formando tejidos conectados a su alrededor. Estas estructuras tridimensionales tienen que poder garantizar la vascularidad y permitir la formación de estructuras homólogas a los órganos que se intentan sanar o sustituir, por lo que suelen tener una forma de esponja o de tejido²⁸.

El proceso de regeneración del tejido alrededor del soporte se da de manera simultánea a la degradación de este último por acción hidrolítica. De manera que al final tendríamos un tejido nuevo o sanado, mientras que el material soporte ha sido completamente degradado y absorbido por el cuerpo^{18,29}.

En estos dispositivos juegan un papel fundamental las interacciones material-células y se buscan materiales no solo que actúen como soporte mecánico, sino que además ayuden a las células en sus procesos de adhesión, proliferación, diferenciación, etc^{31,32}.

- **Implantes temporales:** Los implantes temporales son aquellos dispositivos médicos que sirven para fijar, servir de soporte o estabilizar tejidos de manera temporal mientras el cuerpo se sana a sí mismo. Entre estas aplicaciones se encuentran los dispositivos de fijación de huesos (tornillos, placas etc.) o catéteres para mantener vías abiertas (catéteres urinarios, *stents* en venas etc.).

En estos materiales prima el conocimiento de los procesos cinéticos de degradación del material y poder desarrollar materiales con tiempos y procesos de degradación ajustados. Además de estas propiedades/ características también es importante que los polímeros/materiales presentes radiopacidad ya que ayudan a la implantación de los materiales mediante técnicas de guiado por rayos-X³³. La radiopacidad además ayuda durante el seguimiento de la posición del implante con el tiempo y al control de los subproductos de la degradación del mismo.

- **Dispositivos de liberación de fármacos:** los dispositivos de liberación de fármacos controlados son implantes médicos cuya finalidad es contener y liberar de manera

controlada dentro del cuerpo humano un fármaco o molécula bioactiva. Eso se consigue normalmente mediante materiales con gran capacidad de degradación³⁴⁻³⁶. La idea principal es que los medicamentos estén dispersos y física o químicamente unidos a las cadenas del polímero base, de manera que vayan liberándose al medio circundante cuando los procesos de degradación hidrolítica entren en juego.

En este caso la clave es conocer muy bien los procesos de degradación del polímero y cómo interactúan con las diferentes moléculas potencialmente utilizables en terapias médicas. De esta manera se pueden diseñar implantes que liberen de manera controlada el fármaco dentro del propio cuerpo humano, mitigando los efectos secundarios de la sobredosificación de los medicamentos orales³⁷.

Poli (ϵ -caprolactona) y copolímeros en aplicaciones médicas

Dentro de los polímeros biodegradables los poliésteres tales como el poli(ácido láctico) (PLA), el poli(ácido glicólico) (PGA) o la poly(ϵ -caprolactona) (PCL) han adquirido importancia gracias a la capacidad de degradación hidrolítica de los grupos éster y su buena biocompatibilidad.

En el siguiente apartado se van a describir brevemente las propiedades y principales usos de los polímeros poli (ϵ -caprolactona) (PCL) y sus copolímeros en aplicaciones médicas. A modo de ilustración, en la Figura III se puede ver un esquema con algunos ejemplos de aplicaciones biomédicas y el uso del PCL y el copolímero poli(D,L-lactida-co-epsilon-caprolactona) (PDLCL).

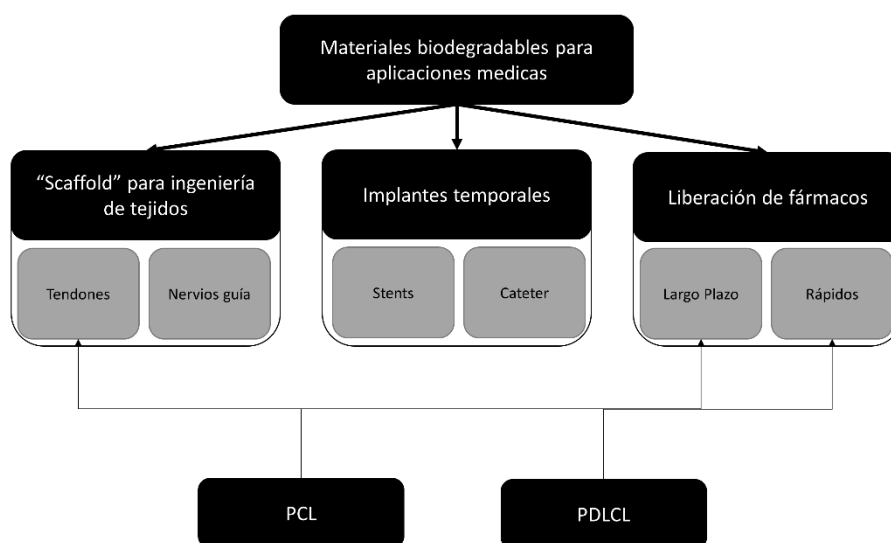


Figura III. Ejemplos de aplicaciones biomédicas del polímero poli(ϵ -caprolactona) (PCL) y copolímero poli(D,L-lactida-co-epsilon-caprolactona) (PDLCL).

El PCL es un polímero que se obtiene mediante polimerización por apertura de anillo del monómero ϵ -caprolactona³⁸ (véase la Figura IV). Esta polimerización puede darse con el uso de diferentes catalizadores como el octoato de estaño y/o utilizando diferentes temperaturas y tiempos de reacción^{38,39}. De esta manera se consiguen polímeros de pesos moleculares e índices de polidispersidad variados y por lo tanto, se pueden obtener polímeros con propiedades y tiempos de biodegradación diferentes y ajustables.

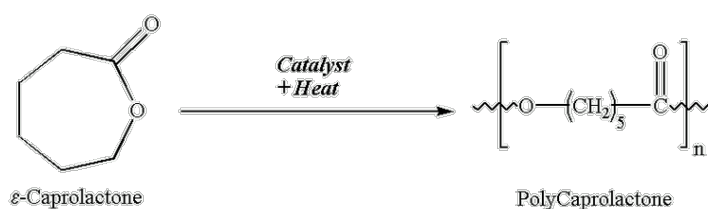


Figura IV. Reacción por apertura de anillo de ϵ -caprolactona para obtener poli(ϵ -caprolactona).

El PCL es un polímero semicristalino ($\chi_c = 45\% - 55\%$) termoplástico de baja temperatura de transición vítrea ($T_g \approx -60\text{ }^\circ\text{C}$) y temperatura de fusión relativamente alta ($T_m \approx 60\text{ }^\circ\text{C}$)^{40,41}. Estas propiedades hacen que a temperatura ambiente posea un comportamiento

mecánico dúctil (debido a la formación de cristales) y una gran capacidad de plastificación tanto a temperatura ambiente como en temperaturas del cuerpo humano ($T \approx 37 \text{ }^\circ\text{C}$)⁴⁰. Sin embargo, debido a su alta capacidad de cristalización el PCL es más estable frente a la degradación hidrolítica que otros poliésteres, por lo que tiene tiempos de degradación largos⁴².

En cuanto al procesado, es un polímero fácilmente procesable debido a su carácter termoplástico y su poca sensibilidad a los procesos que implican disolventes, temperatura alta o esterilización⁴³. Todo esto lo hace que sea un buen candidato para su uso como material de aplicación médica, especialmente dentro de la ingeniería de tejidos y como dispositivo de liberación de fármacos de larga duración. Algunos dispositivos que incluyen PCL o sus derivados ya han sido aprobados por la asociación americana de alimentos y medicamentos (FDA) para su aplicación en humanos como el ‘Capronor’⁴⁴.

En cuanto a los copolímeros poli(lactida- ϵ -caprolactona) son producto de la polimerización simultánea de los monómeros ϵ -caprolactona y ácido láctico o lactonas^{45,46} (véase Figura V). Las propiedades resultantes dependen fuertemente de la estructura del copolímero resultante (por bloques o al azar) y la composición molar obtenida^{16,47-49}.

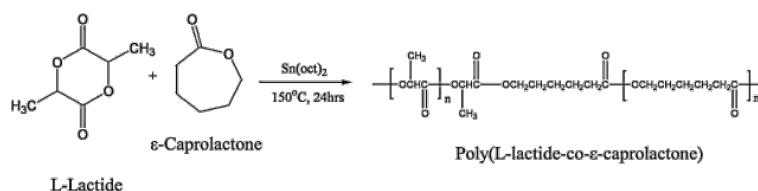


Figura V. Reacción por apertura de anillo de ϵ -caprolactona y lactona para obtener poli(L-lactida-co- ϵ -caprolactona).

Las composiciones más habituales suelen oscilar entre 70:30 a 85:15 proporción Lactida/caprolactona⁴⁵, dando lugar a polímeros con carácter elastómero con temperaturas de transición vítrea entre los 20 y los 30 grados centígrados^{50,51}. Los polímeros resultantes son de carácter amorfo, aunque se ha demostrado que las fases de lactida pueden reorganizarse con el tiempo formando fases cristalinas⁵². Este proceso de cristalización está favorecido dentro del cuerpo humano por estar en condiciones cercanas a la temperatura de transición vítrea y causa un aumento significativo en la velocidad de degradación, ya que las fases cristalinas son menos hidrolizables. Es por ello, que en los

últimos años se han ido desarrollando copolímeros y terpolímeros con mezclas racémicas de D- y L-lactida, que inhiben la formación de cristales⁵³. Como consecuencia de estos trabajos, se han obtenido copolímeros termoplásticos de gran capacidad elástica y de muy rápida degradación (14 semanas).

Estos copolímeros con capacidad elastomérica han adquirido interés en lo últimos años dentro de la ingeniería de tejidos para la regeneración de músculo, tendón o ligamentos gracias a la gran capacidad de recuperación elástica. Esta propiedad permite la estimulación mecánica de las células, que promueve diferentes mejoras como: mayor proliferación, producción de matriz extracelular y diferentes expresiones genéticas⁵⁴. Gracias a todo lo anterior descrito, estos copolímeros PLCL son buenos candidatos para la ingeniería de tejidos en nervios guía⁵⁵, tratamiento de estenosis esofágica⁵⁶ o tejido uretral⁵⁷.

Composites y materiales multifuncionales

Las aplicaciones biomédicas requieren de materiales con diversas funcionalidades y/o propiedades muy específicas difíciles de encontrar en materiales monolíticos. Por ello, el uso de materiales compuestos es una alternativa cada vez más habitual. Así, esta tesis se va a centrar en el uso de dos refuerzos en concreto, el sulfato de bario y los nanotubos de carbono que gracias a su escala sub-micro y nanométrica pueden otorgar nuevas propiedades y funcionalidad a los polímeros de base ampliando el rango de aplicaciones. La Figura VI muestra el ejemplo de los composites estudiados en esta tesis y las aplicaciones médicas en las que podrían ser utilizados.

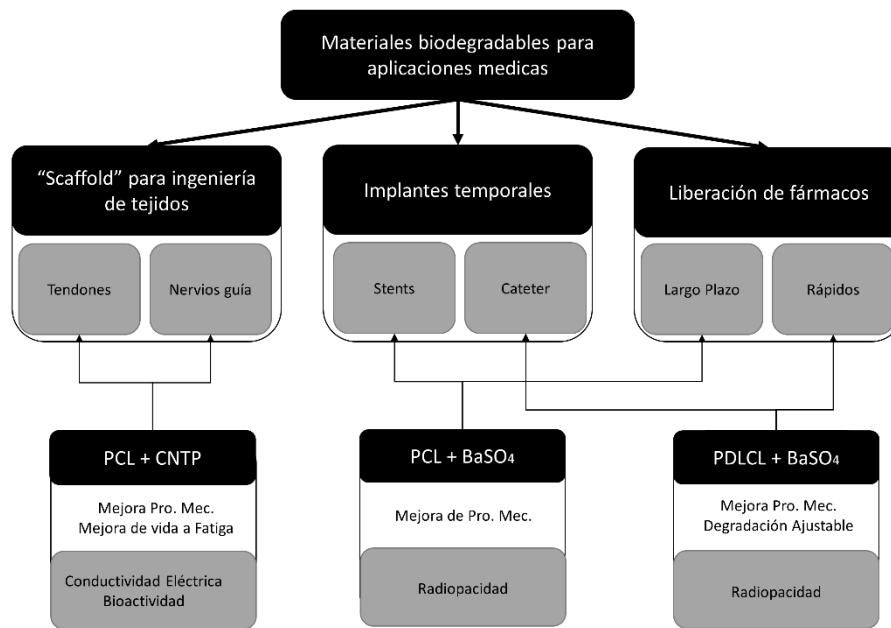


Figura VI .Uso de composites multifuncionales en aplicaciones médicas.

A continuación se incluye un resumen de las principales características y usos de los refuerzo empleados en este trabajo de tesis; el sulfato de bario (BaSO_4) y lo nanotubos de carbono (CNT).

Sulfato de bario

Los polímeros biodegradables aportan grandes ventajas frente a los implante metálicos en cuanto a biocompatibilidad, evitar el efecto *stress-shielding* y segundas cirugías. Sin embargo, suelen ser transparentes frente a las imágenes de rayos-X que es la técnica más utilizada a la hora de posicionar un implante o controlar su ubicación. Para poder solucionar esta desventaja, se han empezado a incluir refuerzos de alto peso molecular como el óxido de bismuto⁵⁸, óxido de hierro⁵⁹ y el sulfato de bario⁶⁰ junto con los polímeros. De esta manera, los composites resultantes adquieren la capacidad de ser radiopacos (RO). A modo de ejemplo en la Figura VII se observa la diferencia de un implante sin (imagen (a)) y con nano-partículas radiopacas de Fe_3O_4 (imagen (b)).

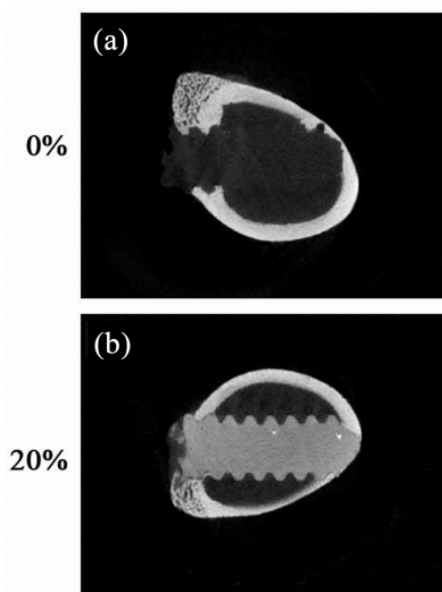


Figura VII. Tomografía computarizada de implantes de polilactida con y sin nano-partículas de Fe_3O_4 ⁵⁹.

Dentro de estos refuerzos, el sulfato de bario ha sido aprobado para su uso médico por la asociación americana de alimentos y medicamentos (FDA) y es utilizada en medicina como contraste de rayos-X. Por lo tanto, su uso junto con materiales biodegradables ha causado un gran interés para aplicaciones como catéteres biodegradables⁶⁰⁻⁶².

Por el contrario es un refuerzo que presenta variados resultados desde el punto de vista mecánico^{63,64}, incluyendo disminución de propiedades significativas con algunos polímeros⁶⁵, por lo que es necesario ampliar el conocimiento de la interacciones matriz refuerzo en estos composites.

Nanotubos de carbono

Los nanotubos de carbono son formas alotrópicas del carbón descubiertas por Iijima en 1991⁶⁶ y que desde entonces han sido utilizadas en multitud de aplicaciones como electrodos, componente de micro/nano electrónica o refuerzos mecánicos.

Pueden ser sintetizados de diferentes maneras como la ablación laser o la deposición química-catalítica en fase gaseosa⁶⁷. El resultado es una lámina de grafeno plegada sobre si misma formando un tubo. Una distinción principal dentro los nanotubos es si están formados por una única capa (en inglés “*Single Wall Carbon Nanotubes*” o SWCN) o por

varias capas de manera concéntrica (en inglés “*Multiple Wall Carbon Nanotubes*” o MWCNT) (véase Figura VIII). Estos últimos son los más comunes y tienen normalmente entre 5 y 20 capas dando lugar a diámetros de tubo de entre 20 y 100 nanómetros. Por último, según los procesos de fabricación la longitud de los tubos oscila entre las 0,5 y las 5 micras⁶⁸.

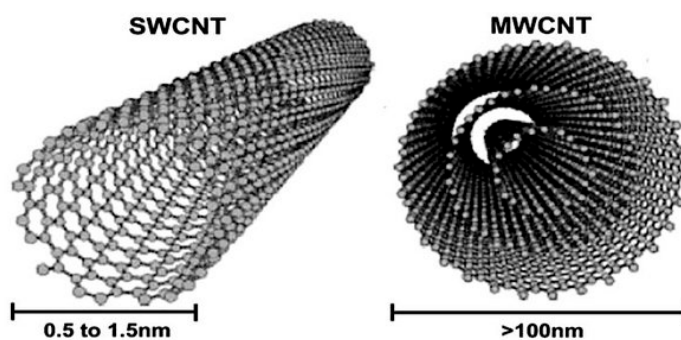


Figura VIII. Estructura de los nanotubos (izquierda) monocapa o SWCNT y (derecha) multicapa o MWCNT⁶⁹.

Dependiendo de la estructura electrónica y de los defectos del proceso de fabricación los nanotubos tienen diferentes propiedades eléctricas, pero en general los MWCNT son muy buenos conductores eléctricos y por esta razón se utilizan en aplicaciones eléctricas y electrónicas⁶⁷. Como refuerzo en matrices poliméricas han demostrado aumentar la conductividad eléctrica, sobre todo si se alcanza un valor crítico en el que los nanotubos están bien dispersos y conectados. Este estado se denomina normalmente como “Percolación”. Gracias a la alta relación de aspecto de estas nano-partículas este estado se puede conseguir con porcentajes bajos de carga⁷⁰. Además de esto tienen unas altísimas propiedades mecánicas específicas con valores teóricos de rigidez cercanos a 1TPa⁷¹ (por encima de 0.5 TPa en ensayos mediante AFM⁷²) y una alta resistencia mecánica, lo que los hace muy buenos candidatos como refuerzo mecánico.

Dentro de las aplicaciones biomédicas es uno de los nano-refuerzos más estudiados en variedad de aplicaciones como agente de contraste en aplicaciones de diagnóstico⁷³, biosensores electromecánicos⁷⁴ o liberación genética y fármacos^{75,76}. Dentro del área de trabajo de estas tesis destacaría su uso en ingeniería de tejidos junto con polímeros biodegradables ya que ha demostrado ser un buen sustrato para la adhesión celular y promover las señales de las células neuronales⁷⁷⁻⁷⁹.

Por último, un aspecto muy importante para la aplicación de los nanotubos y especialmente en aplicaciones médicas es la modificación superficial de estos. Las propiedades que pueden aportar a un composite como la conductividad eléctrica o la mejora mecánica dependen fuertemente de estar muy bien dispersos en la matriz polimérica. Por desgracia debido a las interacciones físico-químicas los nanotubos de carbono han demostrado ser partículas difíciles de dispersar tanto en ambientes hidrófilos como hidrófobos^{80,81}.

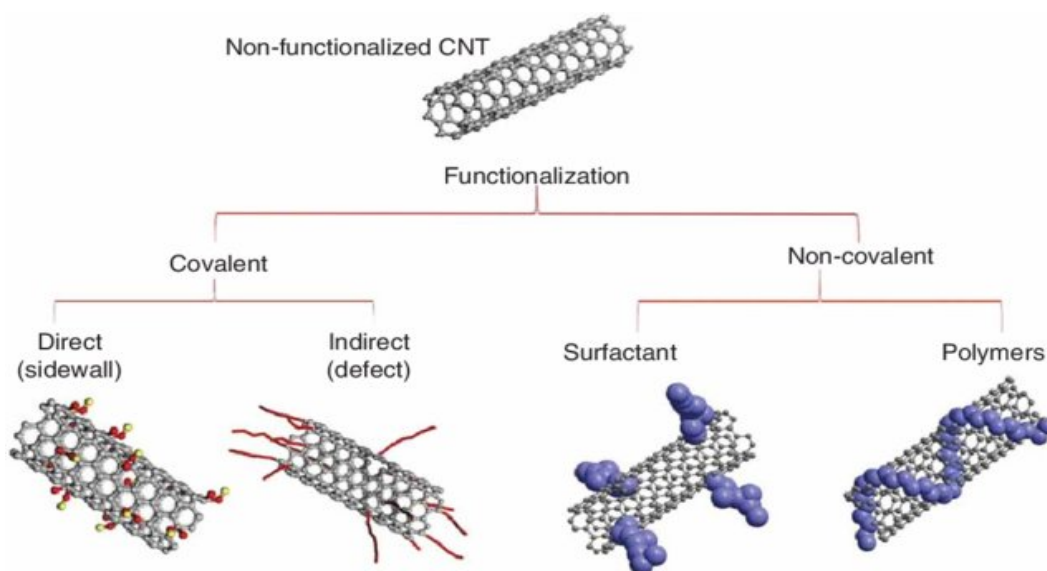


Figura IX. Ejemplos de funcionalización en nanotubos de carbono⁸².

Esta modificación superficial se conoce habitualmente como “funcionalización” y normalmente se lleva a cabo uniéndose a diferentes moléculas de manera covalente o no covalente como se muestra en la Figura IX.

Las funcionalizaciones covalentes están asociadas a cambios en la hibridación de sp^2 a sp^3 de las uniones carbono-carbono para enlazar diferentes moléculas. Esto genera defectos en la estructura hexagonal de los nanotubos y tiene consecuencias en las propiedades, sobre todo eléctricas. Las funcionalizaciones no covalentes están basadas en uniones más débiles como fuerzas de *van der Waals* o interacciones π - π y por lo tanto inducen menores cambios en la estructura principal del carbono, pero representan uniones de interfase menos robustas^{83,84}. Por otra parte la funcionalización de los nanotubos abre

nuevas oportunidades para adherir moléculas que puedan mejorar aspectos como las biocompatibilidad⁸⁵.

En esta tesis se estudiará el uso de nanotubos funcionalizados con poli(dopamina), una molécula bioinspirada en la adhesión de los moluscos con capacidad de proporcionar bioactividad a los materiales recubiertos^{86,87}.

Fatiga en materiales de implantes médicos

A la hora de seleccionar los materiales es habitual valorar su biocompatibilidad, tiempo de biodegradación y sus propiedades físico-químicas. Sin embargo, teniendo en cuenta que los tejidos blandos del cuerpo humano (como cartílago, piel músculos o venas) presentan un comportamiento viscoelástico^{88 89} y que muchos de los órganos del cuerpo humano están sometidos a esfuerzos cíclicos de tensión y/o deformación^{90 91}, no se debe olvidar el estudio de las propiedades mecánicas y dinámicas. Y más aún cuando se ha demostrado que las propiedades mecánicas (rigidez, deformación) y viscoelásticas de los biomateriales tienen un efecto significativo en la actividad celular (proliferación, diferenciación, etc.) de las células madre⁹²⁻⁹⁶. Por tanto, tener un material con las propiedades dinámicas adecuadas, que se mantienen a lo largo del tiempo, es fundamental para conseguir una regeneración adecuada del tejido dañado.

Para poder diseñar implantes médicos de manera adecuada es necesario disponer de las curvas de Tensión-Ciclos (normalmente llamadas curvas S-N) ya que nos indican la vida a fatiga de un material según el nivel de tensión al que va a ser sometida y nos permiten calcular la confianza estadística de que un implante vaya a sobrevivir a su vida de diseño. Un ejemplo de esto se puede ver en la Figura X.

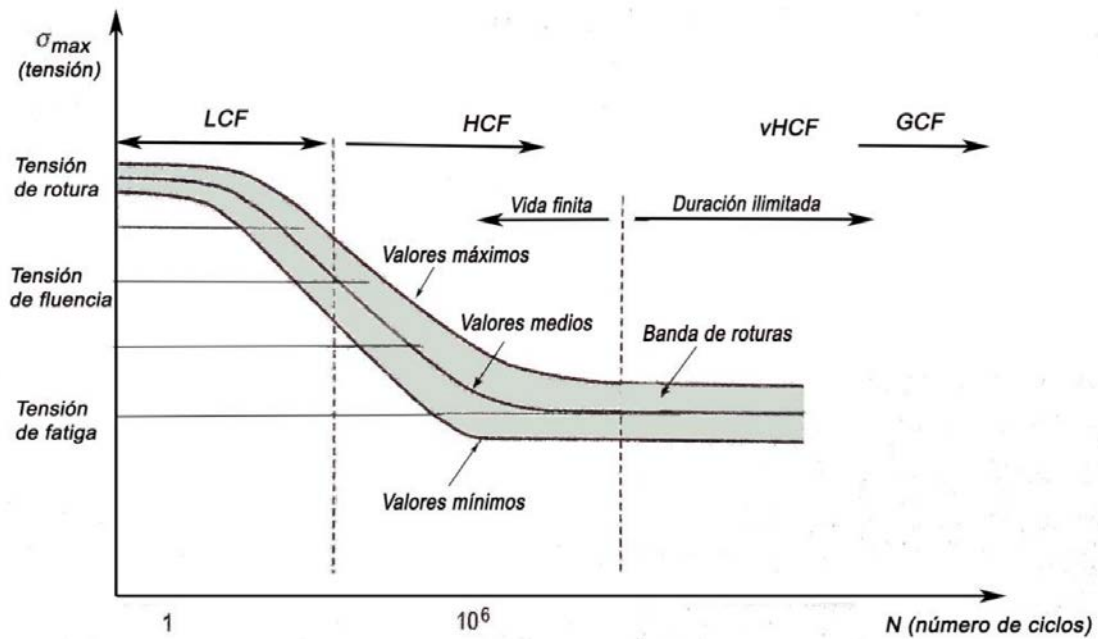


Figura X Curva S-N para materiales dividida en 4 zonas en función de la duración en ciclos: LCF (low cycle fatigue), HCF (high cycle fatigue) vHCF (very high cycle fatigue) y GCF (giga cycle fatigue)⁹⁷.

Por otro lado también es muy importante conocer la evolución de las propiedades de los materiales durante las cargas cíclicas. Especialmente con materiales poliméricos cuyas propiedades viscoelásticas hacen que ante la presencia de tensión continuada y temperatura puedan sufrir efectos de deformación acumulada por efecto de “Creep”, debido a la movilidad de las cadenas poliméricas.

Como puede verse en la Figura XI esto da lugar a que los polímeros puedan sufrir deformación plástica acumulada cuando se ven sometidos a una tensión constante en el tiempo llegando al fallo mecánico por inestabilidad plástica (Zona 3). En el caso de un polímero a fatiga el fenómeno es el mismo y además puede ir acrecentado por el calor producido mediante la histéresis, que favorece todos los procesos relacionados con la movilidad de sus cadenas poliméricas.

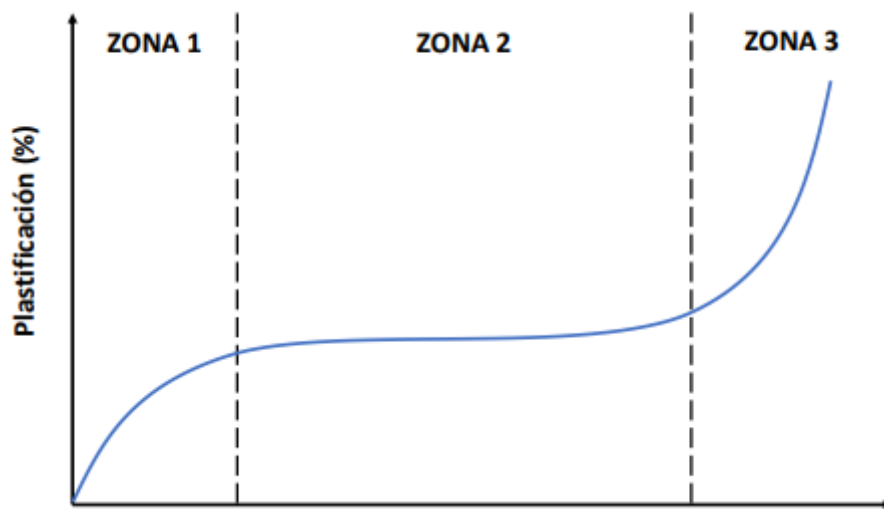


Figura XI. Curva de “Creep” de un polímero sometido a tensión constante.

Por último el otro factor determinante para entender en profundidad la fatiga es la mecánica de la fractura en polímeros. Al igual que en los materiales metálicos, la mecánica de la fractura se encarga de estudiar los fallos en los materiales con presencia de grietas. En los polímeros la generación de microhuecos⁹⁸ en las zonas de concentración de tensiones termina en la coalescencia de estos que acaba formando grietas. Estas grietas inician su crecimiento ante tensiones cíclicas terminando en un fallo frágil. Este crecimiento de grieta viene gobernado normalmente por la Ley de Paris⁹⁹, ejemplificada en la Figura XII, donde puede verse que la velocidad de crecimiento de grieta por ciclo (da/dN) crece de manera exponencial con el factor de intensidad de tensiones K regido por la fórmula (1):

$$K = \sigma \sqrt{\pi \cdot a} \quad (1)$$

Donde “ σ ” es la tensión sometida al material y “ a ” al tamaño de la grieta.

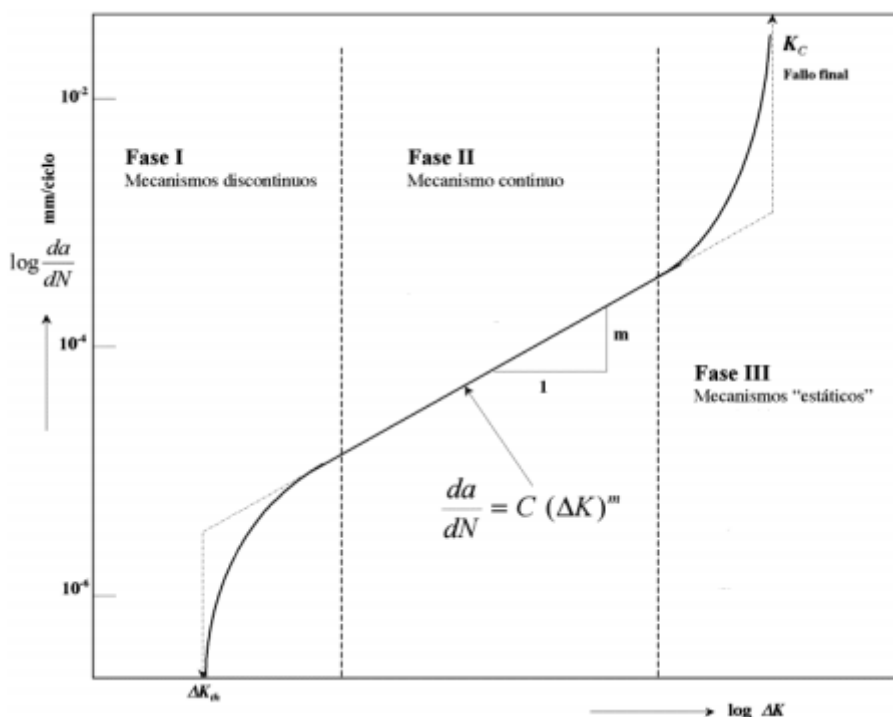


Figura XII. Curva característica de propagación de grieta en materiales. Ley de Paris⁹⁹.

Existe en la literatura una cierta carencia en el número de artículos sobre el estudio de las propiedades dinámicas y, en concreto, de la resistencia de fatiga de los materiales para implantes médicos. Y este incluye al PCL y sus compuestos. Los pocos estudios encontrados en la bibliografía¹⁰⁰⁻¹⁰³, se realizan para un único nivel de deformación o, como mucho, para tres niveles de tensiones y las muestras presentan la forma de scaffold. Los scaffolds, debido a la cantidad de factores morfológicos que introducen (número de poros, interconexión entre poros, etc.), dificultan discernir si los resultados obtenidos son por el propio material o por la morfología de la muestra. Por estas razones no se puede considerar al PCL un material adecuadamente caracterizado a fatiga, aspecto clave para conocer la resistencia a fatiga del material en función de la tensión.

Es por ello, que en la presente tesis doctoral se pretende analizar el comportamiento dinámico del PCL realizando ensayos de fatiga a films de PCL bajo condiciones fisiológicas (37 °C + medio acuoso) sometidos a distintas tensiones y analizando no sólo la duración/ciclos que soportan las muestras, a través de la curva S-N obtenida, sino que también el daño/deformación que sufren por estar sometidas a fatiga, la energía disipada

(histéresis) y su morfología del fallo. Todo ello para adquirir los conocimientos que completen el gap existente en el comportamiento a fatiga de este biopolímero y sus composites reforzados con nanotubos de carbono.

Referencias

1. Larrañaga, A. & Lizundia, E. A review on the thermomechanical properties and biodegradation behaviour of polyesters. *Eur. Polym. J.* **121**, 109296 (2019).
2. Piskin, E. Journal of Biomaterials Science , Biodegradable polymers as biomaterials. 37–41 (1994).
3. Chandra, R. & Rustgi, R. Biodegradable polymers. *Prog. Polym. Sci.* **23**, 1273–1335 (1998).
4. Nair, L. S. & Laurencin, C. T. Biodegradable polymers as biomaterials. *Prog. Polym. Sci.* **32**, 762–798 (2007).
5. Park, H., Temenoff, J. S. & Mikos, A. G. Biodegradable Orthopedic Implants. *Eng. Funct. Skelet. Tissues* 55–68 (2007) doi:10.1007/978-1-84628-366-6_4.
6. Ulery, B. D., Nair, L. S. & Laurencin, C. T. Biomedical applications of biodegradable polymers. *J. Polym. Sci. Part B Polym. Phys.* **49**, 832–864 (2011).
7. Martina, M. & Hutmacher, D. W. Biodegradable polymers applied in tissue engineering research: a review. *Polym. Int.* **56**, 145–157 (2007).
8. Ikada, Y. & Tsuji, H. Biodegradable polyesters for medical and ecological applications. *Macromol. Rapid Commun.* **21**, 117–132 (2000).
9. Lu, Y. & Chen, S. C. Micro and nano-fabrication of biodegradable polymers for drug delivery. *Adv. Drug Deliv. Rev.* **56**, 1621–1633 (2004).
10. Asghari, F., Samiei, M., Adibkia, K., Akbarzadeh, A. & Davaran, S. Biodegradable and biocompatible polymers for tissue engineering application: a review. *Artif. Cells, Nanomedicine Biotechnol.* **45**, 185–192 (2017).
11. Grizzi, I., Garreau, H., Li, S. & Vert, M. Hydrolytic degradation of devices based on poly(dl-lactic acid) size-dependence. *Biomaterials* **16**, 305–311 (1995).
12. Smith, R., Oliver, C. & Williams, D. F. The enzymatic degradation. **21**, 991–1003 (1987).
13. Bergsma, J. E. *et al.* In vivo degradation and biocompatibility study of in vitro pre-degraded as-polymerized polylactide particles. *Biomaterials* **16**, 267–274 (1995).
14. Van Minnen, B., Stegenga, B., Van Leeuwen, M. B. M., Van Kooten, T. G. & Bos, R. R. M. A long-term in vitro biocompatibility study of a biodegradable polyurethane and its degradation products. *J. Biomed. Mater. Res. - Part A* **76**, 377–385 (2006).
15. Shih, C. Chain-end scission in acid catalyzed hydrolysis of poly (d,l-lactide) in solution. *J. Control. Release* **34**, 9–15 (1995).
16. Fernández, J., Etxeberria, A. & Sarasua, J. R. Effects of repeat unit sequence distribution and residual catalyst on thermal degradation of poly(l-lactide/ε-caprolactone) statistical copolymers. *Polym. Degrad. Stab.* **98**, 1293–1299 (2013).
17. Göpferich, A. Mechanisms of polymer degradation and erosion1. *Biomater. Silver Jubil. Compend.* **17**, 117–128 (1996).

18. Pietrzak, W. S. Principles of development and use of absorbable internal fixation. *Tissue Eng.* **6**, 425–433 (2000).
19. Middleton, J. C. & Tipton, A. J. Synthetic biodegradable polymers as orthopedic devices. *Biomaterials* **21**, 2335–2346 (2000).
20. Larsen, M. W., Pietrzak, W. S. & DeLee, J. C. Fixation of osteochondritis dissecans lesions using poly(l-lactic acid)/poly(glycolic acid) copolymer bioabsorbable screws. *Am. J. Sports Med.* **33**, 68–76 (2005).
21. Böstman, O. & Pihlajamäki, H. Clinical biocompatibility of biodegradable orthopaedic implants for internal fixation: A review. *Biomaterials* **21**, 2615–2621 (2000).
22. Hegggers, J. P. *et al.* Biocompatibility of Silicone Implants. *Ann. Plast. Surg.* **11**, 38–45 (1983).
23. Singh, R. P. & Ramarao, P. Accumulated polymer degradation products as effector molecules in cytotoxicity of polymeric nanoparticles. *Toxicol. Sci.* **136**, 131–143 (2013).
24. Engelberg, I. & Kohn, J. Physico-mechanical properties of degradable polymers used in medical applications: A comparative study. *Biomaterials* **12**, 292–304 (1991).
25. Bergström, J. S. & Hayman, D. An Overview of Mechanical Properties and Material Modeling of Polylactide (PLA) for Medical Applications. *Ann. Biomed. Eng.* **44**, 330–340 (2016).
26. Vieira, A. C. *et al.* Mechanical study of PLA-PCL fibers during in vitro degradation. *J. Mech. Behav. Biomed. Mater.* **4**, 451–460 (2011).
27. Ugartemendia, J. M., Muñoz, M. E., Sarasua, J. R. & Santamaria, A. Phase behavior and effects of microstructure on viscoelastic properties of a series of polylactides and polylactide/poly(ϵ -caprolactone) copolymers. *Rheol. Acta* **53**, 857–868 (2014).
28. Larrañaga, A. *et al.* A study of the mechanical properties and cytocompatibility of lactide and caprolactone based scaffolds filled with inorganic bioactive particles. *Mater. Sci. Eng. C* **42**, 451–460 (2014).
29. Hutmacher, D. W. *Scaffolds in tissue engineering bone and cartilage. The Biomaterials: Silver Jubilee Compendium* vol. 21 (Woodhead Publishing Limited, 2000).
30. Freed, L. E. *et al.* Biodegradable Polymer Scaffolds for Tissue Engineering. *Nat. Biotechnol.* **12**, 689–693 (1994).
31. Yang, X. B. *et al.* Human osteoprogenitor growth and differentiation on synthetic biodegradable structures after surface modification. *Bone* **29**, 523–531 (2001).
32. Mueller-Schulte, D. *et al.* Surface Modification of Polymers to Permit Endothelial Cell Growth. *Cells Mater.* **1**, 1 (1991).
33. Chan, W. A., Bini, T. B., Venkatraman, S. S. & Boey, F. Y. C. Effect of radio-opaque filler on biodegradable stent properties. *J. Biomed. Mater. Res. Part A* **79A**, 47–52 (2006).
34. Sanchez-Rexach, E. *et al.* Novel biodegradable and non-fouling systems for controlled-release based on poly(ϵ -caprolactone)/Quercetin blends and biomimetic bacterial S-layer coatings. *RSC Adv.* **9**, 24154–24163 (2019).
35. Sanchez-Rexach, E. *et al.* Miscibility, interactions and antimicrobial activity of poly(ϵ -caprolactone)/chloramphenicol blends. *Eur. Polym. J.* **102**, 30–37 (2018).
36. Sanchez-Rexach, E., Meaurio, E. & Sarasua, J. R. Recent developments in drug eluting devices with tailored interfacial properties. *Adv. Colloid Interface Sci.* **249**, 181–191

- (2017).
37. Larrañaga, A. *et al.* Antioxidant functionalized polymer capsules to prevent oxidative stress. *Acta Biomater.* **67**, 21–31 (2018).
 38. Labet, M. & Thielemans, W. Synthesis of polycaprolactone: A review. *Chem. Soc. Rev.* **38**, 3484–3504 (2009).
 39. STOREY, R. F. & TAYLOR, A. E. Effect of Stannous Octoate on the Composition, Molecular Weight, and Molecular Weight Distribution of Ethylene Glycol-Initiated Poly(ϵ -Caprolactone). *J. Macromol. Sci. Part A* **35**, 723–750 (1998).
 40. Jimenez, G., Ogata, N., Kawai, H. & Ogihara, T. Structure and thermal/mechanical properties of poly(ϵ -caprolactone)-clay blend. *J. Appl. Polym. Sci.* **64**, 2211–2220 (1997).
 41. López-Rodríguez, N., López-Arraiza, A., Meaurio, E. & Sarasua, J. R. Crystallization, morphology, and mechanical behavior of polylactide/poly(ϵ -caprolactone) blends. *Polym. Eng. Sci.* **46**, 1299–1308 (2006).
 42. Larrañaga, A., Aldazabal, P., Martin, F. J. & Sarasua, J. R. Hydrolytic degradation and bioactivity of lactide and caprolactone based sponge-like scaffolds loaded with bioactive glass particles. *Polym. Degrad. Stab.* **110**, 121–128 (2014).
 43. Woodruff, M. A. & Hutmacher, D. W. The return of a forgotten polymer - Polycaprolactone in the 21st century. *Prog. Polym. Sci.* **35**, 1217–1256 (2010).
 44. Darney, P. D., Monroe, S. E., Klaisle, C. M. & Alvarado, A. Clinical evaluation of the Capronor contraceptive implant: Preliminary report. *Am. J. Obstet. Gynecol.* **160**, 1292–1295 (1989).
 45. Fernández, J. *et al.* Synthesis and characterization of poly (l-lactide/ ϵ -caprolactone) statistical copolymers with well resolved chain microstructures. *Polymer (Guildf)*. **54**, 2621–2631 (2013).
 46. Liu, F., Zhao, Z., Yang, J., Wei, J. & Li, S. Enzyme-catalyzed degradation of poly(l-lactide)/poly(ϵ -caprolactone) diblock, triblock and four-armed copolymers. *Polym. Degrad. Stab.* **94**, 227–233 (2009).
 47. Fernández, J., Etxeberria, A., Ugartemendia, J. M., Petisco, S. & Sarasua, J. R. Effects of chain microstructures on mechanical behavior and aging of a poly(L-lactide-co- ϵ -caprolactone) biomedical thermoplastic-elastomer. *J. Mech. Behav. Biomed. Mater.* **12**, 29–38 (2012).
 48. Fernández, J., Etxeberria, A. & Sarasua, J. R. Synthesis, structure and properties of poly(L-lactide-co- ϵ -caprolactone) statistical copolymers. *J. Mech. Behav. Biomed. Mater.* **9**, 100–112 (2012).
 49. In Jeong, S. *et al.* Morphology of elastic poly(L-lactide-co- ϵ -caprolactone) copolymers and in vitro and in vivo degradation behavior of their scaffolds. *Biomacromolecules* **5**, 1303–1309 (2004).
 50. Fernández, J., Etxeberria, A. & Sarasua, J. R. In vitro degradation studies and mechanical behavior of poly(ϵ -caprolactone-co- δ -valerolactone) and poly(ϵ -caprolactone-co-L-lactide) with random and semi-alternating chain microstructures. *Eur. Polym. J.* **71**, 585–595 (2015).
 51. Fernández, J., Larrañaga, A., Etxeberria, A. & Sarasua, J. R. Effects of chain microstructures and derived crystallization capability on hydrolytic degradation of poly(l-lactide/ ϵ -caprolactone) copolymers. *Polym. Degrad. Stab.* **98**, 481–489 (2013).

52. Amestoy, H., Larrañaga, A., Ugartemendia, J. M. & Sarasua, J. R. Phase-structural evolution in polylactides during an initial 7 day degradation period in PBS. in *Society of Plastics Engineers - EUROTECH 2013* (2013).
53. Fernández, J., Larrañaga, A., Etxeberria, A., Wang, W. & Sarasua, J. R. A new generation of poly(lactide/ε-caprolactone) polymeric biomaterials for application in the medical field. *J. Biomed. Mater. Res. - Part A* **102**, 3573–3584 (2014).
54. Lee, J. *et al.* Regeneration of Achilles' Tendon: The role of dynamic stimulation for enhanced cell proliferation and mechanical properties. *J. Biomater. Sci. Polym. Ed.* **21**, 1173–1190 (2010).
55. Chiriac, S., Facca, S., Diaconu, M., Gouzou, S. & Liverneaux, P. Experience of using the bioresorbable copolyester poly(DL-lactide-ε-caprolactone) nerve conduit guide Neurolac™ for nerve repair in peripheral nerve defects: Report on a series of 28 lesions. *J. Hand Surg. (European Vol.* **37**, 342–349 (2012).
56. Yu, X. *et al.* A shape memory stent of poly(ε-caprolactone-co-DL-lactide) copolymer for potential treatment of esophageal stenosis. *J. Mater. Sci. Mater. Med.* **23**, 581–589 (2012).
57. Sartoneva, R. *et al.* Comparison of a poly-L-lactide-co-ε-caprolactone and human amniotic membrane for urothelium tissue engineering applications. *J. R. Soc. Interface* **8**, 671–677 (2011).
58. Kusiak, E. & Zaborski, M. Characteristic of natural rubber composites absorbing X-radiation. *Compos. Interfaces* **19**, 433–439 (2012).
59. Chang, W. J. *et al.* Development and testing of X-ray imaging-enhanced poly-L-lactide bone screws. *PLoS One* **10**, 1–12 (2015).
60. Isotalo, T. *et al.* Biocompatibility testing of a new bioabsorbable X-ray positive SR-PLA 96/4 urethral stent. *J. Urol.* **162**, 1764–1767 (1999).
61. Lämsä, T. *et al.* Biocompatibility of a new bioabsorbable radiopaque stent material (BaSO₄ containing poly-L,D-lactide) in the rat pancreas. *Pancreatology* **6**, 301–305 (2006).
62. Martínez De Arenaza, I., Sadaba, N., Larrañaga, A., Zuza, E. & Sarasua, J. R. High toughness biodegradable radiopaque composites based on polylactide and barium sulphate. *Eur. Polym. J.* **73**, 88–93 (2015).
63. Wang, K., Wu, J., Ye, L. & Zeng, H. Mechanical properties and toughening mechanisms of polypropylene/barium sulfate composites. *Compos. Part A Appl. Sci. Manuf.* **34**, 1199–1205 (2003).
64. Wang, K., Wu, J. & Zeng, H. Microstructure and fracture behavior of polypropylene/barium sulfate composites. *J. Appl. Polym. Sci.* **99**, 1207–1213 (2006).
65. Siaueira, G., Bras, J. & Dufresne, A. Cellulose whiskers versus microfibrils: Influence of the nature of the nanoparticle and its surface functionalization on the thermal and mechanical properties of nanocomposites. *Biomacromolecules* **10**, 425–432 (2009).
66. Iijima, S. Helical microtubules of graphitic carbon. *Nature* **354**, 56–58 (1991).
67. Monthieux, M. *et al.* Carbon Nanotubes. in *Springer Handbooks* vol. PartF1 193–247 (2017).
68. Belin, T. & Epron, F. Characterization methods of carbon nanotubes: A review. *Mater. Sci. Eng. B Solid-State Mater. Adv. Technol.* **119**, 105–118 (2005).
69. Ribeiro, B., Botelho, E. C., Costa, M. L. & Bandeira, C. F. Carbon nanotube buckypaper

- reinforced polymer composites: A review. *Polimeros* **27**, 247–255 (2017).
70. Li, J. *et al.* Correlations between percolation threshold, dispersion state, and aspect ratio of carbon nanotubes. *Adv. Funct. Mater.* **17**, 3207–3215 (2007).
 71. Yao, N. & Lordi, V. Young's modulus of single-walled carbon nanotubes. *J. Appl. Phys.* **84**, 1939–1943 (1998).
 72. Sun, X. & Wang, Y. Mechanical Properties of Carbon Nanotubes. in *Textile Engineering* 53–57 (ASMEDC, 2002). doi:10.1115/IMECE2002-39484.
 73. Gong, H., Peng, R. & Liu, Z. Carbon nanotubes for biomedical imaging: The recent advances. *Adv. Drug Deliv. Rev.* **65**, 1951–1963 (2013).
 74. Ojeda, I. *et al.* Grafted-double walled carbon nanotubes as electrochemical platforms for immobilization of antibodies using a metallic-complex chelating polymer: Application to the determination of adiponectin cytokine in serum. *Biosens. Bioelectron.* **74**, 24–29 (2015).
 75. Liu, Z., Sun, X., Nakayama-Ratchford, N. & Dai, H. Supramolecular Chemistry on Water-Soluble Carbon Nanotubes for Drug Loading and Delivery. *ACS Nano* **1**, 50–56 (2007).
 76. Liu, Z. *et al.* Supramolecular stacking of doxorubicin on carbon nanotubes for in vivo cancer therapy. *Angew. Chemie - Int. Ed.* **48**, 7668–7672 (2009).
 77. Lovat, V. *et al.* Carbon nanotube substrates boost neuronal electrical signaling. *Nano Lett.* **5**, 1107–1110 (2005).
 78. Bédier, A. *et al.* Elucidation of the role of carbon nanotube patterns on the development of cultured neuronal cells. *Langmuir* **28**, 17363–17371 (2012).
 79. Matta-Domjan, B. *et al.* Biophysical interactions between pancreatic cancer cells and pristine carbon nanotube substrates: Potential application for pancreatic cancer tissue engineering. *J. Biomed. Mater. Res. - Part B Appl. Biomater.* **106**, 1637–1644 (2018).
 80. Xie, X. L., Mai, Y. W. & Zhou, X. P. Dispersion and alignment of carbon nanotubes in polymer matrix: A review. *Mater. Sci. Eng. R Reports* **49**, 89–112 (2005).
 81. Vaisman, L., Wagner, H. D. & Marom, G. The role of surfactants in dispersion of carbon nanotubes. *Adv. Colloid Interface Sci.* **128–130**, 37–46 (2006).
 82. Karimi, M. *et al.* Carbon nanotubes part I: Preparation of a novel and versatile drug-delivery vehicle. *Expert Opin. Drug Deliv.* **12**, 1071–1087 (2015).
 83. Hirsch, A. & Vostrowsky, O. Functionalization of carbon nanotubes. *Top. Curr. Chem.* **245**, 193–237 (2005).
 84. Hirsch, A. Functionalization of single-walled carbon nanotubes. *Angew. Chemie - Int. Ed.* **41**, 1853–1859 (2002).
 85. Shim, M., Kam, N. W. S., Chen, R. J., Li, Y. & Dai, H. Functionalization of Carbon Nanotubes for Biocompatibility and Biomolecular Recognition. *Nano Lett.* **2**, 285–288 (2002).
 86. Sun, Y. *et al.* Peptide decorated nano-hydroxyapatite with enhanced bioactivity and osteogenic differentiation via polydopamine coating. *Colloids Surfaces B Biointerfaces* **111**, 107–116 (2013).
 87. Cui, J. *et al.* Polydopamine-functionalized polymer particles as templates for mineralization of hydroxyapatite: Biomimetic and in vitro bioactivity. *RSC Adv.* **6**, 6747–6755 (2016).

88. Fung, Y. C. *Biomechanics: Mechanical Properties of Living Tissues*. (Springer-Verlag New York, 1993). doi:10.1007/978-1-4757-2257-4.
89. Maurel, W., Thalmann, D., Wu, Y. & Thalmann, N. M. *Biomechanical Models for Soft Tissue Simulation*. (Springer-Verlag Berlin Heidelberg, 1998). doi:10.1007/978-3-662-03589-4.
90. Wren, T. A. L., Lindsey, D. P., Beaupré, G. S. & Carter, D. R. Effects of creep and cyclic loading on the mechanical properties and failure of human Achilles tendons. *Ann. Biomed. Eng.* **31**, 710–717 (2003).
91. Martin, R. B., Burr, D. B., Sharkey, N. A. & Fyhrie, D. P. Fatigue and Fracture Resistance of Bone. in *Skeletal Tissue Mechanics* 423–482 (Springer, New York, NY, 2015). doi:https://doi.org/10.1007/978-1-4939-3002-9_8.
92. Keung, A. J., Healy, K. E., Kumar, S. & Schaffer, D. V. Biophysics and dynamics of natural and engineered stem cell microenvironments. *Wiley Interdiscip. Rev. Syst. Biol. Med.* **2**, 49–64 (2010).
93. Vining, K. H. & Mooney, D. J. Mechanical forces direct stem cell behaviour in development and regeneration. *Nat. Rev. Mol. Cell Biol.* **18**, 728–742 (2017).
94. Engler, A. J., Sen, S., Sweeney, H. L. & Discher, D. E. Matrix Elasticity Directs Stem Cell Lineage Specification. *Cell* **126**, 677–689 (2006).
95. Huang, D. *et al.* Viscoelasticity in natural tissues and engineered scaffolds for tissue reconstruction. *Acta Biomater.* **97**, 74–92 (2019).
96. Kumar, A., Placone, J. K. & Engler, A. J. Understanding the extracellular forces that determine cell fate and maintenance. *Dev.* **144**, 4261–4270 (2017).
97. Avilés, R. *Métodos de cálculo de fatiga para ingeniería. Metales*. (Ediciones Paraninfo, 2015).
98. Pruitt, L. A., Rama Sreekanth, P. S., Badgayan, N. D. & Sahoo, S. K. Fatigue of Polymers. *Ref. Modul. Mater. Sci. Mater. Eng.* 1–15 (2017) doi:10.1016/b978-0-12-803581-8.00904-8.
99. González, J. L. A. and J. J. *Mecánica de Fractura*. (Universidad del País Vasco, 2002).
100. Panadero, J. A., Vikingsson, L., Gomez Ribelles, J. L., Sencadas, V. & Lanceros-Mendez, S. Fatigue prediction in fibrin poly- ϵ -caprolactone macroporous scaffolds. *J. Mech. Behav. Biomed. Mater.* **28**, 55–61 (2013).
101. Fernández, J., Auzmendi, O., Amestoy, H., Diez-Torre, A. & Sarasua, J. R. Mechanical properties and fatigue analysis on poly(ϵ -caprolactone)-polydopamine-coated nanofibers and poly(ϵ -caprolactone)-carbon nanotube composite scaffolds. *Eur. Polym. J.* **94**, 208–221 (2017).
102. Ergun, A., Yu, X., Valdevit, A., Ritter, A. & Kalyon, D. M. In vitro analysis and mechanical properties of twin screw extruded single-layered and coextruded multilayered poly(caprolactone) scaffolds seeded with human fetal osteoblasts for bone tissue engineering. *J. Biomed. Mater. Res. - Part A* **99 A**, 354–366 (2011).
103. Panadero, J. A. *et al.* Mechanical fatigue performance of PCL-chondroprogenitor constructs after cell culture under bioreactor mechanical stimulus. *J. Biomed. Mater. Res. - Part B Appl. Biomater.* **104**, 330–338 (2016).

Objetivos y metodología

El **objetivo general** de esta tesis es el desarrollo de composites poliméricos multifuncionales que presente nuevas propiedades tales como la radiopacidad, la conductividad eléctrica o la bioactividad para su uso en ingeniería tisular o/y regeneración de tejidos tales como, materiales de **liberación de fármacos** detectables por rayos-X, **catéteres urinarios** de biodegradación rápida posicionables mediante asistencia de rayos-X, *scaffolds* bioactivos para **regeneración ósea** o para **regeneración de nervios**.

Para este propósito se han realizado estudios de composites de poli(ϵ -caprolactona) (PCL) y el terpolímeros poli(D,L-L-lactida-co- ϵ -caprolactona) (PDLCL) reforzados con micro- y nano-refuerzos tales como el sulfato de bario (BaSO_4), nanotubos de carbono de pared múltiple (MWCNT) y nanotubos de carbono funcionalizados con poli(dopamina) o polivinilpirrolidona (PDA o PVP). El **objetivo principal** de este trabajo es conseguir mediante los refuerzos, materiales no solo con propiedades mejoradas, si no que tengan nuevas propiedades útiles para la biomedicina como son la radiopacidad, la bioactividad o la conductividad eléctrica.

Para poder alcanzar el objetivo principal, el trabajo se ha dividido en alcanzar **cuatro objetivos parciales**. Cada uno de estos objetivos queda recogido en un capítulo de esta tesis.

- **CAPITULO 1** - Estudiar los composites de PCL y BaSO_4 : Determinar el porcentaje necesario de refuerzo para obtener la radiopacidad equivalente a la de un material metálico. Estudiar los efectos del refuerzo en las propiedades mecánicas y posibles cambios en la estructura cristalina del polímero.
- **CAPITULO 2** - Estudiar los composites de PDLCL y BaSO_4 : Determinar el porcentaje necesario de refuerzo para obtener la radiopacidad equivalente a la de un material metálico. Estudiar el efecto en las propiedades mecánicas y posibles cambios en la estructura del polímero. Analizar mediante un estudio de degradación *in vitro* simulando condiciones del cuerpo humano ($T \approx 37^\circ\text{C}$ y $\text{pH} \approx 7.4$) el efecto de las partículas en la cinética de degradación del polímero, la evolución de las propiedades mecánicas con los días de degradación hidrolítica y el mantenimiento de la capacidad radiopaca.

- **CAPITULO 3** - Determinar el espesor de funcionalización de PDA en composites MWCNT para reforzar PCL que de mejores propiedades mecánicas. Estudiar el efecto de la funcionalización en la estructura cristalina del polímero. Analizar el efecto de la funcionalización en las propiedades mecánicas y la interfase matriz/refuerzo mediante técnicas dinámico mecánicas. Investigar el posible efecto de bioactividad en *scaffolds* de PCL con MWCNT recubiertos de PDA mediante ensayos in vitro en fluidos que simulen el cuerpo humano (*simulated body fluid* o SBF).
- **CAPITULO 4** – Estudios de comportamiento a fatiga del PCL y PCL reforzado con MWCNT:
 - **Capítulo 4.1** – Estudiar el comportamiento a fatiga de films de PCL simulando condiciones del cuerpo humano (medio líquido y $T \approx 37\text{ }^{\circ}\text{C}$). Obtener las curvas S-N para el diseño de componentes en ingeniería biomédica de PCL. Entender los factores que afectan a la vida a fatiga como la viscoelasticidad, la mecánica de la fractura y la temperatura. Analizar la pérdida de rigidez del PCL durante la vida a fatiga para poder ajustar el diseño de componentes biomédicos.
 - **Capítulo 4.2** – Estudiar la mejora de vida a fatiga al reforzar con MWCNT films de PCL simulando condiciones del cuerpo humano (medio líquido y $T \approx 37\text{ }^{\circ}\text{C}$) a altas tensiones (9 MPa). Evaluar el efecto de la funcionalización de PVP en los MWCNT en la vida a fatiga. Determinar los mecanismos principales que influyen en el cambio de vida a fatiga del material.

Chapter 1: Crystallization behavior and mechanical properties of poly (ϵ -caprolactone) reinforced with barium sulphate sub-micron particles.

Summary

Poly(ϵ -caprolactone) (PCL) was mixed with sub-micron particles of barium sulphate to obtain biodegradable radiopaque composites. X-ray images comparing with aluminum samples show that with 15 wt.% of barium sulphate (BaSO_4) is sufficient to present radiopacity. Thermal studies by Differential Scanning Calorimetry (DSC) show a statistically significant growth in PCL degree of crystallinity from 46% to 52% for 25 wt.% of BaSO_4 . Non-isothermal crystallization tests were performed at different cooling rates to evaluate crystallization kinetics. The study reveals the nucleation effect of BaSO_4 changing also the morphology and quantity of the primary crystals of PCL also corroborated by Polarized Light Optical Microscopy (PLOM). These results fitted well with Avrami-Ozawa- Jeziorny model and show a secondary crystallization which contributes to an increase of crystal fraction with internal structure reorganization. The addition of barium sulphate particles in composite formulations with PCL improves stiffness but not strength for all compositions due to possible cavitation effects induced by debonding of reinforcement interphase.

Introduction

In past recent years there has been an increasing interest in biodegradable polymers for biomedical applications as temporary surgical implants and templates for tissue engineering. Polyesters based on polylactides and polylactones present tremendous interest in this field because of their biocompatibility and tunable mechanical properties and biodegradability¹⁻⁶. Among these polymers, poly(ϵ -caprolactone) (PCL) stands out, widely used in tissue engineering and drug delivery platforms⁷⁻¹².

Despite its success as implantable material, in comparison to metals its low radiopacity makes it difficult to detect by X-ray imaging techniques. Hence to overcome this difficulty the use of composites with high radiopaque fillers is being investigated. Barium sulphate (BaSO_4)¹³⁻¹⁵, ferrous oxide (Fe_3O_4)¹⁶ and bismuth oxide (Bi_2O_3)¹⁷⁻¹⁸ have been previously reported as radiopaque composite fillers, being BaSO_4 the most commonly used in medical applications currently. Barium sulphate (BaSO_4) is a standard in medical

applications, approved by the FDA, and used for X-ray assisted implantation to control the position of polymer implants and drug delivery systems during biodegradation^{9,19,20}.

The incorporation of BaSO₄ has been reported to be an alternative to improve the toughness of, for example, polylactides²¹⁻²². However, its use also might affect negatively other mechanical properties depending on the particle content. For instance, barium sulphate as an inorganic reinforcement has been already reported to be used with various polymer matrices such as polyethylene, polypropylene and poly (lactic acid); reporting that mechanical performance is reduced at large filler contents²³⁻²⁶. The fail in mechanical properties is often explained in term of poor compatibility of the matrix/reinforcement interface²⁷. In the particular case of PCL a number of authors have demonstrated the poor compatibility with other fillers²⁸⁻³⁰. These two facts, the relative content of the particle and the matrix/reinforcement interface, play an important role for the correct use of PCL based devices. On the one hand, to obtain sufficient radiopacity weight percentages of about 25% are necessary for commonly used BaSO₄ particles in medical applications. On the other hand, the particle content which ensure sufficient radiopacity must preserve or improve the mechanical properties of the base material. Therefore, an equilibrium must be found between these two variables.

Moreover, incorporating inorganic particles in a crystallizable polymer matrix affects the crystallization kinetics, crystal morphology and final degree of crystallinity of the base polymer^{22,31}. Therefore, in this work a complete study of crystallization of PCL in presence of BaSO₄ particles is presented. PCL at human body conditions (≈ 37 °C) is above its glass transition temperature ($T_g \approx -60$ °C). At these conditions mechanical properties of PCL are soft and strongly related to degree of crystallinity. In fact, previous researches show important effect of fillers on polymer crystallinity depending the composition, content, size and morphology of the reinforcement^{29,30,32}.

There is a growing evidence in literature that recognizes the importance of the development of biodegradable radiopaque polymeric systems for being used as medical devices. Studies over the past two decades have provided important information on physical-mechanical properties of PCL. However, to date the relationship between crystallization behavior-mechanical properties-radiopacity when added BaSO₄ particles has not yet been extensively studied. The aim of this research work has therefore been to

study the role of BaSO₄ in the crystallization behavior, mechanical properties in term of the particle/matrix interface and radiopacity stabilising the minimum BaSO₄ content needed to preserve the mechanical performance.

Materials and methods

Poly(ϵ -caprolactone) (PCL) CAPA6500, with weight average molecular weight (M_w) of 147.6 KDa and a dispersity index (D) of 1.49 was provided by Solvay (Perstorp). Barium sulfate (BaSO₄) was provided by Fluka Analytical (Sigma Aldrich). Particle size was determined by Dynamic Light Scattering (DLS) on a Zetasizer ZS90 ZEN3690 (Malvern Instrument) showing an average diameter of 577 ± 125 nm.

Sample preparation

PCL with BaSO₄ composites were prepared by melt mixing in a conical twin-screw mixer MC5 (Xplore) at 150 °C and 150 rpm for 30 min. Compositions with 5wt.%, 15wt.%, 25wt.% and 35 wt.% BaSO₄ were prepared (see Name-code in Table 1). Sheets of 1mm thickness of neat PCL and composites were prepared from pellets by compression molding in a hot press Dr. Collin P200E (Germany), at 150 °C and 25 MPa.

The amount of barium sulphate present in samples after processing was measured by Thermogravimetric Analysis (TGA) in a TGA model Q50 (TA instruments). Samples of 10-15 mg were heated from room temperature to 500 °C at a rate of 10 °C min⁻¹ under a nitrogen atmosphere. Three different samples (n=3) were used to determine the content of BaSO₄ in the samples. A slide difference was found between the actual and real content of the particle (see Table 1-1).

Table 1-1. Name-Code of composite samples showing real barium sulphate content after processing calculated by TGA analysis.

Sample (Name- Code)	BaSO ₄ content (wt.%)	Real BaSO ₄ content (wt.%)
PCL	0	0
PCL_05BaSO ₄	5	8.4
PCL_15BaSO ₄	15	14.2
PCL_25BaSO ₄	25	25.0
PCL_35BaSO ₄	35	32.5

Non-Isothermal crystallization kinetics

Before the non-isothermal crystallization treatments the thermal history of the samples was erased by increasing the temperature to 100 °C and then non-isothermal crystallization treatments were carried out from melt by cooling the samples at cooling rates of 1 °C min⁻¹, 5 °C min⁻¹ and 10 °C min⁻¹. Thermal properties of the samples were measured in a subsequent Differential Scanning Calorimeter (DSC) run by heating from -85 °C to 100 °C at a rate of 20 °C min⁻¹ on a nitrogen atmosphere. The DSC employed was a Q80 Differential Scanning Calorimeter (DSC) (TA instruments) calibrated with pure indium and sapphires. In all cases, three different samples (n=3) weighting 7 ± 1 mg were used. Cooling cycles were monitored. The melting temperature was determined (T_m) from the endothermic peak position and the melt enthalpy (ΔH_m) was obtained calculating the area under the melting peak.

Crystal morphology

Spherulitic morphology of samples was observed with a Polarized Light Optical Microscope (PLOM) LEICA DM LM (LEICA). Samples were dissolved in dichloromethane to obtain films by solvent casting on a microscope glass slide. Non-isothermal crystallization treatments were conducted by a heat controlling Mettler FP90 hot stage (Mettler Toledo) at the conditions described previously.

Mechanical testing

Tensile testing was conducted in an Instron 5565 universal testing machine according to ISO 37-2 standard. Samples of 4 mm width were cut from the molded sheets and at least five samples (n=5) were employed for mechanical properties measurements. Testing was performed at a crosshead speed of 10 mm min⁻¹. Young's modulus (E) with a linear fitting at initial 2% of strain, yield strength (σ_y), stress at break (σ_b) and strain at break (ε_b) were determined.

X-ray Images

Radiographs of samples were taken using an X-radiographic standard clinical machine. As a reference 1mm aluminum plate was employed. All the samples including the reference and neat PCL were tested using the same intensity for comparative purposes.

Results

Crystallization behavior and crystal morphology

The incorporation of barium sulphate (BaSO_4) decrease the melting temperature and increase the degree of crystallinity of poly(ϵ -caprolactone) (PCL) as revealed by Diferential Scanning Calorimetry (DSC) (see **Figure 1-1** and Table 1-2). The melting temperature monotonously decrease from 67 °C for neat PCL to 63.4 °C when incorporating 35 wt.% of BaSO_4 suggesting smaller and less perfect crystalline structures. The degree of crystallinity (X_c) of PCL and its composites was calculated according to equation 1 where ΔH_m is the melting enthalpy, ΔH_m° is the melting enthalpy of 100 % crystalline PCL taken as 139 J g^{-1} ³³ and X_{BaSO_4} the real barium sulphate fraction in samples obtained by Thermogravimetric Analysis (TGA) (see Table 1).

$$X_c(\%) = \frac{\Delta H_m}{\Delta H_m^\circ} * \left(\frac{1}{1 - X_{\text{BaSO}_4}} \right) \quad (1)$$

The degree of crystallinity increases from 46% to 52% which is statistically significant for compositions of 25 wt.% and 35 wt.% ($p=0.03$ and $p=0.007$).

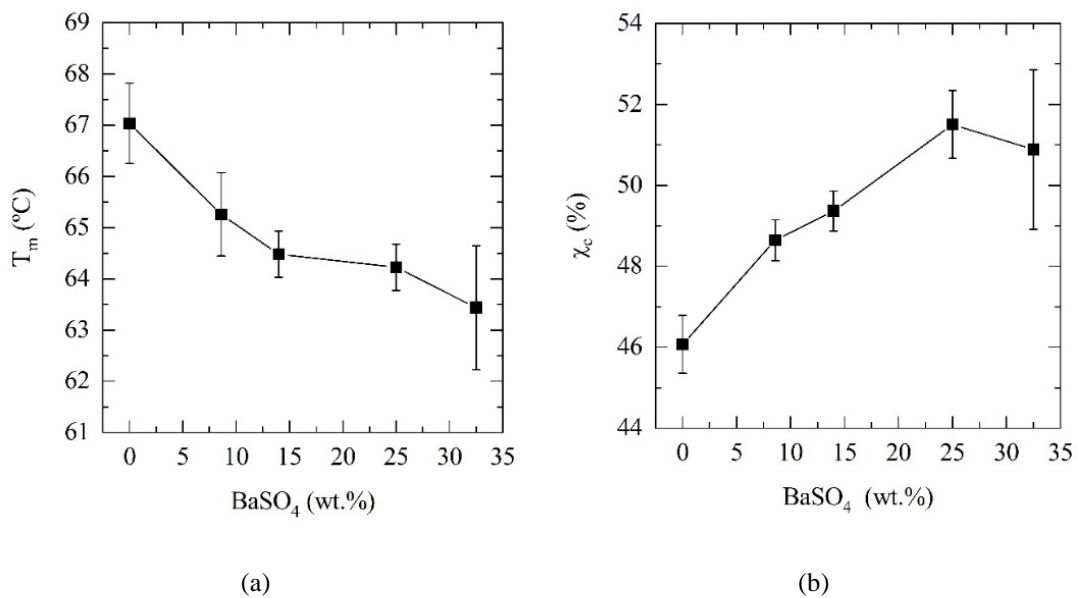


Figure 1-1. (a) Melting temperature and (b) Degree of crystallinity of neat PCL and its barium sulphate (BaSO_4) composites.

Table 1-2. Thermal properties and degree of crystallinity of poly(ϵ -caprolactone) (PCL) and its BaSO₄ composites. T_m: Melting temperature, ΔH_m : Melting enthalpy, X_c: Degree of crystallinity

Sample (Name-Code)	BaSO ₄ content (wt. %)	T _m (°C)	ΔH_m (J/g)	X _c (%)
PCL	0	67.0 ± 0.8	70.5 ± 1.1	46
PCL_05BaSO ₄	8.4	65.3 ± 0.8	68.2 ± 0.7	49
PCL_15BaSO ₄	14.2	64.5 ± 0.5	64.8 ± 0.6	49
PCL_25BaSO ₄	25.0	64.2 ± 0.5	59.1 ± 1.0	52
PCL_35BaSO ₄	32.5	63.4 ± 1.2	52.6 ± 2.0	51

PCL and its BaSO₄ composites were subjected to non-isothermal crystallization treatments *in-situ* in a Polarized Light Optical Microscopy (PLOM). The resultant crystal morphology after samples being cooled from melt at cooling rates of 1 °C min⁻¹, 5 °C min⁻¹ and 10 °C min⁻¹ were studied and compared. As expected, smaller spherulites are observed in samples cooled at higher cooling rates than for their counterparts due to molecules having less time for diffusion. In Figure 1-2 images taken at cooling rates of 1 °C min⁻¹ and 10 °C min⁻¹ are compared for neat PCL and PCL containing 5 wt.% and 35 wt.% of BaSO₄. Regardless the cooling rate, no significant differences were found in crystal size between composites having low particle content, 5 wt.%, and neat PCL. However, the incorporation of higher particle contents, 35 wt.%, does have influence in crystal size. For example, PCL shows a spherulitic structure with average size of 100 μm and clear grain boundaries when cooled at 1 °C min⁻¹; whereas the composite having 35 wt.% BaSO₄ shows an average size of 5 μm. When comparing the crystal morphology of PCL at different cooling rates, the result reveals highly distorted and more planar spherulitic structure at higher cooling rates. However, when BaSO₄ particles are incorporated this spherulitic morphology, though distorted as in neat PCL, is become rounder.

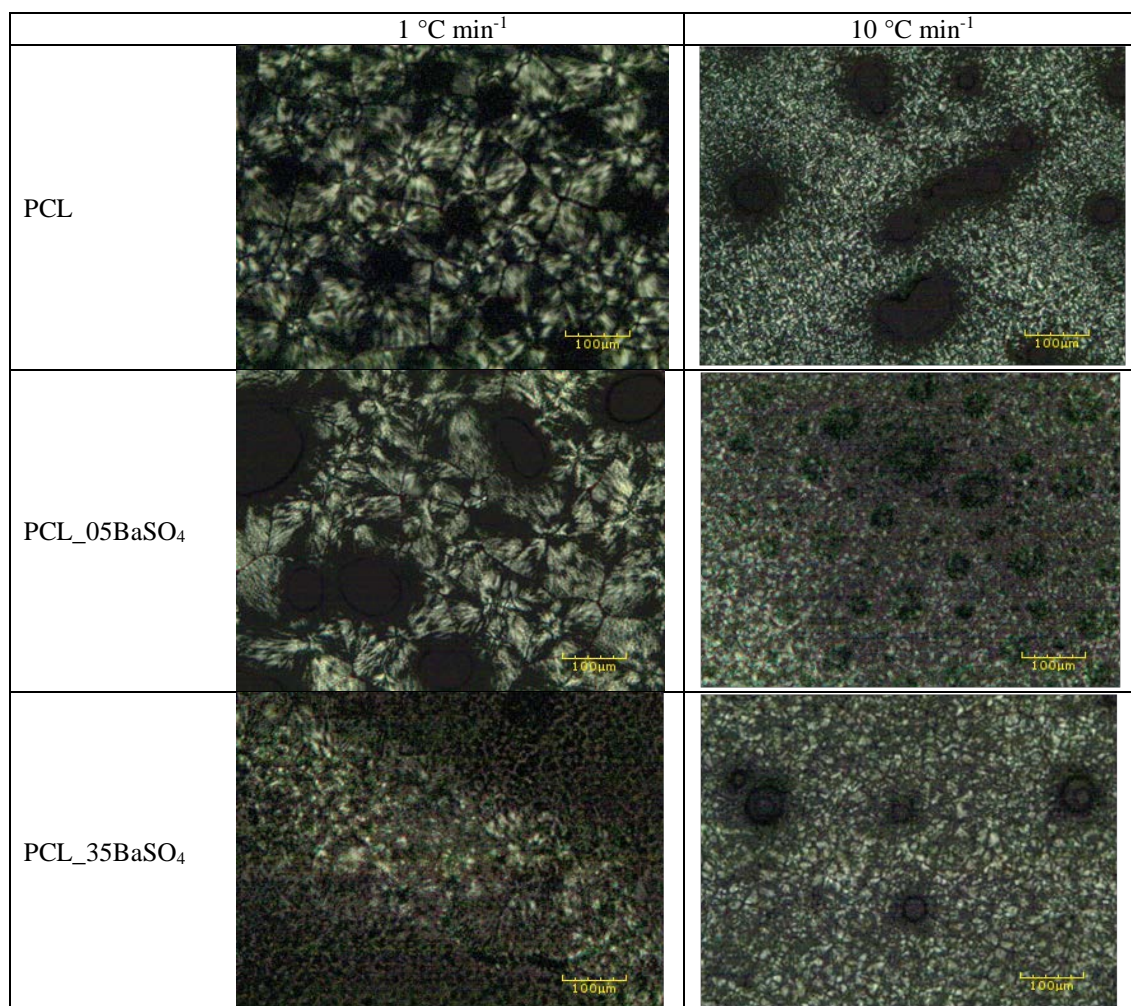


Figure 1-2. Crystal morphology for neat PCL and its composites having 5 and 35 wt.% of BaSO₄ after non-isothermal crystallization at cooling rates of (left column) 1 °C min⁻¹ and (right column) 10 °C min⁻¹. Black holes in micrographs correspond to air bubbles formed during *in-situ* crystallization treatments.

Non-isothermal crystallization and kinetics analysis

To analyze in more detail the non-isothermal crystallization, cooling curves from DSC were analyzed for PCL and its BaSO₄ composite cooled at cooling rates of 1 °C min⁻¹, 5 °C min⁻¹, 10 °C min⁻¹ (see Figure 1-3). A crystallization peak is observed between 30-40 °C for all compositions, yet in composites, this is observed some degrees at higher temperature suggesting a heterogeneous nucleation induced by BaSO₄ particles. At higher cooling rates the crystallization peaks translate to lower temperatures for neat PCL and composite samples (see Table 1-3).

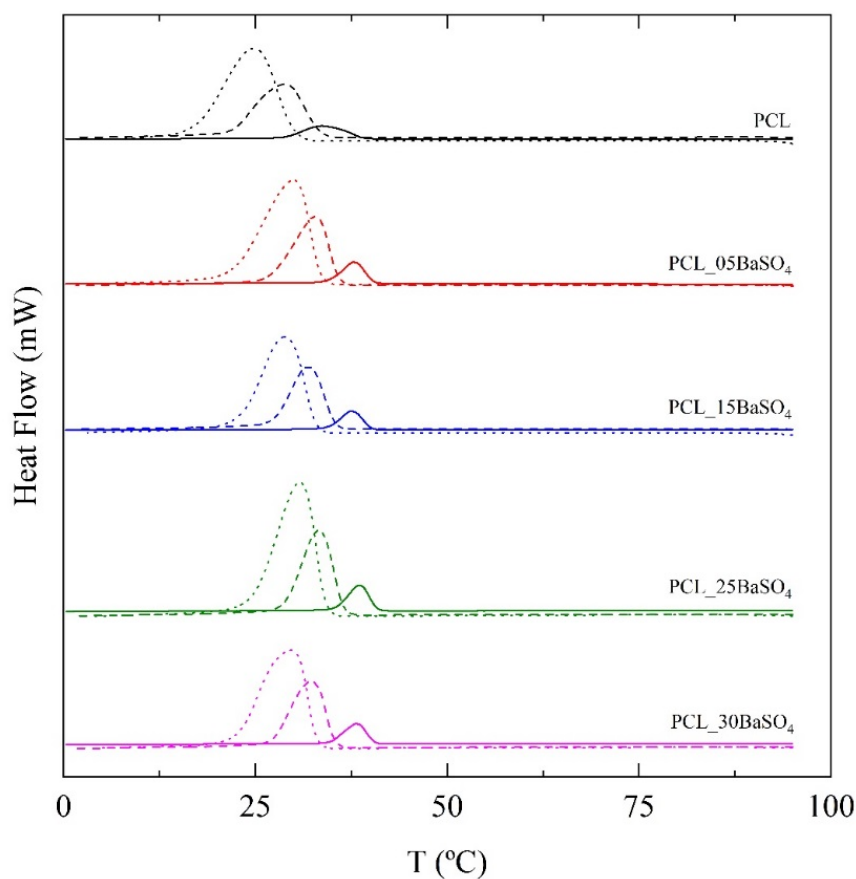


Figure 1-3. Cooling curves obtained by Differential Scanning Calorimetry (DSC) for neat PCL and its BaSO₄ composites at different cooling rates. (solid line) 1 °C min⁻¹ (dash line) 5 °C min⁻¹ (dot line) 10 °C min⁻¹.

Table 1-3. Crystallization temperature and crystallization enthalpy of PCL and its BaSO₄ composites at different cooling rates.

Sample (Name-Code)	Cooling rate (°C min ⁻¹)	T _c (°C)	ΔH _c (J g ⁻¹)
PCL	1	33.7	62.3
	5	28.7	57.7
	10	24.8	54.1
PCL_05BaSO ₄	1	37.8	67.9
	5	32.8	62.6
	10	29.9	59.6
PCL_15BaSO ₄	1	37.5	68.1
	5	31.8	63.0
	10	28.8	60.4
PCL_25BaSO ₄	1	38.5	71.2
	5	33.2	66.5
	10	30.7	63.7
PCL_35BaSO ₄	1	38.1	70.7
	5	32.2	65.9
	10	29.6	63.0

Moreover, the crystallization degree during cooling increases with BaSO₄ content as deduced from the increase of the crystallization enthalpy (see Figure 1-4). Therefore, the presence of the inorganic particles in PCL not only provides nucleation sites and accelerate crystallization kinetics but lead to higher degree of crystallinity. Furthermore, lower cooling rates favor both nucleation and the final degree of crystallinity in neat PCL and its composites, respectively. The crystallization peak temperatures and crystallization enthalpy for each composition at the selected different cooling rates are summarized in Table 1-3.

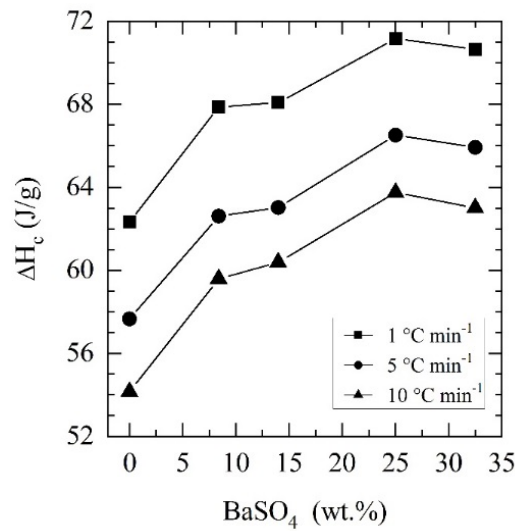


Figure 1-4. The increase of crystallization enthalpies of PCL and its BaSO₄ composites obtained at (■) 1 °C min⁻¹ (●) 5 °C min⁻¹ (▲) 10 °C min⁻¹ cooling rates from melt.

The evolution of the degree of crystallinity with time is shown in Figure 1-5 for the different cooling rates. Crystallization kinetics was studied analyzing degree of crystallinity in function of temperature according to equation 2 where T_0 and T_∞ are initial and final temperatures of the crystallization process, dH_c is the crystallization enthalpy at temperature difference dT and at temperature T . The crystallization time during the process was assessed according to equation 3 where T_c is the crystallization temperature at crystallization time t and Φ is the cooling rate.

$$X(T) = \int_{T_0}^T \left(\frac{dH_c}{dT} \right) dT / \int_{T_0}^{T_\infty} \left(\frac{dH_c}{dT} \right) dT \quad (2)$$

$$t = (Tc - T)/\Phi \quad (3)$$

In accordance with DSC results, the evolution of the degree of crystallinity over time indicates the nucleating effect of BaSO₄ particles advancing the onset of crystallization in regard to PCL. Moreover, the results revealed that crystallization might be accelerated by the presence of BaSO₄. This fact is assessed by employing crystallization models.

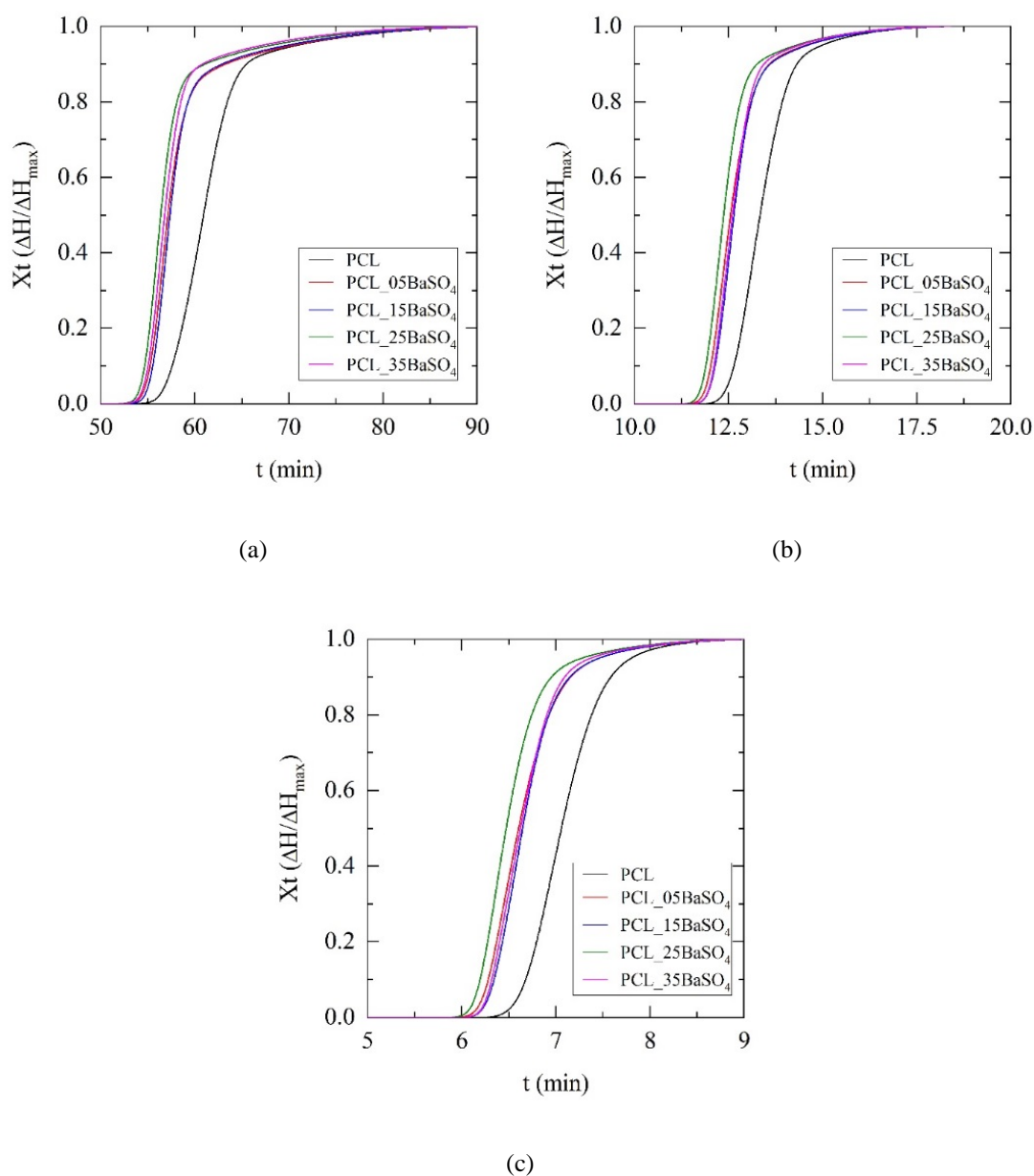


Figure 1-5. Degree of crystallinity versus time of PCL and its BaSO₄ composites at different cooling rates. (a) 1 °C min⁻¹ (b) 5 °C min⁻¹ (c) 10 °C min⁻¹.

For crystallization kinetic analysis Avrami-Ozawa-Jeziorny (A-O-J) model was employed. Polymer crystallization kinetics can be described by Avrami's model for phase changes at isothermal conditions³⁴ by equation 4 where $1-X_t$ is the non-crystallized volume fraction, "n" is a parameter which defines the type of crystal growth and Z_t is a combined factor of nucleation rate and crystal growth rate. At non-isothermal conditions Ozawa model³⁵ could be employed by following equation 5. Note that both equations are quite similar, however the Z_t and "n" parameters do not have the same physical meaning because the temperature varies constantly in non-isothermal crystallization. For our study Ozawa model could not be employed as some bibliographic results show that this model does not fit satisfactorily the PCL crystallization process^{36,37}. Therefore, the change on Z_t proposed by Jeziorny³⁸ was applied for Avrami's model being used at non-isothermal conditions. Equation 6 describes the change proposed by Jeziorny in order to unify the Avrami's and Ozawa's models for non-isothermal conditions. In this equation Φ is the cooling rate and Z_c a factor obtained from non-isothermal conditions with equivalent meaning of Z_t in Avrami models. In order to obtain "n" and Z_c factors, a linear fitting must be applied for $\log(-\ln(1-X_t))$ versus $\log(t)$ curves.

$$1 - X_t = e^{-Z_t \cdot t^n} \quad (4)$$

$$1 - X_t = e^{-Z_t \cdot \Phi^n} \quad (5)$$

$$\log(Z_c) = \frac{\log(Z_t)}{\Phi} \quad (6)$$

Figure 1-6 shows the double logarithmic curves of PCL and its composites fitting the crystallization model proposed. The experimental data do not fit in simple linear manner and show in all cases a more complex crystallization behavior. This finding is consistent with reported bibliographic results for PCL suggesting the existence of a secondary crystallization process^{36,37,39}. This secondary crystallization is common in other polymers with similar thermal properties like HDPE, when the working conditions are high above the glass transition temperature⁴⁰. Therefore, in this work a double linear behavior was considered for data fitting obtaining positive results ($r \geq 0.9$).

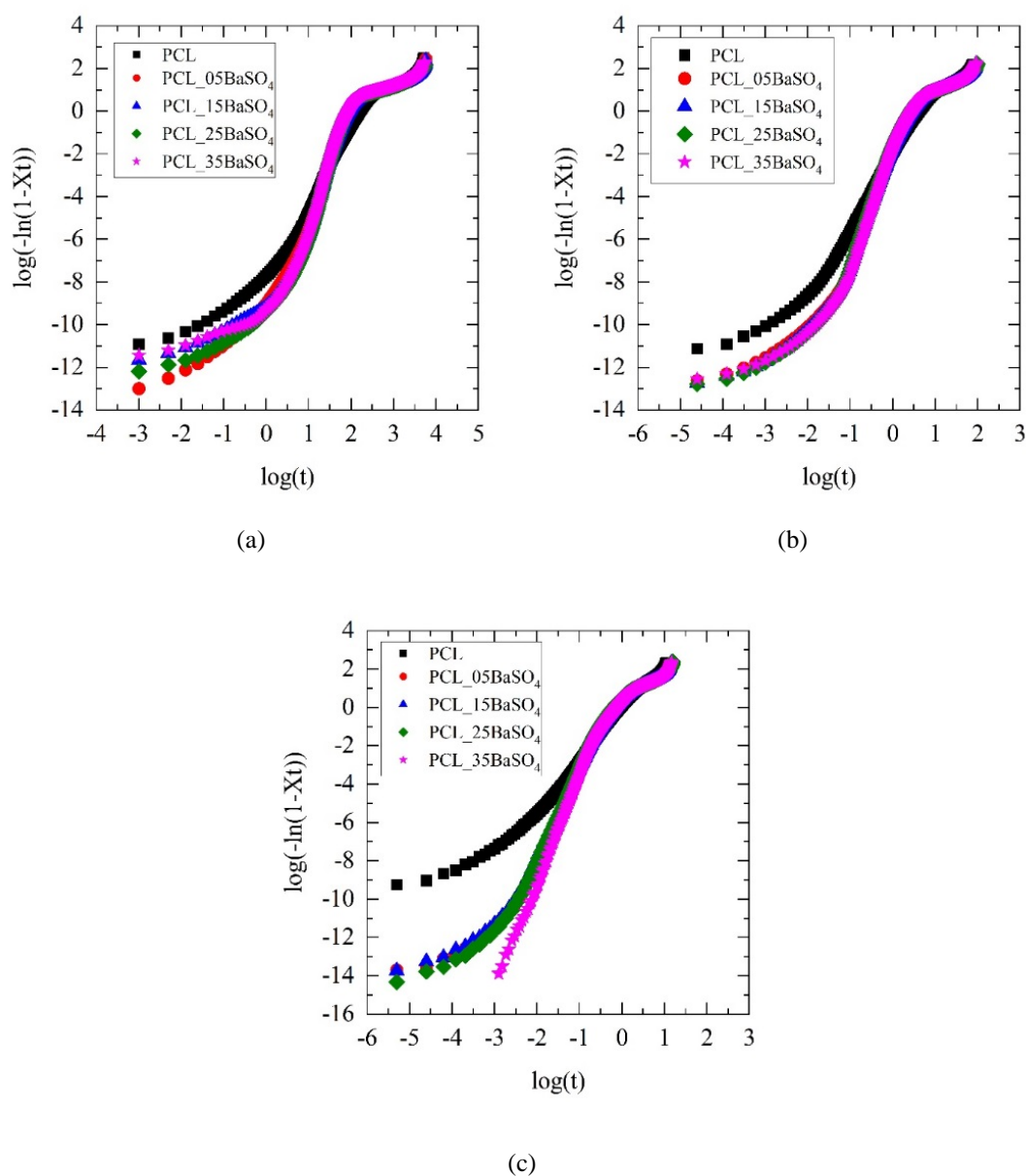


Figure 1-6. $\log(-\ln(1-X_t))$ versus $\log(t)$ of PCL and its BaSO_4 composites at different cooling rates to adjust the Avrami-Ozawa-Jeziorny model. (a) $1\text{ }^\circ\text{C min}^{-1}$ (b) $5\text{ }^\circ\text{C min}^{-1}$ (c) $10\text{ }^\circ\text{C min}^{-1}$.

Figure 1-7 shows an example of the simple and double linear model adjustment of crystallization kinetics of PCL and its BaSO_4 composites. The value of the double fitting model parameters (n_i and Z_{ci}) are summarized in Table 1-4.

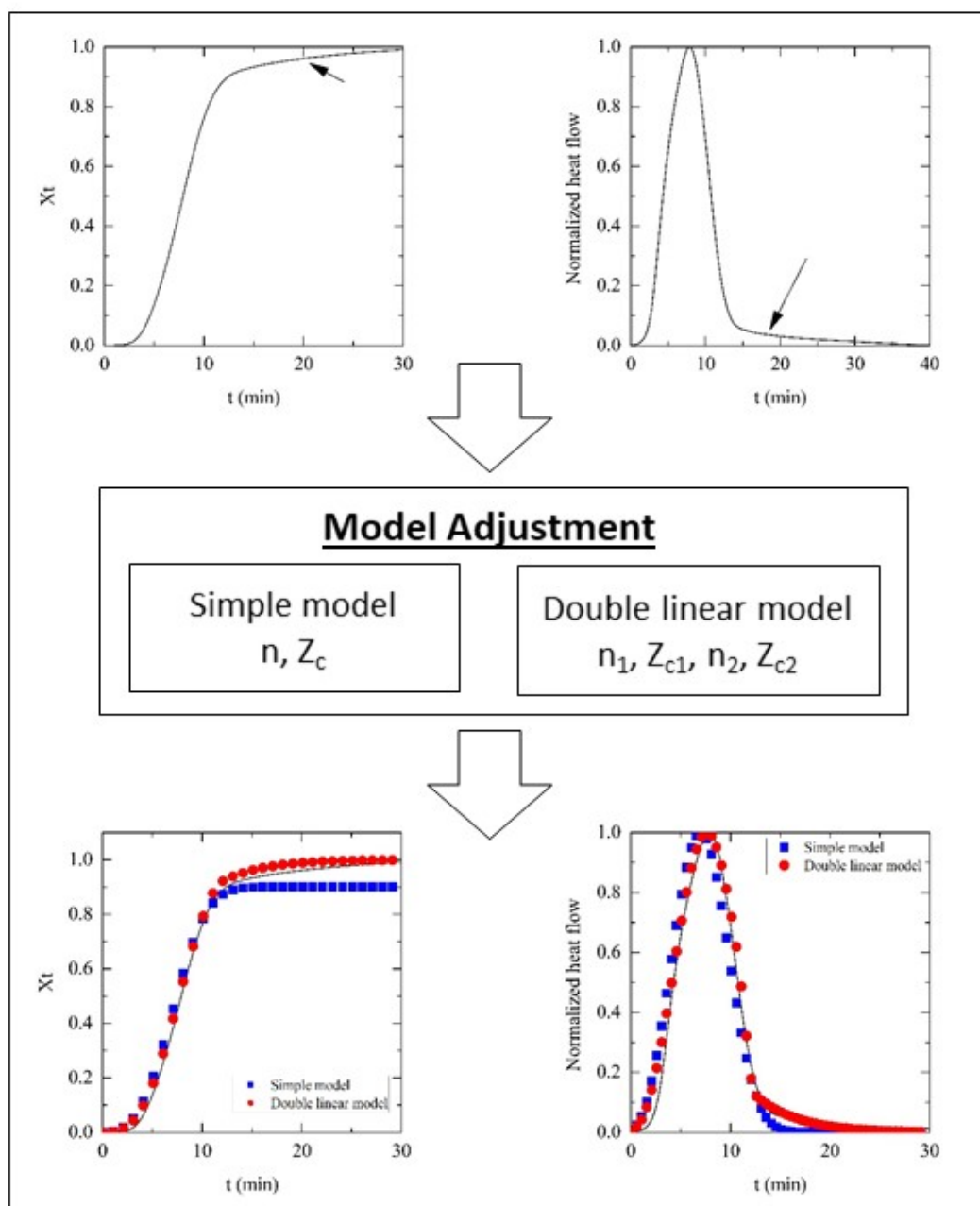


Figure 1-7. Example of simple (blue) and double linear (red) fitting model of experimental results of crystallization kinetics for PCL and its composites. Black arrows indicate the double-fitting area corresponding to the secondary crystallization. Data shown correspond to neat PCL at $1\text{ }^{\circ}\text{C min}^{-1}$ cooling rate

For the first linear fitting, n_1 is always higher for composite samples and is close to the theoretical factor of four corresponding to a three dimensional crystallization according to the model. In contrast, neat PCL presents a factor closer to 3 and slightly decreases

when cooling rate is increased. The value in composite samples do not change with cooling rate and is independent for BaSO₄ quantity. For the same sample, Z_{c1} rises abruptly with cooling rate due to the usual effect of nucleation enhancing by fast cooling. The increase in particle content shows an incremental effect in this factor at high cooling rates, 10 °C min⁻¹, whereas for low cooling rates, 1 °C min⁻¹, all samples have similar behavior.

Table 1-4. The parameters of the double linear Avrami-Ozama-Jeziorny model for PCL and its BaSO₄ composites at different cooling rates.

Sample (Name-Code)	Φ (°C min ⁻¹)	$Z_{c1} * 10^6$	n_1	r_1	$Z_{c2} * 10^6$	n_2	r_2
PCL	1	393	3.06	0.96	112010	1.12	0.90
	5	26661	3.00	0.97	134567	1.24	0.96
	10	93981	2.46	0.97	138174	1.65	0.98
PCL_05BaSO ₄	1	311	3.76	0.94	156060	1.01	0.91
	5	22345	3.68	0.94	157177	1.08	0.95
	10	130814	3.69	0.97	149402	1.33	0.96
PCL_15BaSO ₄	1	353	3.68	0.91	171962	0.98	0.92
	5	24246	3.73	0.95	159310	1.09	0.94
	10	145824	3.65	0.97	161103	1.30	0.95
PCL_25BaSO ₄	1	266	3.86	0.91	173790	0.99	0.90
	5	25408	3.79	0.95	169341	1.05	0.94
	10	169961	3.81	0.97	170617	1.22	0.93
PCL_35BaSO ₄	1	339	3.70	0.91	136477	1.08	0.89
	5	21298	3.72	0.95	144059	1.17	0.94
	10	229399	3.92	0.97	147983	1.39	0.92

The kinetics study according to this model shows that nucleation of PCL crystals is led by the presence of BaSO₄ particles in a primary crystallization process to form spherulitic morphology. In fact, PLOM images showed that for low cooling rates nucleation and growth of crystals in PCL was favored. The presence of BaSO₄ leads to heterogeneous nucleation points at the interfaces starting the crystallization process earlier than in neat PCL with an increase in degree of crystallinity observed also in previous results. When cooling rate is increased, however, the nucleating effect becomes more relevant since the effect of particles on crystallization of PCL is enhanced.

Secondary crystallization is also important; up to a 40% of total crystallization has been attributed for it⁴¹. Three reasons might be proposed to explain it: (1) New lamellae are formed in amorphous phase; (2) lamellae become thicker; or (3) new lamellae grow at particle interfaces. This secondary crystallization just after primary crystallization (pointed with a black arrow in Figure 1-7) is observable in the DSC normalized cooling

curves (Figure 1-3) and crystallinity versus time plots (Figure 1-5). An inclination which can be attributed to secondary crystallization can be observed. Irrespective to BaSO₄ content, the value of n_2 factor is low between 1 and 2, suggesting a process more related to molecular reorganization than crystal growth. For the same sample, this factor increases with cooling rate; leading to a distorted spherulitic crystals in accordance with the results obtained from PLOM.

Mechanical properties

The stiffness of PCL is significantly increased with the barium sulphate content in composites, with values of Young's modulus ranging from 308 MPa for non-reinforced PCL to 397 MPa for its 35 wt.% BaSO₄ composite counterpart. This effect in modulus is statistically significant starting from 15 wt.% composite ($p=0.018$) (see Figure 1-8c and Table 1-5).

The yield strength remains constant irrespective of the presence of BaSO₄ content, until 35 wt.% BaSO₄ for which a decrease is found ($p=0.03$) (see Figure 1-8). Focusing on the shape of plasticization peak curves at yield point, one can observe that the region becomes narrower and appears at lower strains as the BaSO₄ content increases in composites (see Figure 1-8b). Moreover, yield plateau stress after plasticization peak decrease to lower stress levels being significant for composition up to 15% ($p=0.04$) (see Figure 1-8e). This drop in stress after peak is an indicative of cavitation induced by debonding of matrix-reinforcement interphase and thus it might be conclude that filler content has a negative effect.

Regarding ductility, some decrease of elongation at break is observed at higher amounts of reinforcement in composites in regard to neat PCL. However, it is noticeable that all samples regardless de BaSO₄ amount remain ductile with values of elongation at break higher than 557% (see Table 1-5 and Figure 1-8f). This result is statistically significant for 5wt.% ($p=0.01$) and the decrease tendency for high content is notable ($p=0.065$ for 35wt.% of BaSO₄).

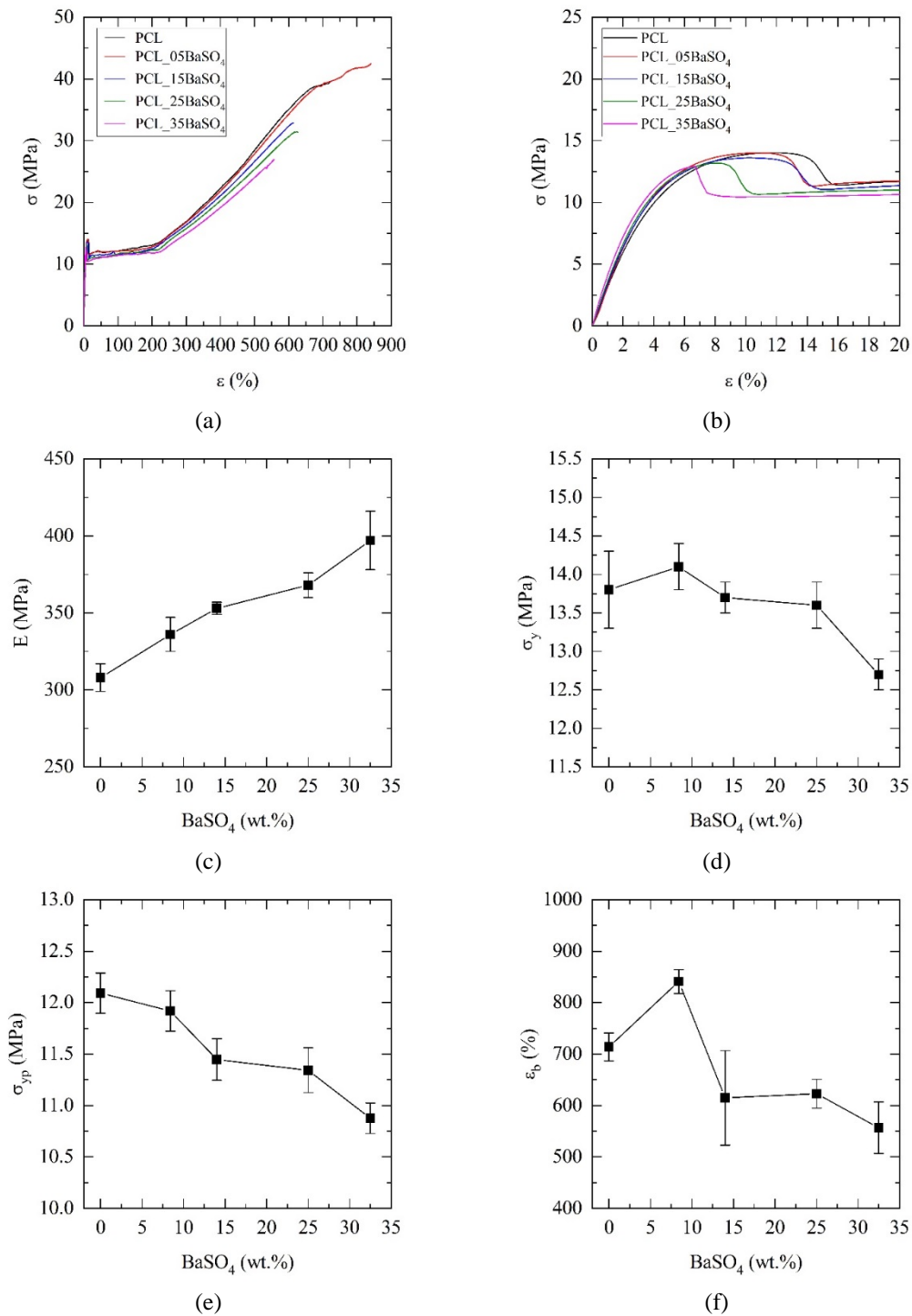


Figure 1-8. Mechanical behavior of PCL and its BaSO₄ composites (a) Stress-Strain curves (b) Zoom of the plastification peak at yield point. Evolution of the mechanical properties (c) Young's modulus (d) Yield Stress (e) Yield Plateau (f) Elongation at break.

Table 1-5. Values of the mechanical properties measured by tensile test for neat PCL and its BaSO₄ composites. Young modulus (E), Yield stress and yield strain (σ_y , ϵ_y), yield plateau stress (σ_{yp}) and elongation at break (ϵ_b)

Sample (Name-Code)	E* (MPa)	σ_y (MPa)	ϵ_y (%)	σ_{yp} (MPa)	ϵ_b (%)
PCL	308 ± 9	13.8 ± 0.5	10.2 ± 1.5	12.1 ± 0.2	714 ± 27
PCL_05BaSO ₄	336 ± 11	14.1 ± 0.3	10.9 ± 0.8	11.9 ± 0.2	841 ± 23
PCL_15BaSO ₄	353 ± 4	13.7 ± 0.2	9.9 ± 0.3	11.4 ± 0.2	615 ± 92
PCL_25BaSO ₄	368 ± 8	13.6 ± 0.3	8.8 ± 0.7	11.3 ± 0.2	623 ± 28
PCL_35BaSO ₄	397 ± 19	12.7 ± 0.2	6.5 ± 0.3	10.1 ± 0.1	557 ± 50

* E is defined by linear fitting at first 2% of strain

The results demonstrate that the BaSO₄ particles in PCL are acting in the linear strain zone at low strains of the tensile stress-strain curve (see Figure 1-8a) as a usual stiff reinforcement for polymers. The increase in modulus in PCL with inorganic reinforcements is quite common^{28,30,36,42}. The effect of the matrix/particle interfaces become relevant and affect the mechanical properties at higher strain values of the stress-strain curves. If the interface adhesion is poor²⁹ it is not expected an increase in yield strength; debonding at the interfaces would prevent the reinforcing effect at the strain value at which appears the yield point. Interface debonding and cavitation explains the behavior of the yield region in which the strain is observed to appear at lower strain values and yield stress hence drops for high amounts of BaSO₄. Previous works provided for PCL composites are consistent with this behavior, evidencing a decrease in yield stress even when compatibilizing agents for the interface were used to improve the adhesion level²⁸. Barium sulphate as reinforcement with PCL behaves in a similar manner as calcium sulphates showing increments at medium reinforcement amounts and then falling down at >15 wt.%³². The behavior observed here for PCL matrix have also been effects corroborated for BaSO₄ composites with other semicrystalline matrices such as polypropylene (PP) or polyethylene (PE)^{23,43,44}. In this work the falling in yield strength was not observed up to a high amounts (35 wt.%) of BaSO₄ particles. This fact suggests a contributing effect of the crystal nucleation and growth in presence of particles observed also by DSC and PLOM, leading to increased degree of crystallinity in PCL composites that compensates the detrimental effects of cavitation and debonding.

Finally, the impact of BaSO₄ particles in strain capacity of the polymer matrix can be discussed with sub-micron and nano sizes particles having being proved that they provide

an enhancement in toughness in PLA at low particle amounts ($\leq 10\%$ wt.)^{44,45}. However, for higher particle amounts a decrease in toughness is expected since debonding and cavitation occurs leading to a decrease in the strain capacity in composite formulations. Micron sized holes, coalescence and finally cracks developed during stretching of samples lead finally to decreasing values of elongation at break, as it was observed here for PCL/BaSO₄ composites. Therefore, it can be concluded that addition of BaSO₄ particles in quantities from 5 to 25 wt.% is optimal for polymer composites of PCL without a detrimental effect in toughness.

X-ray imaging and radiopacity assessment

Figure 1-9 shows the X-ray images of 1mm thickness films of PCL and its 5 wt.%, 15 wt.%, 25 wt.% and 35 wt.% barium sulphate composites compared to 1mm thickness aluminum film. Barium sulphate particles increase the radiopacity of PCL, as expected. Samples are detectable with 5 wt.% of barium sulphate and have comparable radiopacity of aluminum at particle amounts of 25 wt.%.

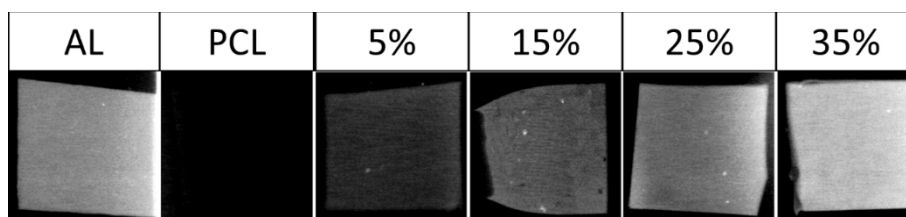


Figure 1-9. X-ray images of Aluminum, PCL and its barium sulphate composites.

Conclusions

The main goal of the current study was to study the relationship between crystallization behavior, mechanical properties and radiopacity of poly(ϵ -caprolactone) (PCL) and its barium sulphate (BaSO₄) composites. In this work we have prepared samples of PCL with different BaSO₄ contents (0, 5, 15, 25 and 35 wt. %) of sub-micron particles with average size of 577 nm.

Thermal studies show a statistically significant grow in PCL degree of crystallinity during cooling from melt in presence of BaSO₄ particles. Non-isothermal crystallization kinetics of PCL in absence and presence of BaSO₄ particles were conducted at 1 °C min⁻¹, 5 °C

min⁻¹ and 10 °C min⁻¹ cooling rates from melt. The study reveals the nucleating effect of BaSO₄ changing the morphology and degree of crystallinity of the primary crystals of PCL, also corroborated by Polarized Light Optical Microscopy (PLOM). The experimental data fitted well to Avrami-Ozawa- Jeziorny model and the corresponding parameters were determined revealing a secondary crystallization, which contributes to an increase of the degree of crystallinity with internal structure reorganization.

The addition of barium sulphate particles in composite formulations with PCL improves stiffness but the other relevant mechanical properties (strength, elongation and toughness) are not optimal. This is attributed to the debonding and cavitation at particle/matrix interfaces in which adhesion plays a pivotal role.

Moreover, X-ray images show that with 15 wt.% of BaSO₄ is sufficient to present radiopacity for devices to be visible for use in medical imaging techniques.

One of the more significant findings to emerge from this study is that PCL presents sufficient radiopacity with tough mechanical properties when mixed with 25 wt.% of BaSO₄ sub-micron particles. These finding would be of broad use to the scientific and biomedical communities as this composite fulfilled the required conditions for monitoring implants and drug delivery devices by X-ray imaging techniques.

References

1. Nair, L. S. & Laurencin, C. T. Biodegradable polymers as biomaterials. *Prog. Polym. Sci.* **32**, 762–798 (2007).
2. Larrañaga, A., Aldazabal, P., Martin, F. J. & Sarasua, J. R. Hydrolytic degradation and bioactivity of lactide and caprolactone based sponge-like scaffolds loaded with bioactive glass particles. *Polym. Degrad. Stab.* **110**, 121–128 (2014).
3. Fernández, J., Auzmendi, O., Amestoy, H., Diez-Torre, A. & Sarasua, J. R. Mechanical properties and fatigue analysis on poly(ε-caprolactone)-polydopamine-coated nanofibers and poly(ε-caprolactone)-carbon nanotube composite scaffolds. *Eur. Polym. J.* **94**, 208–221 (2017).
4. Vert, M., Li, S. M., Spenlehauer, G. & Guerin, P. Bioresorbability and biocompatibility of aliphatic polyesters. *J. Mater. Sci. Mater. Med.* **3**, 432–446 (1992).
5. Albertsson, A. C. & Varma, I. K. Recent developments in ring opening polymerization of lactones for biomedical applications. *Biomacromolecules* **4**, 1466–1486 (2003).
6. Ugartemendia, J. M., Larrañaga, A., Amestoy, H. & Sarasua, J. R. Supramolecular evolution over an initial period of biodegradation of lactide and caprolactone based medical (co)polyesters. *Polym. Degrad. Stab.* **108**, (2014).

7. Sanchez-Rexach, E. *et al.* Novel biodegradable and non-fouling systems for controlled-release based on poly(ϵ -caprolactone)/Quercetin blends and biomimetic bacterial S-layer coatings. *RSC Adv.* **9**, 24154–24163 (2019).
8. Kenawy, E. R., Abdel-Hay, F. I., El-Newehy, M. H. & Wnek, G. E. Processing of polymer nanofibers through electrospinning as drug delivery systems. *Mater. Chem. Phys.* **113**, 296–302 (2009).
9. Venugopal, J., Ma, L. L. & Ramakrishna, S. Biocompatible nanofiber matrices for the engineering of a dermal substitute for skin regeneration. *Tissue Eng.* **11**, 847–854 (2005).
10. Cui, J., Kratz, K. & Lendlein, A. Shape-Memory Properties of Radiopaque Micro-Composites from Amorphous Polyether Urethanes Designed for Medical Application. *MRS Proc.* **1190**, 1190-NN03-22 (2009).
11. Sanchez-Rexach, E., Martínez de Arenaza, I., Sarasua, J. R. & Meaurio, E. Antimicrobial poly(ϵ -caprolactone)/thymol blends: Phase behavior, interactions and drug release kinetics. *Eur. Polym. J.* **83**, 288–299 (2016).
12. Larrañaga, A. & Sarasua, J. R. Effect of bioactive glass particles on the thermal degradation behaviour of medical polyesters. *Polym. Degrad. Stab.* **98**, 751–758 (2013).
13. Lämsä, T. *et al.* Biocompatibility of a new bioabsorbable radiopaque stent material (BaSO₄ containing poly-L,D-lactide) in the rat pancreas. *Pancreatology* **6**, 301–305 (2006).
14. Laukkarinen, J., Lämsä, T., Nordback, I., Mikkonen, J. & Sand, J. A novel biodegradable pancreatic stent for human pancreatic applications: a preclinical safety study in a large animal model. *Gastrointest. Endosc.* **67**, 1106–1112 (2008).
15. Wang, K., Wu, J. & Zeng, H. Microstructure and fracture behavior of polypropylene/barium sulfate composites. *J. Appl. Polym. Sci.* **99**, 1207–1213 (2006).
16. Luo, C., Chen, G., Zhu, K. & Yuan, X. Preparation of X-ray developable LDPE/SA-BaSO₄ composites and their thermal and mechanical properties. *Polym. Compos.* **37**, 1396–1406 (2016).
17. Yang, J. *et al.* Morphologies, mechanical properties and thermal stability of poly(lactic acid) toughened by precipitated barium sulfate. *Russ. J. Phys. Chem. A* **89**, 2092–2096 (2015).
18. Chen, X., Wang, L., Shi, J., Shi, H. & Liu, Y. Effect of barium sulfate nanoparticles on mechanical properties and crystallization behaviour of HDPE. *Polym. Polym. Compos.* **18**, 145–152 (2010).
19. Siaeira, G., Bras, J. & Dufresne, A. Cellulose whiskers versus microfibrils: Influence of the nature of the nanoparticle and its surface functionalization on the thermal and mechanical properties of nanocomposites. *Biomacromolecules* **10**, 425–432 (2009).
20. Lepoittevin, B. *et al.* Poly(ϵ -caprolactone)/clay nanocomposites prepared by melt intercalation: mechanical, thermal and rheological properties. *Polymer (Guildf)*. **43**, 4017–4023 (2002).
21. Avella, M. *et al.* Preparation and characterisation of compatibilised polycaprolactone/starch composites. *Polymer (Guildf)*. **41**, 3875–3881 (2000).
22. Liu, J. *et al.* Microstructure and properties of polycaprolactone/calcium sulfate particle and whisker composites. *Polym. Compos.* **33**, 501–508 (2012).

23. Wu, D., Wu, L., Sun, Y. & Zhang, M. Rheological properties and crystallization behavior of multi-walled carbon nanotube/poly(ϵ -caprolactone) composites. *J. Polym. Sci. Part B Polym. Phys.* **45**, 3137–3147 (2007).
24. Huang, Y. *et al.* Nonisothermal crystallization kinetics of modified bamboo fiber/PCL composites. *J. Appl. Polym. Sci.* **116**, NA-NA (2010).
25. Jeziorny, A. Parameters characterizing the kinetics of the non-isothermal crystallization of poly(ethylene terephthalate) determined by D.S.C. **19**, 1142–1144 (1978).
26. Pires, L. S. O., Fernandes, M. H. F. V. & de Oliveira, J. M. M. Crystallization kinetics of PCL and PCL–glass composites for additive manufacturing. *J. Therm. Anal. Calorim.* **134**, 2115–2125 (2018).
27. Chen, X., Wang, L., Liu, Y., Shi, J. & Shi, H. Nonisothermal crystallization kinetics of high-density polyethylene/barium sulfate nanocomposites. *Polym. Eng. Sci.* **49**, 2342–2349 (2009).
28. Eder, M. & Wlochowicz, A. Kinetics of non-isothermal crystallization of polyethylene and polypropylene. *Polymer (Guildf)*. **24**, 1593–1595 (1983).
29. Wang, K., Wu, J., Ye, L. & Zeng, H. Mechanical properties and toughening mechanisms of polypropylene/barium sulfate composites. *Compos. Part A Appl. Sci. Manuf.* **34**, 1199–1205 (2003).
30. Cao, X., Zhang, H., Chen, M. & Wang, L. Preparation, characterization, and properties of modified barium sulfate nanoparticles/polyethylene nanocomposites as T-shaped copper intrauterine devices. *J. Appl. Polym. Sci.* **131**, 1–7 (2014).
31. Martínez De Arenaza, I., Sadaba, N., Larrañaga, A., Zuza, E. & Sarasua, J. R. High toughness biodegradable radiopaque composites based on polylactide and barium sulphate. *Eur. Polym. J.* **73**, 88–93 (2015).

**Chapter 2: Formation of a rigid amorphous phase
at Poly(D,L-Lactide- ϵ -
caprolactone)/barium sub-micro particle
interphase and its effect on hydrolytic
degradation and mechanical properties**

Summary

Poly(D,L-Lactide- ϵ -caprolactone) (81%D,L-LA,L/19%CL), PDLCL, was synthesized and mixed with barium sulphate sub-micron particles to obtain biodegradable radiopaque composites. An in vitro hydrolytic degradation study was performed at 37 °C and pH 7.4 to evaluate the changes in molecular, physical and mechanical properties induced by BaSO₄ on PDLCL over time. DSC and DMTA analysis gave strong evidence of molecular interactions of PDLCL chains with barium sulphate. BaSO₄ particles increase the glass transition temperature (T_g) of the neat polymer, translates the storage modulus falling at T_g to higher temperatures and reduces the viscoelasticity related parameters lost modulus E'' and tan δ lost peak. The composites tensile strength increased 110% at human body temperature (37 °C) for the 35 wt.% BaSO₄ composite in regard to neat PDLCL maintaining high deformation at break (>300%) thus increasing also toughness. BaSO₄ delays the degradation process of PDLCL to longer times. The degradation rate constant (KMW) in composites decreases monotonously from 0.056 to 0.021 Km³/g.day for PDLCL; however, the water absorption rate and mass lost rate is similar in composites and neat PDLCL which suggest that no changes are occurring by the introduction of the radiopaque filler in both water diffusion and end-chain scission mechanism of PDLCL. GPC curves in composites show a bimodal behavior that is not present in neat PDLCL which is explained by the existence of a rigid hydrolysable amorphous phase (RAP) leading to matrix/particle reinforcement at PDLCL/BaSO₄ interface. Interphase chains and good adhesion are thus found at PDLCL/BaSO₄ interfaces. The good adhesion due to the RAP in PDLCL explains the good compatibility and outstanding mechanical properties of PDLCL/BaSO₄ composites.

Introduction

Poly (L-lactide- ϵ -caprolactone)s (PLCLs) present excellent properties for medical applications because of their good biocompatibility, high hydrolytic degradability in comparison with Poly (L-lactide) (PLLA) and Poly (ϵ -caprolactone) (PCL), and adjustable mechanical properties with composition making it possible new polymeric biomaterials presenting mechanical behavior from glassy rigid to elastomeric¹⁻⁵. For

these reasons PLCLs are being investigated for temporary sutures, catheters, stents, tissue engineering and drug delivery systems⁶⁻⁹.

Barium sulphate (BaSO_4) is a standard in medical applications. Approved by FDA it can be used for X-ray assisted polymer systems to detect either the location of implants or scaffolds in the human body, the drug delivery during biodegradation, or for the detection of sub-products during degradation *in vivo*¹⁰⁻¹⁵.

Biodegradable polymer properties in aqueous medium vary with time. For a correct design of medical devices is necessary to know how many days the polymeric biomaterial will keep sufficient mechanical properties maintaining shape and when it is completely reabsorbed. All these factors depend on polymer degradation kinetics since it is well known that the incorporation of reinforcements lead to changes on it¹⁶⁻¹⁸.

Figure 2-1 shows a scheme of the hydrolytic degradation of polyesters like polylactides and polylactones investigated in this work. This is only a simple representation scheme of a complex degradation behavior yet useful to rationalize the principal mechanisms involved in such polyesters in hydrolytic medium. When a biodegradable polymer is implanted in the human body, the process starts with water absorption by diffusion mechanism. The rate of water absorption (R_1) depends on several factors like material hydrophobicity, surface roughness and water permeability. Water diffusion is a key factor always. When water cannot be easily diffuse into the polymer, hydrolysis only can affect the surface and then the degradation mode is known as “surface degradation”. If water can fill in all the polymer volume gradually, this is known as “bulk degradation”, where the polymer losses molecular weight and mass. The surface degradation behavior is the predominant one in biodegradable polyesters shaped with low area/volume aspect ratio at nano/microscale^{16,19}.

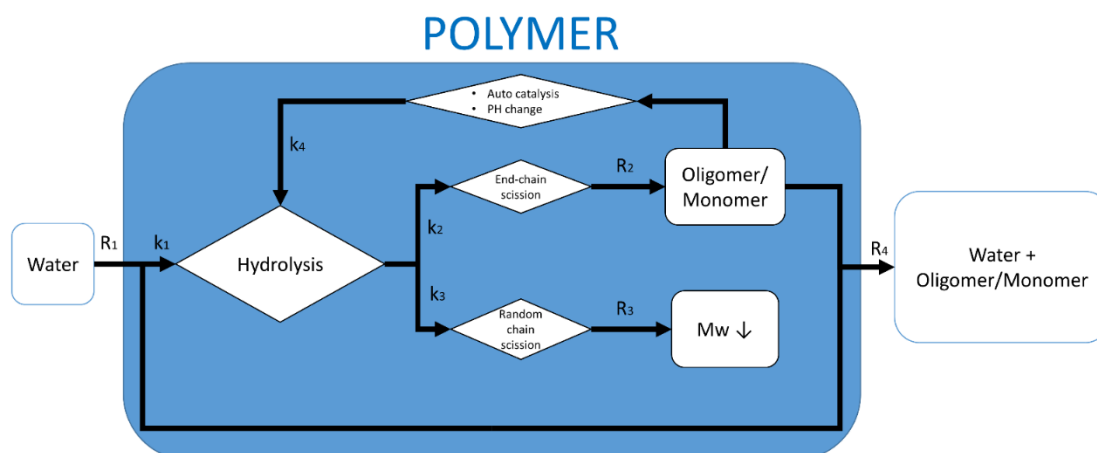


Figure 2-1. Biodegradable polyesters degradation scheme.

After water diffusion, the water molecules absorbed can react with ester groups starting hydrolytic degradation. The hydrolysis reactivity constant (k_1) depends on factors such as the temperature, pH, the catalytic effect of species and the chemical composition of the polymer^{20–22}: It depends also on factors related with polymer structure: molecular weight and distribution and crystal/amorphous morphology and structure. Biodegradation kinetics studies have identified two main mechanisms in polymer hydrolysis^{22–24}. When water affects polymer chain extremes there is said exists an “end-chain scission” mechanism. The principal consequence of this mechanism is sliding small chains and monomers from polymer backbone long chains. As we can see in the scheme (

Figure 2-1) these sub-products can enhance the hydrolysis effect leading to changes of the PH of the medium to more acidic values and then an auto-catalytic effect may occur by carboxylic groups. Several studies in bibliography say that this mechanism reactivity (k_2) is greater than the other (k_1) in an order of 10 times²⁴.

When water can affect groups in the middle of the backbone chains there is a “random chain scission” mechanism. The reactivity in such a case (k_3) is less probable, but its consequences are more notable since sliding chains in the middle of the chains have a huge effect in the reduction of the molecular weight of the polymer chains. According to Shih et al its effectiveness reducing molecular weight is 1000 times higher than that following a end-chain scission mechanism²⁴. It is also important to note that the rate of

molecular weight reduction (R_3) is dependent on molecular weight itself. First, when polymer chains are longer, random chain scission have a huge effect and the molecular weight falls fast. Then degradation rate is reduced gradually in an exponential decreasing manner until a critical molecular weight is obtained. When the molecular weight is lower than this critical value the water diffusion is in equilibrium and part of the low molecular weight molecules, oligomers and monomers, can be diffused out of the polymer macroscopic surface, starting the weight loss. This weight loss rate (R_4) is directly related to the oligomer and monomer production rate (R_2), thus to the chain scission mechanism.

The hydrolytic degradation dynamics is complex and can be drastically affected by changing the different variables. Polymer shape for example can be determinant. When polymers have high volume/low area ratio, water diffusion equilibrium takes time and degradation products tend to accumulate. These products change de pH in polymer and speed up the degradation process in a process known as “autocatalytic degradation effect”. On the other hand, high area/low volume shapes do not accumulate the degradation products due to the high water diffusion. These effects are described in the bibliography with examples of different geometries such as plates, films, particles or scaffolds shapes¹⁷.

Taken all these factors together we can now understand how a reinforcement can affect the degradation kinetics in biodegradable polyester composites. First, the reinforcement can affect the superficial properties like the local hydrophilicity/hydrophobicity and produce changes in the water absorption rate (R_1). Second, some inorganic particles can interact with water and then change the hydrolysis reactivity (k_1). Further some particles can affect matrix-reinforcement by means of interphase chains leading to a rigid amorphous phase (RAP), or promote crystallinity fraction becoming less effective to some types of hydrolysis mechanism²⁵. Finally, some fillers can cancel PH changes and autocatalytic effects of monomers and oligomers (k_4) delaying the degradation rate¹⁸.

This paper presents a complete study of changes in degradation and mechanical properties of Poly(D,L-Lactide- ϵ -caprolactone) (PDLCL) reinforced with barium sulphate radiopaque filler particles in simulated human body fluid conditions (37 °C and pH 7.4). The use of rac-Lactide (50%L-lactide,50%D-lactide) as a comonomer in PDLCL during the synthesis was a choice for starting with an amorphous polymer to avoid the crystal

formation during the degradation process and hence to have a homogeneous and relatively simple degradation process in the sense that polymer crystallinity is avoided during the hydrolytic degradation of PDLCL and its composites and therefore the effect of reinforcement on the degradation mechanisms can be studied without such an interference.

Materials and methods

The poly (D,L-Lactide- ϵ -Caprolactone) terpolymer (PDLCL) was synthesized by ring opening polymerization (ROP) according to the procedure described by Fernandez et al²⁶. Three monomer were used, (D,L-lactide and L-Lactide) provided by Purac Biochem (Netherlands) with >95% purity and (ϵ -Caprolactone) provided by Merk (Germany) with >98% purity. PDLCL was characterized by proton Nuclear Magnetic Resonance (¹H, NMR) and Gel Permeation Chromatography (GPC). Results are summarized in Table 2-1.

Obtained PDLCL is a terpolymer with randomness character of $R=0.99$. On one hand, it has 19% molar fraction of ϵ -caprolactone with average sequence length (L_{CL}) of 1.25. On the other hand Lactide molar fraction is divided in L-Lactide chains with L_{LA} of 5.45 and D,L-lactide RAC chains with average length of 1.71 respectively.

Table 2-1. Principal characterization parameters of PDLCL by proton NMR and GPC.

Molar composition*	81.4% D,L-LA 18.6% ϵ -CL
Microstructural parameters: block lengths (l_i) and randomness (R)*	$l_{LA}=5.45$ $l_{L-LA}=l_{D-LA}=1.71$ $l_{CL}=1.25$ $R=0.99$
Molecular weight**	$M_w=127$ Kg mol ⁻¹ $D=1.94$

*Proton NMR

** GPC.

Barium sulphate particles were provided by Fluka Analytical (Sigma Aldrich). Particle size was determined by dynamic light scattering technique on a Zetasizer ZS90 (Malvern) showing a distribution of 577 ± 125 nm. For hydrolytic degradation study phosphate buffer saline (PBS) with pH 7.4 was used, provided by Fluka analytical (Sigma Aldrich).

Sample preparation

PDLCL with BaSO₄ composites were prepared by melt mixing using a twin extruder mixer by DSM (Xplore model) 5 at 150 °C and 150 rpm for 1h. The nonreinforced PDLCL and three other compositions with 15, 25 and 35 wt. % of BaSO₄ were prepared in the same processing conditions. Finally plates of 1mm were prepared in the hot press Collin P200E at 150 °C and 25 MPa compression for all four compositions.

Thermal Gravimetric analysis (TGA) was used to obtain real wt. % of barium sulphate in composites, in a TGA model Q50 (TA instruments). Three samples (n=3) of 10-15 mg were heated from room temperature to 500 °C at a rate of 10 °C min⁻¹ under nitrogen atmosphere. Results are presented in Table 2-2 with code names used in this work for all compositions.

Table 2-2. BaSO₄ content measured with TGA.

Name code	Theoretical BaSO ₄ content (wt.%)	BaSO ₄ wt. by TGA (%)
PDLCL	0	0
PDLCL15	15	17 ± 0.5
PDLCL25	25	24 ± 2.2
PDLCL35	35	32 ± 1.1

Molecular and calorimetric analysis

Molecular weight of polymers were determined by Gel Permeation Chromatography (GPC) using a Waters 1515 GPC equipment with two Styragel columns (10²-10⁴ Å). Chloroform was used as eluent at a flow rate of 1mL min⁻¹ and polystyrene standards (Shodex Standards, SM-105) were used to obtain the calibration curve. Composite samples were filtered before GPC analysis with a cellulose pore filter (pore size 200 nm) to ensure the elimination of BaSO₄ particles. The thermal behavior of PDLCL and composites was carried out on a differential scanning calorimeter (DSC) model Q80 (TA instruments). Samples of 7 ± 1 mg were heated from -30 °C to 120 °C at 20 °C min⁻¹ on a nitrogen atmosphere.

Mechanical properties and thermal dynamical analysis

ISO 37-2 shape samples were punched with a cutting mold from 1 mm plates. Tensile tests were performed on a Instron 5565 testing machine. Temperature controlled chamber 3119-600 series was used to perform the tests at 37±0.5 °C. Three samples (n=3) were

tested for each composition at 10 mm min^{-1} deformation rate. The temperature controlled chamber limited the testing of PDLCL and its composites to 300% of strain.

The stiffness of PDLCL and its composites was calculated as a secant modulus at 2% ($E_{2\%}$). At $37 \text{ }^\circ\text{C}$, all samples tested are elastomeric and do not present yield point, hence stress at 10% of strain is presented as a strength ($S_{10\%}$) comparison of the materials. All the samples at $37 \text{ }^\circ\text{C}$ passed along the limit of testing (300% of strain) of the testing machine.

Dynamic Mechanical Thermal Analysis (DMTA) was used in a Mettler Toledo DMA/SDTA861e. Samples of $1 \times 4 \times 10 \text{ mm}$ were tested in tension mode from 0 to $60 \text{ }^\circ\text{C}$ at 1 Hz frequency. To ensure that the samples during the tests work in the elastic region, maximum load of 0.3 N and maximum displacement of $30 \text{ }\mu\text{m}$ was set. An offset of 50% was fixed to complete the tests in tension-tension mode.

In vitro hydrolytic degradation study

In vitro degradation study was used to evaluate the changes in properties at different days of biodegradation. From 1 mm plates, $10 \times 10 \text{ mm}$ samples were prepared for the hydrolytic degradation study. Three samples ($n=3$) for each composition, for day of study ($0, 3, 7, 14, 21, 28, 35, 42, 56, 70$ and 98 days respectively), were submerged in 20 ml of PBS ($\text{pH } 7.4$) and stored in an oven at $37 \pm 0.5 \text{ }^\circ\text{C}$ to simulate human body conditions. All samples were weighed before being submerged in PBS to obtain day 0 weight (W_0). For mechanical characterization samples of $10 \times 4 \times 1 \text{ mm}$ were submerged in 8 ml of PBS with an area/liquid relation of 0.1 ml. mm^{-2} .

Degradation Kinetics evolution

Three samples for composition ($n=3$) were extracted at each corresponding day under the hydrolytic medium and dried with absorbent paper to eliminate superficial water and then weighed to know wet weight (W_w). Finally, samples were dried off in vacuum at 50 mBar for 48 h and weighed again to obtain dry weight (W_d) at room temperature.

Water Absorption percentage (%WA) and Remaining Weight (%RW) were obtained using next formulas (1 and 2):

$$\% WA = \frac{W_w - W_d}{W_d} \cdot 100 \quad (1)$$

$$\% RW = \frac{W_d}{W_0} \cdot 100 \quad (2)$$

To compare the molecular weight evolution with degradation days, dried samples were characterized in a GPC to obtain PDLCL molecular weight averages in weight (M_w) and dispersity (D) both for neat PDLCL and its composites with BaSO₄. The same procedure described for the day zero characterization of samples was used in all cases.

The degradation rate was quantified by using the well-known logarithmic relation for bulk degradation in polymers (eq. 3)

$$\ln M_w = \ln M_{w0} - K_{M_w} * t \quad (3)$$

M_w is the weight average molecular weight in g/mol (Da) at degradation day t in the hydrolytic medium selected, M_{w0} (Da) the molecular weight at day zero, and K_{M_w} the apparent degradation rate constant (Da/day). Another common factor to compare degradation is the half degradation life time $t_{1/2}$ (day) that we can calculate with the next formula (4):

$$t_{1/2} = \ln 2 * 1/K_{M_w} \quad (4)$$

Evolution of thermal and mechanical properties during hydrolytic degradation

On one hand parts of 7 ± 1 mg were obtained from complete dried samples at different days of degradation for DSC analysis in the same conditions described above for day 0 characterization. On the other hand samples of $1 \times 4 \times 10$ were dried with absorbent paper to quit the superficial water before testing and then tested using DMTA analysis in the same conditions described above for day 0 characterization. Finally photographs of samples with a 4 Mega Pixel camera were taken at different days of degradation to see the changes in solids to glassy morphology with degradation and the type of residues generated in hydrolysis.

Radiopacity

Samples used in hydrolytic degradation study were irradiated with X-radiographic standard clinical machine to get radiograph of composites at different time of degradation. In order to compare radiopacity all samples were tested in the same polymer background and using same intensity including 1 mm aluminum plates as reference samples.

Results and Discussion

Thermal and molecular analysis by DSC and GPC

Table 2-3 summarizes the glass transition temperature (T_g) and molecular properties of PDLCL compositions obtained by DSC and GPC. DSC curves do not show any melting peak for any PDLCL composition, so we have a complete amorphous matrix at day 0 as expected for a rac-lactide based terpolymer^{26,27} in both neat PDLCL and of all composites with BaSO₄. The glass transition temperature of PDLCL appears to slightly grow progressively from a value of 29.6 ± 0.35 °C for the neat polymer to 31.2 ± 0.25 °C for the 35 wt.% BaSO₄ composite with the results not being statistically significant. These results are qualitatively somewhat different from others results with this composite system²⁸. In our case the increase of T_g suggests some kind of interaction in matrix-reinforcement interphase improving adhesion. DMTA analysis is presented below to follow with the thermal analysis.

Table 2-3. Glass transition temperature and molecular mass properties by DSC and GPC of PDLCL and its barium sulphate composites.

	T_g (°C)	M_w (kDa)	D (M_w/M_n)
PDLCL	29.6 ± 0.35	74.6 ± 1.5	1.83 ± 0.02
PDLCL15	29.9 ± 0.22	86.1 ± 0.5	1.89 ± 0.03
PDLCL25	30.5 ± 0.43	96.0 ± 1.6	1.90 ± 0.06
PDLCL35	31.2 ± 0.25	94.5 ± 1.7	1.86 ± 0.10

If we compare the GPC curves and average molecular weight (M_w) values after and before processing we can observe a fall in molecular weight (M_w) for PDLCL and its composites, i.e.: from 127 kDa to 74.6 kDa for the neat polymer. This is common when biodegradable polyesters are submitted to high temperatures during processing. As can

be seen from Table 2-3 barium sulphate is preventing this thermal degradation of PDLCL in composites formulations.

Tensile tests and dynamic- mechanical thermal analysis

The tensile test curves for PDLCL and its composites evidence a fully elastomeric behavior for both neat polymer and its composite compositions. **Table 2-4** shows the tensile test mechanical properties and those obtained from DMTA analysis for PDLCL and PDLCL with its barium sulphate composites. On one hand for tensile tests, $E_{2\%}$ is secant modulus at 2% of strain, $S_{10\%}$ is strength at 10% of strain and ϵ_r elongation at break. On the other hand for DMTA $E'_{0^\circ\text{C}}$ correspond for storage modulus at 0°C , $T_{1\text{GPa}}$ is temperature where store modulus is equal to 1 GPa and $\tan\delta$ is viscoelastic rate (E'/E''). These tension test results performed at 37°C show a marked increment of the secant modulus in PDLCL with incorporation of BaSO_4 particles (+59%) which is statistically significant for PDLCL15 reinforced with 15 wt% of barium sulphate ($p>0.05$); further the stiffness of composites PDLCL25 and PDLCL35 shows a large dispersion with no significant change in regard to PDLCL15.

Table 2-4. Mechanical properties of PDLCL and barium sulphate composites from standard tension test at 37°C and DMTA analysis.

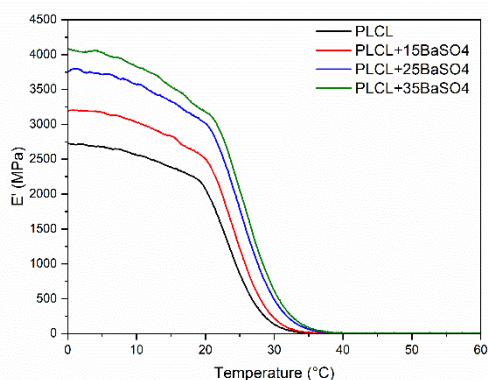
	$E_{2\%}$ (MPa)	$S_{10\%}$ (KPa)	ϵ_r (%)*
PDLCL	2.2±0.4	180±20	> 300
PDLCL15	3.6±0.9	320±90	> 300
PDLCL25	3.5±0.5	330±20	> 300
PDLCL35	3.1±0.5	380±50	> 300
DMTA			
	$E'_{0^\circ\text{C}}$ (MPa)	$T_{1\text{GPa}}$ ($^\circ\text{C}$)	$\tan\delta$
PDLCL	2740 ± 130	24.4 ± 1.16	2.10 ± 0.03
PDLCL15	3230 ± 106	25.7 ± 0.91	1.95 ± 0.03
PDLCL25	3730 ± 174	27.6 ± 1.56	1.89 ± 0.05
PDLCL35	4120 ± 211	28.3 ± 1.13	1.85 ± 0.02

* Use of temperature chamber limit strain rate to 300%.

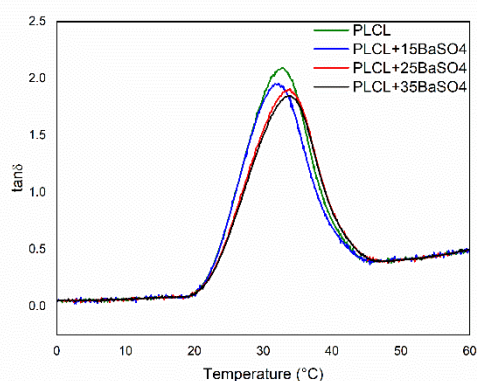
For the results of the tensile strength $S_{10\%}$ a gradual increment with barium sulphate content is observed from 180 KPa for PDLCL to 380 KPa (+110%) for PDLCL35, being the change statistically significant for all compositions ($p>0.05$). Finally, as the values of elongation of > 300% obtained for all neat PDLCL and composites indicate, barium

sulphate particles do not lead to significant changes in the elastomeric behavior, regardless the composition in this range, remaining it in a large extent.

Figure 2-2.A shows the evolution of storage modulus (E') with temperature from DMTA analysis. As can be observed for every polymer composition tested the glass transition temperature appears in the range of 20-30 °C. Below the T_g the behavior of PDLCL and its composites is glassy with storage modulus values measured at 0 °C of 2740 ± 130 , 3230 ± 106 , 3730 ± 174 , 4120 ± 211 for PDLCL, PDLCL15, PDLCL25 and PDLCL35 respectively. It can also be observed when the filler content increases the fall of stiffness is translated to higher temperature suggesting a good PDLCL/ $BaSO_4$ interphase adhesion.



(a)



(b)

Figure 2-2. DMTA curves for PDLCL and PDLCL with barium sulphate composites. a) Storage modulus (E'); b) Tangent delta ($\tan\delta$).

Figure 2-2.b shows the $\tan \delta$ evolution with temperature for PDLCL and its composites. $\tan \delta$ expresses the ratio of the loss modulus over the storage modulus. Hence it is a measure of the viscose dissipation over the storage elastic energy stored in this region of viscoelasticity around the T_g . As can be observed the $\tan \delta$ peak is slightly dropping with barium sulphate content, reducing viscoelasticity. As it is observed the peak values are 2.10 ± 0.03 , 1.95 ± 0.03 , 1.98 ± 0.06 , 1.85 ± 0.02 for PDLCL, PDLCL15, PDLCL25 and PDLCL35 respectively.

$\tan \delta$ peak values can be used to analyse the interphase behavior in composites²⁹. Viscoelasticity at transition glass temperature is related to polymer chain mobility and then $\tan \delta$ peak reduction needs to be proportional to volume fraction of polymer if only one phase is present. Hence we can use formula (5) in order to model this behavior:

$$\frac{\tan \delta_{\text{Composite}}}{\tan \delta_{\text{PDLCL}}} = 1 - b * V_r \quad (5)$$

Where V_r is volume fraction of reinforcement and b the parameter to adjust. When $b=1$, $\tan \delta$ reduction is proportional to volume fraction and then the assumption of one phase is correct. If $b \geq 1$, viscoelasticity is dropping more quickly than reduction of volume fraction and then the existence of a new less viscoelastic phase can be assumed. Finally if $b \leq 1$ this second phase need to be more viscoelastic than neat polymer. This new phase is generally accepted as polymer chains in composite interphase and b can model the interaction between polymer and reinforcement. Figure 2-3 shows $\tan \delta$ peak values for PDLCL and composites including the linear regression with $R=0.85$ and $b= 1.2$ ($b \geq 1$ for al composition with confidence level of 95%). These result suggest a good interaction between barium sulphate an PDLCL based on the reduction of chain mobility in the composite-matrix intherphase.

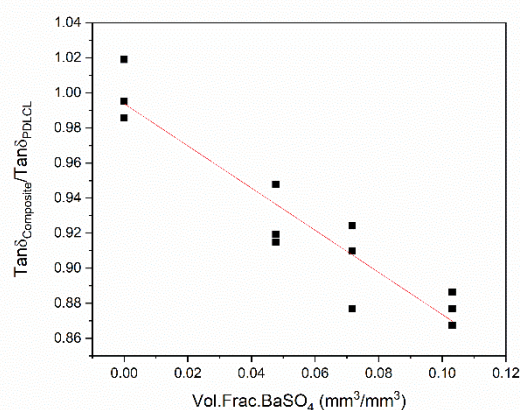


Figure 2-3. Evolution of $\text{Tan}\delta$ according to equation (5) with barium sulphate volume fraction.

In **Table 2-4** also it is shown the temperature at which the storage modulus drops below 1 GPa for PDLCL and its composites. This point is translated from 24.4 for PDLCL to 28.3°C for PDLCL35, which is in agreement with the glass transition results obtained by DSC results, and suggests the existence of a rigid amorphous phase (RAP) in PDLCL in contact surfaces with BaSO₄ providing interface interaction and good adhesion.

Evolution of thermal properties during in vitro hydrolytic degradation

It can be observed in DSC curves of PDLCL and its BaSO₄ composites at different days of degradation that none of the PDLCLs show neither crystallinity nor melting peaks, only the signal corresponding to the glass transition temperature (T_g) appears. This demonstrates the existence of a fully amorphous state in all samples which is an expected result since the block lengths of lactide or ϵ -caprolactone) in chain microstructure of PDLCL used in this work are very short ($l_{LA}=5.45$, $l_{L-LA}=l_{D-LA}=1.71$; $l_{CL}=1.25$) and the randomness character is $R=0.99$ indicating the presence of a near random Bernouillian distribution of motifs in a statistical copolymer ($R=1$)¹. Hence the crystallization ability of this terpolymer is not thermodynamically possible³⁰.

Table 2-5 summarized results of thermal analysis by DSC of PDLCL and its BaSO₄ composites for day 0 and day 21 of hydrolytic degradation. On one hand, the drop in glass transition temperature in first 21 days of degradation ($\Delta T_{g \text{ Day 0 to day21}}$) is linearly correlated with barium sulphate w.t. content ($R=0.9$), suggesting that BaSO₄ are not only

decreasing chains mobility in composites at day 0, also is preventing chains excisions, since this is the main mechanism of T_g reduction in polymer hydrolytic degradation.

Table 2-5. Results of thermal analysis for PDLCL and its barium sulphate composites.

	Tg Day 0	Tg Day 21	$\Delta Tg_{\text{Day 0 to day 21}}$ (°C)	ΔC_p (J/(g*°C))	X_{MAP}	X_{RAP}
PDLCL	29.6	25.6	4.0	4.29 E-05	1,000	0
PDLCL+15BaSO4	29.9	26.3	3.6	9.33 E-06	0,217	0,783
PDLCL+25BaSO4	30.5	28.0	2.5	7.95 E-06	0,185	0,815
PDLCL+35BaSO4	31.2	29.3	1.9	6.64 E-06	0,155	0,845

On the other hand variation of the specific heat capacity at the $T_g(\Delta C_p)$ can be used to understand changes in structural phases of polymers³¹. Since there is not any phase changes in barium sulphate in the range of 20 to 40 °C, change of C_p at glass transition temperature only can be attributed to polymer phases. DSC result have proved that these PDLCL polymer matrix do not present crystalline phases, hence ΔC_p in neat PDLCL is consequence of mobile amorphous phase (MAP). Hence, based on these assumptions, reduction in ΔC_p with barium sulphate content can be related with new polymer phase with less chain mobility (generally named rigid amorphous phase or RAP) an this reduction need to be proportional to the drop of MAP mass phase. Hence we can use the formula (6) and (7) to evaluate the mass fraction of mobile amorphous fraction (X_{MPA}) and rigid amorphous fraction (X_{RAP}):

$$\chi_{MAP} = \frac{\Delta C_{p_{composite}}}{\Delta C_{p_{PDLCL}}} \quad (6)$$

$$\chi_{RAP} = 1 - \chi_{MAP} \quad (7)$$

Figure 2-4 clearly show a linear correlation of RAP fraction and barium sulphate content ($R=0.97$) and suggest the existence of a degree of interaction and good adhesion at the interfaces between PDLCL and BaSO₄ particles that explain the good compatibility and mechanical properties found in PDLCL/BaSO₄ composites.

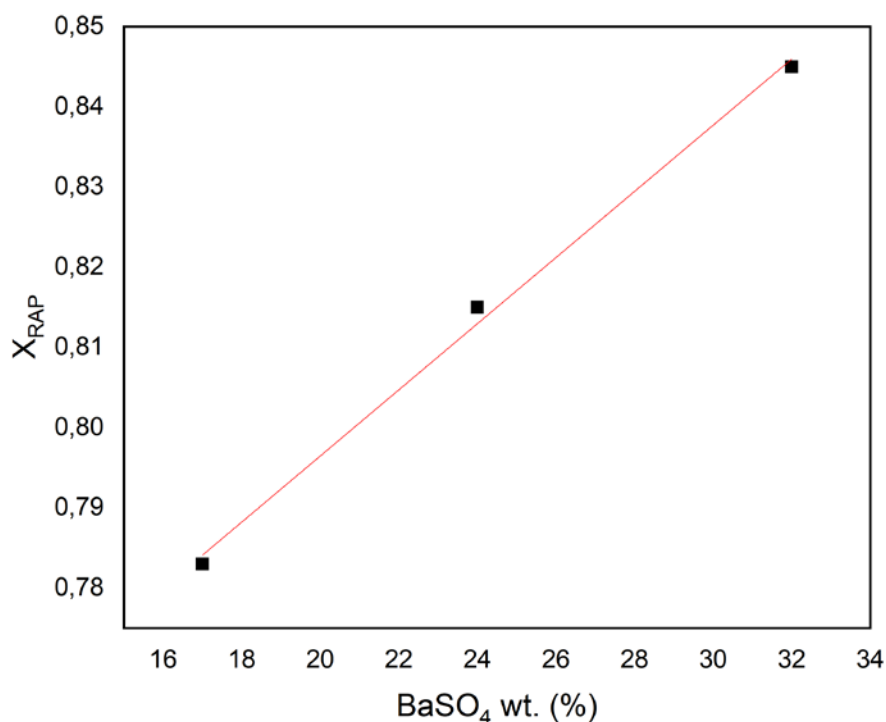


Figure 2-4. Variation of rigid amorphous phase fraction (RAP) of PDLCL composites with barium sulphate content.

Evolution of the mechanical properties during *in vitro* hydrolytic degradation

The evolution of the mechanical properties during degradation was followed by DMTA. Figure 2-5 shows the storage modulus evolution with temperature for PDLCL and its BaSO₄ composites at day 21 of degradation. PDLCL at day 21 was not possible to be tested because its advanced state of hydrolytic degradation. It can be observed the glassy state at temperatures below the T_g located around 25 °C with the corresponding value at zero temperature of 1600, 2250 and 2300 MPa for PDLCL15, PDLCL25 and PDLCL35 respectively. In the glassy region the storage modulus slightly and monotonously reduces for each PDCL composition until, around the T_g , a typical fall of about 2-3 orders of magnitude is observed. It is observed also that the fall in mechanical properties speeds up with days of degradation in these composites, i.e. for day 21 the reduction in storage modulus of PDLCL15 is to be about a half of the corresponding value at day zero and is accompanied by a reduction in the T_g value of 7.2 °C.

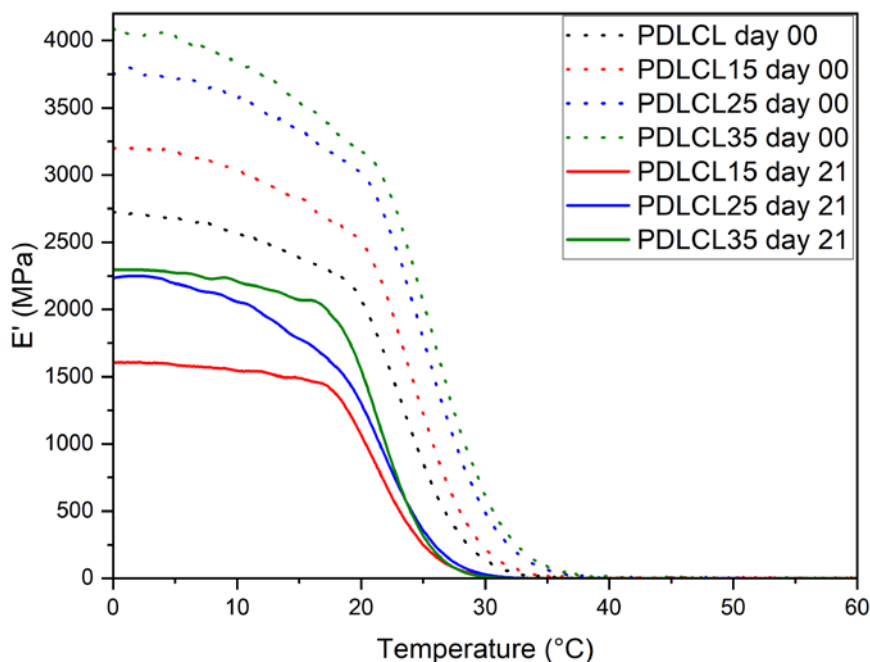


Figure 2-5. Storage modulus curves by DMTA of PDLCL composites at day 0 and 21 of hydrolytic degradation. Neat PDLCL samples were impossible to test due to brittleness induced by hydrolytic degradation at day 21.

Figure 2-6 shows the storage modulus behavior with temperature for PDLCL35 at days 0, 7, 14 and 21 in the hydrolytic degradation medium. The typical and complete storage modulus evolution with temperature of a polymer composite system was possible to be observed for each day of hydrolytic degradation selected in this case because of the high content of BaSO₄ particles in the DMTA tested samples. It can be observed in this figure that the storage modulus of PDLCL35 is steadily decreasing with days under the hydrolytic medium from 4120 ± 211 MPa at day 0 to 2280 ± 326 MPa at day 21. This values are attributed to a combined effect of both a polymer plasticization due to water absorption and the molecular degradation of polymer chains in the hydrolytic medium.

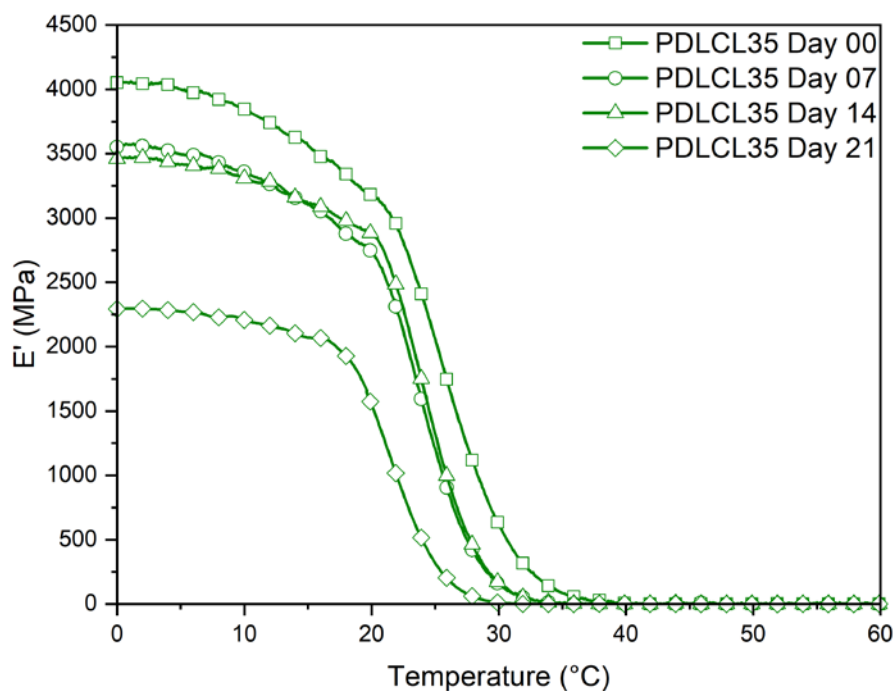


Figure 2-6. DMTA curves of PDLCL+35BaSO₄ composition at different days of degradation.

Hydrolytic degradation kinetics

Figure 2-7 shows the remaining weight values in percentage of PDLCL and its composites after water sorption at different submersion days in the hydrolytic medium. All dates have been corrected with TGA results to only show the effects in polymer mass. It is relevant that all compositions show in this respect a very similar behavior in the first 21 days of study which is in agreement with a bulk degradation scheme for hydrophobic polymers^{26,32}. In this initial period, all samples regardless the composition, maintain a constant weight; however, for PDLCL a reduction of weight starts at 30th day whereas all composites start mass reduction at a critical point of 42th day. Finally, the reduction of weight continues along the period of hydrolysis selected reaching, depending on PDLCL and BaSO₄ content, a value of the remaining weight in percentage reaching values at day 98 ranging from 18 wt.% for PDLCL to 30 % for PDLCL35.

In the intermediate region of time dependent evolution, after the critical time-value, an exponential increase in mass reduction is observed for all PDLCL and its composite

samples with BaSO₄. For this region it can be said that there is a transition from a solid-like to a hydrogel-like behavior since the samples do not maintain their shape becoming an amorphous paste along this period of immersion in the hydrolytic medium.

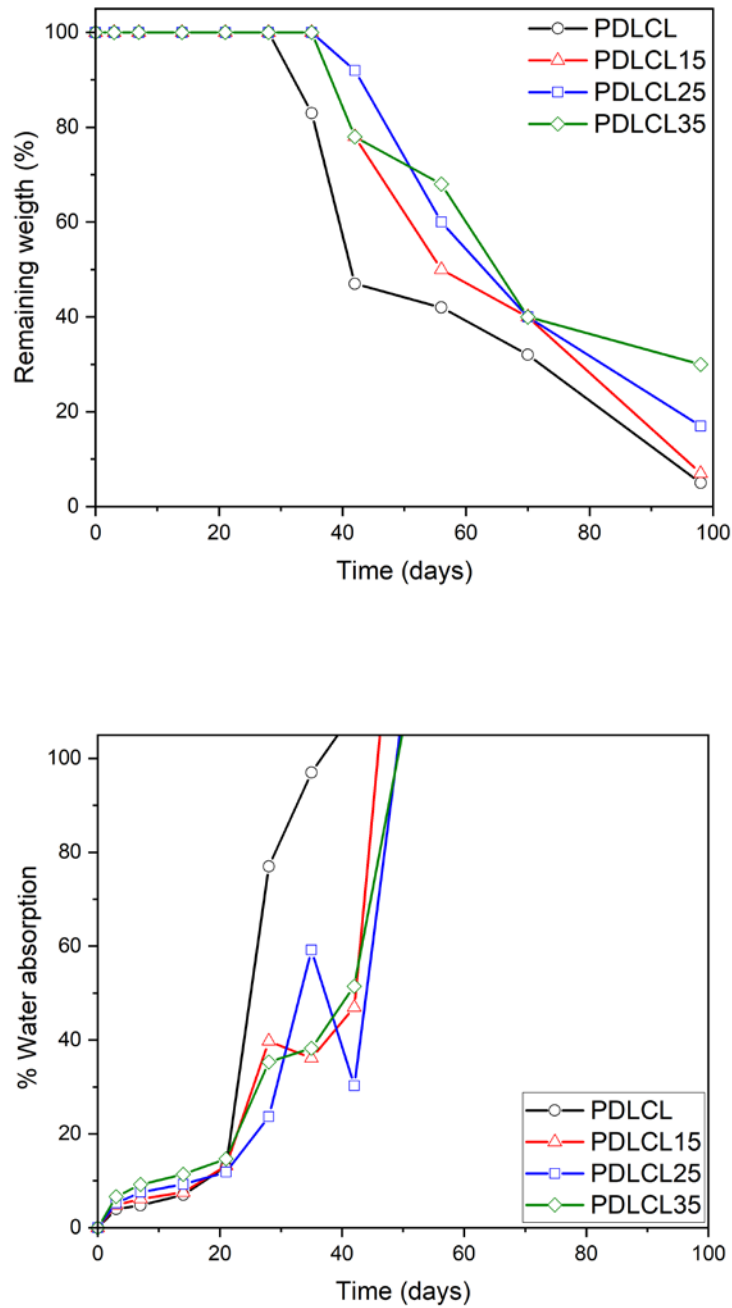


Figure 2-7. Remaining weight (RW%) and water absorption (WA%) evolution during days of degradation.

From these results it is derived that BaSO₄ delays significantly the PDLCL mass reduction initiation. However, qualitatively there is no change comparing neat PLCL and BaSO₄ composites. This is a quite different behavior comparing what is found in other inorganic reinforcements used in poly (lactic acid) (PLA) or poly (amino acid) (PAA) reinforced with Bioglass and Calcium sulphate respectively^{33,34}. In the latter the inorganic particles may lead to changes in the pH of the hydrolytic medium along the time enhancing the hydrolyzation and allowing the diffusion of shorter molecular segments, oligomers and monomers to the outside surface of samples.

Figure 2-8 presents the molecular weight evolution of PDLCL and its composites with BaSO₄ with the degradation time from GPC curves. It is presented in logarithmic scale to show clearly the first order logarithmic behavior of the degradation dynamics in PDLCL and its composites. Relevant points are marked: 1) The last day that samples have sufficient mechanical properties to be tested (blue, o); 2) Critical point from which a constant water absorption occurs (green, o) and 3) last day at which weight lost is observed (red, o).

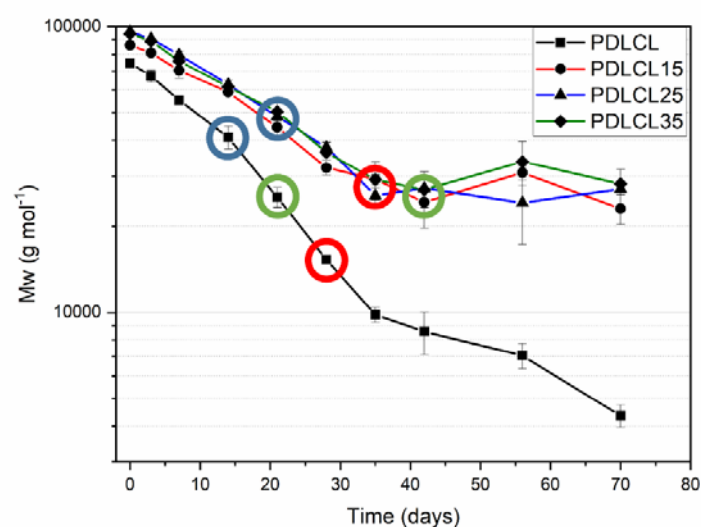


Figure 2-8. Molecular weight evolution with days of degradation of PDLCL and PDLCL with barium sulphate composites.

Table 2-6 resume the principal parameters of logarithmic degradation model using (3) and (4) formulas for first 28 days of degradation. As can be observed all samples present

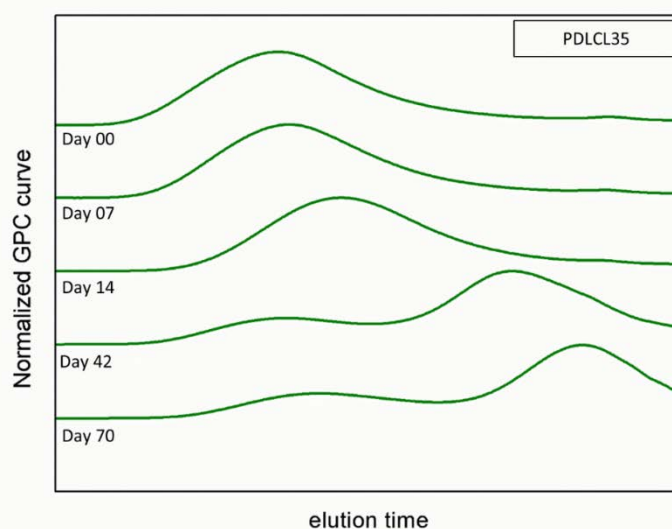
at first, a linear reduction in their reduction behavior at logarithmic scale. The linear correlation at day 28 is good for all compositions ($R \geq 0.95$) and supports the use of a first order logarithmic equation to model the degradation rates in PDLCL and its composites with BaSO₄. It is evident from these data that the introduction of Barium sulfate reduces the degradation rate of PDLCL in composites with an almost linear relation for the exponential constant K_{Mw} with the filler content ($R=0.95$).

Table 2-6. Results of logarithmic fitting for first 28 days of degradation.

	K_{Mw} (KDa/day ⁻¹)	$t_{1/2}$ (day)
PDLCL	0.0562	12.3
PDLCL+15BaSO ₄	0.0348	19.9
PDLCL+25BaSO ₄	0.0340	20.4
PDLCL+35BaSO ₄	0.0214	32.4

After this intermediate period in which the molecular weight reduces following a logarithmic evolution with time, all the samples start their mass loss and shorter segments are thus obtained, and oligomers and monomers diffuse out of the samples surface. These would contribute to enhance the hydrolysis rate with an autocatalytic pH acidic effect but now, diffusing out of the polymer, the molecular weight reduction rate in both neat PDLCLs and its composites is slower^{23,26}.

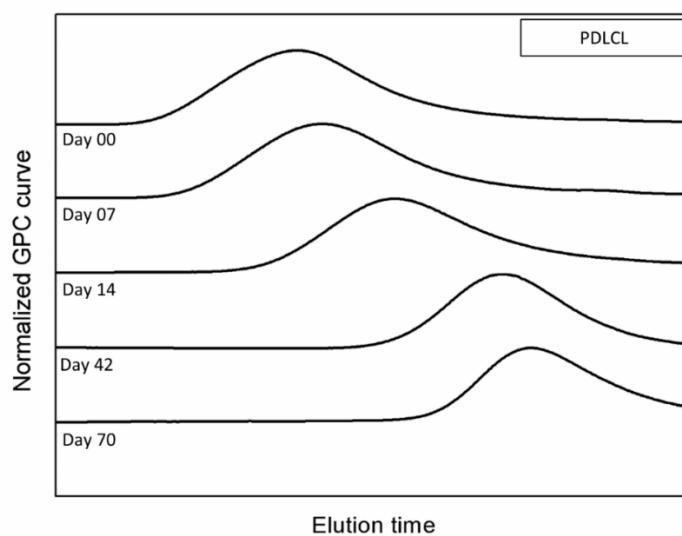
As PDLCL composites are concerned, however, samples show a more complex



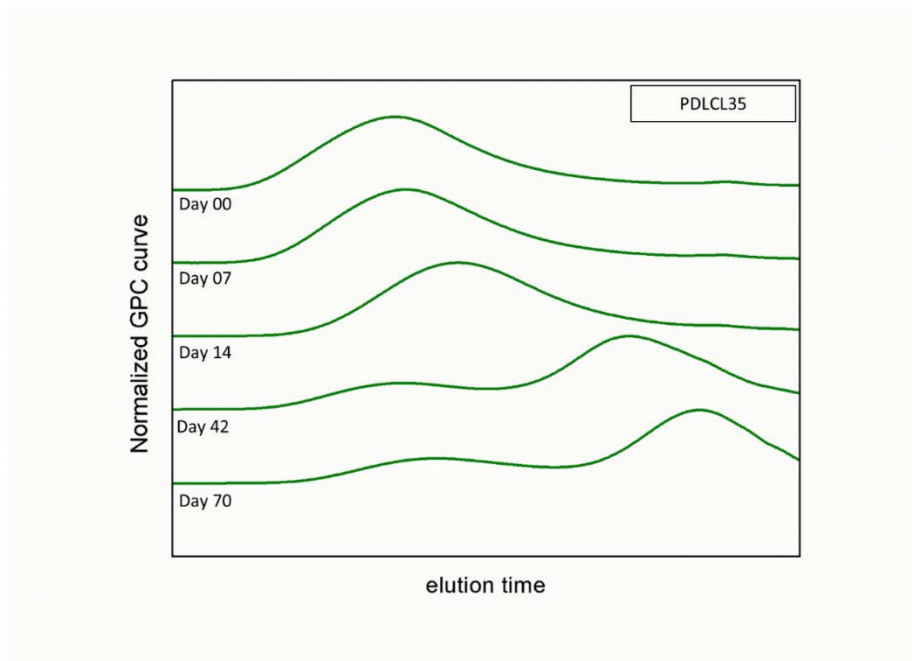
behavior.

(b)

Figure 2-9 presents the normalized GPC curves for neat PDLCL (a) and for its counterpart composite composition with 35 wt.% of barium sulphate (b). For neat PDLCL it can be observed the usual evolution in biodegradation of macromolecules with the peak translating to the right with days of degradation indicating a homogeneous molecular weight decrease along the time in the hydrolytic medium.



(a)



(b)

Figure 2-9. Evolution of GPC curves at different days of degradation: a) PDLCLD; b) PDLCL+35BaSO₄.

However, as can be observed for PDLCL in Figure 2-9b, the molecular weight reduction along the time in the hydrolysis medium changes from its homogeneous behavior in neat PDLCL to a heterogeneous one when BaSO₄ particles are included. At day 42 we can observe that the molecular distribution starts to be bimodal with one little peak corresponding to high molecular weights at lower elution times and another bigger peak corresponding to lower molecular weights. At day 72 this second peak continues the usual degradation behavior translating to the right in the same way of neat PDLCL whereas the little peak at lower elution times appears to be less affected by the increase of time of the sample in the degradation medium. Taking all GPC curves together it can be concluded that the inclusion of barium sulphate particles is creating a double phase molecular degradation behavior in the PDLCL/BaSO₄ composites opposite to the homogeneous degradation found in neat PDLCL, suggesting that the existence of RAP supported by thermal an DMTA analysis have effect on hydrolytic degradation in composites.

Figure 2-10 represents the PDLCL chains in a region close to the filler which appears to be less affected by the random chain scission mechanism happening in neat PDLCL. This particle/matrix interphase in PDLCL composites corresponds to the rigid amorphous

phase (RAP) not contributing to the ΔC_p change at the T_g previously observed and discussed in DSC and DMA sections. Hence there is a double phase amorphous behavior corresponding to composite samples containing a RAP and a MAP in PDLCL matrix. This results in PDLCL/BaSO₄ composites with a lower degradation rate due to the existence of a fraction of RAP together with a usual higher degradation rate similar to that in neat PDLCL for the corresponding fraction of mobile amorphous phase (MAP) in composites. This effect is very similar to that found in semicrystalline biodegradable polymers where the confinement of chains lead to hardly hydrolysable phases in crystalline regions in regard to amorphous ones²⁵.

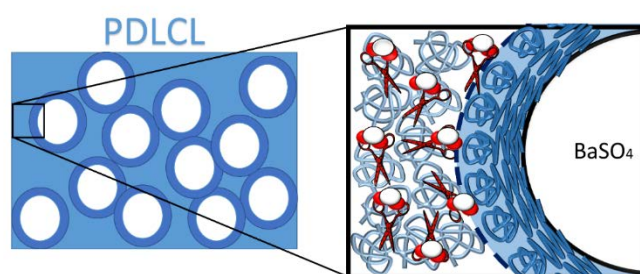


Figure 2-10. Illustration of the interphase between PDLCL macromolecules and BaSO₄ explaining the double phase degradation behavior phase in PDLCL composites.

From this inner structure scheme we can explain the evolution of hydrolytic degradation on mechanical behavior of these composites. Loss of mechanical integrity appears most related to some molecular weight critical value close to 35 KDa (blue circles in **Figure 2-8**). After this point the samples become brittle. It is also remarkable that BaSO₄ particles are enhancing the mechanical life in composites with a reduction of the hydrolytic degradation rate.

Another aspect related to the existence of a critical value of molecular weight below which the water absorption grows exponentially (green circles in **Figure 2-8**). For neat PDLCL and composites samples this value is 25 KDa since below it chains are found to be soluble in water. In addition, BaSO₄ particles are delaying this point in the same way mentioned before, as they lead to a reduction of the degradation rate of PDLCL chains.

Finally, mass lost in composites also appears to be changed with the incorporation of BaSO₄ to PDLCL (red circles in **Figure 2-8**). Therefore, neat PDLCL samples present

the usual degradation evolution starting with the loss of mechanical stability, then pass through a critical point of water absorption and finally a mass reduction process occurs when the oligomers and monomer diffusion is easier at longer hydrolysis times. In composite formulations the behavior changes in regard to composites since the samples start losing their mass until the water absorption behavior changes later. This difference can be explained again by the existence of a rigid amorphous phase in PDLCL at the BaSO₄ particles interphase because the less degraded chains of higher molecular weight in this region can create a more stable network maintaining the shape and stability of the samples at the time that lower molecular weights and oligomers can diffuse out allowing their mass reduction.

Morphology of the hydrolytically degraded samples

Figure 2-11 shows the photomicrographs of neat PDLCL and PDLCL/BaSO₄ composites at different days of degradation in the hydrolytic medium. Initially all samples are glassy solids. At day 28, it can be observed that samples regardless the composition are still glassy solids, yet a degree of deformation depending on BaSO₄ content is observed. At day 42 the samples become homogeneously pasty although maintaining the cohesion in matter. At day 98 PDLCL disappears completely in neat PDLCL. Opposite to this when BaSO₄ is present in composites the PDLCL can be still observed at day 98 in the form of soft and pasty solid.

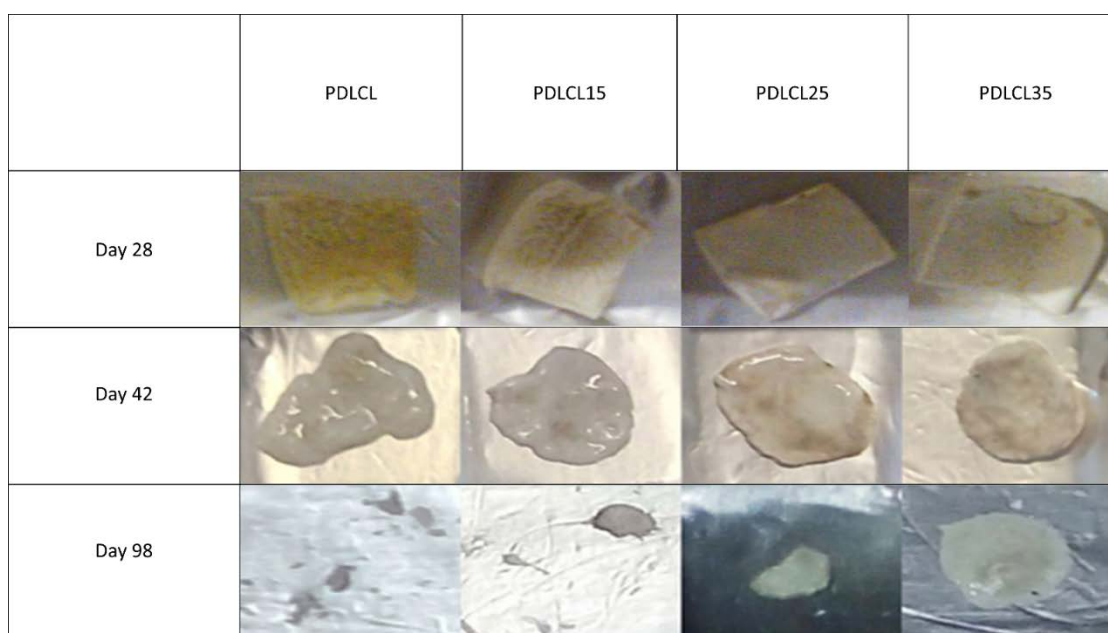


Figure 2-11. Photos of hydrolytic study of PDLCL and PDLCL with barium sulphate composites at different day of degradation.

Radiopacity

Figure 2-12 show X-ray images of 1mm aluminum and PDLCL composites at different days of degradation. At day 0 we can observe that samples with 15% wt. content of BaSO₄ nanoparticles are clearly visible and 25 % BaSO₄ in composites is enough to achieve the same radiopacity as the aluminum sample. At day 21 samples show the mass lost effects with tiny holes, but radiopacity seems to be the same. This suggests that samples are not losing BaSO₄ particles by diffusion mechanism. At day 56 samples are a homogenous paste and as can be seen composites with less quantity of nanoparticles have lost more mass during the degradation process. As can be observed samples near to full degradation can be easily detected with X-ray images, thus is useful for medical application to monitor degradation of samples at human body.

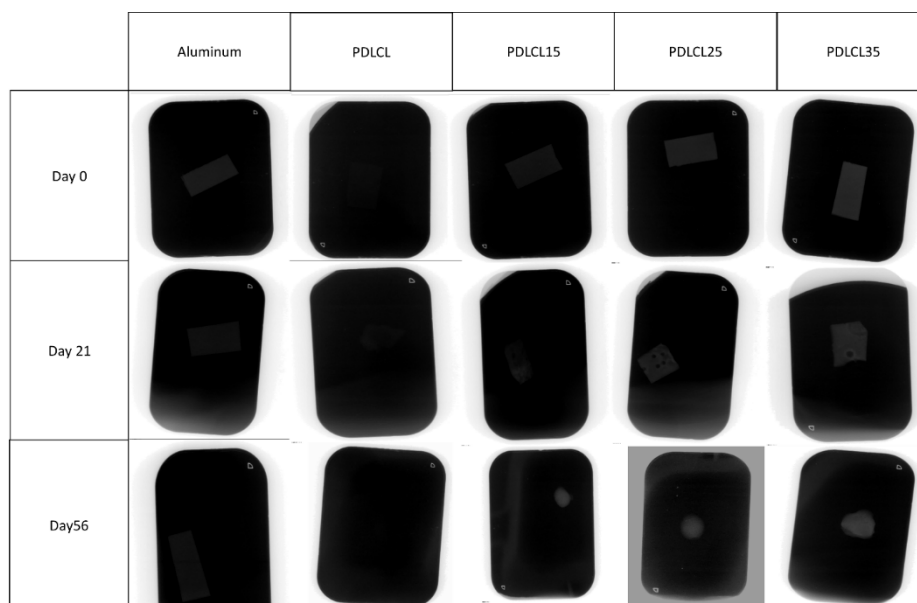


Figure 2-12. X-ray images of Aluminum and composite samples at different days of hydrolytic degradation.

Conclusions

In this investigation poly(D,L-L-lactide- ϵ -caprolactone) (81%D,L-LA/19%CL) was synthesized and mixed with barium sulphate particles to obtain fast biodegradable

radiopaque composites. The aim of the research was to assess the changes induced by BaSO₄ particles in the mechanical and degradation properties of PDLCL in simulated human body conditions (37 °C and pH=7.4). The study was designed also to understand how this filler is affecting hydrolytic degradation dynamics and evaluate the principal mechanisms involved in it.

GPC analysis showed that the presence of BaSO₄ particles in PDLCL composites increases the thermal degradation temperature of the polymer during processing. DSC and DMTA analysis gave a strong evidence of the existence of molecular interactions of PDLCL chains with barium sulphate creating an interphase between the rigid amorphous phase of PDLCL and BaSO₄ sub-micron particles that leads to a slight increase of the glass transition temperature and translates the storage modulus (E') fall at T_g to higher temperatures accompanied with a reduction of viscoelasticity parameters such as the viscose lost (tan δ) and lost modulus (E'').

The good adhesion at the PDLCL/BaSO₄ interphase due to the existing interactions are traduced in an increase of stiffness in composites tensile tested at human body temperature (37°C) with a + 110% for PDLCL35, the 35 wt.% of barium sulphate composite.

BaSO₄ particles change the degradation behavior of PDLCL in the hydrolytic medium selected, delaying it to longer times. Using first order degradation models valid for de hydrolytic degradation of polyesters (R≥0.99), the hydrolytic degradation rate constant of neat PDLCL (K_{MW}) decreased from 0.056 to 0.021Kg/day for the 35 wt.% percent composite which is correlated to the increasing barium sulphate content with R=0.94.

Water absorption rate is similar for neat PDLCL and its composites, so changes in degradation are no related to the water diffusion mechanism involved. The weight loss starting day was delayed with barium sulphate, but the mass loss rate did not change significantly. This is an indication that barium sulphate is not having a great effect on the end-chain scission mechanism of PDLCL hydrolytic degradation.

GPC curves show a bimodal peak for composites that is not present in neat PDLCL. This is due to the existence of a hard hydrolysable phase (rigid amorphous phase, RAP) induced by barium sulphate particles at the matrix/filler interphase. This RAP acts in a

similar way of crystalline phase regions in semicrystalline polymers, which is less sensible to the random-chain scission mechanism, reducing hence the degradation rate in PDLCL and leading to a stiffer and stronger mechanical behavior and a reduction of viscoelastic parameters in PDLCL/BaSO₄ composites during hydrolysis. Thermal analysis did not show either any fusion peak for PDLCL during degradation, thus this more hardly hydrolysable RAP is attributed to the existence of a matrix-reinforcement interphase with PDLCL chains in close interaction and contact with BaSO₄ particles leading to a good interphase adhesion and mechanical properties of composites.

The bi-phasic amorphous structure of PDLCL can also explain the changes produced in the degradation behavior of its composites with BaSO₄. This effect is proportional for BaSO₄ content decreasing the degradation rate and enabling composites to maintain the strength related mechanical properties for a longer time. Further, the hardly hydrolysable RAP phase creates a connected network, allowing to composite samples to delay the time at which samples lost shape and start absorbing water exponentially. Finally, when PDLCL matrix is not affected by the barium sulphate particles in the mobile amorphous phase regions the low molecular weight PDLCL molecules, oligomers and monomer diffusion is more allowed and hence the mass loss rate is not so widely affected.

References

1. Fernández, J., Etxeberria, A. & Sarasua, J. R. Synthesis, structure and properties of poly(L-lactide-co- ϵ -caprolactone) statistical copolymers. *J. Mech. Behav. Biomed. Mater.* **9**, 100–112 (2012).
2. Fernández, J., Etxeberria, A., Ugartemendia, J. M., Petisco, S. & Sarasua, J. R. Effects of chain microstructures on mechanical behavior and aging of a poly(L-lactide-co- ϵ -caprolactone) biomedical thermoplastic-elastomer. *J. Mech. Behav. Biomed. Mater.* **12**, 29–38 (2012).
3. Ugartemendia, J. M., Muñoz, M. E., Sarasua, J. R. & Santamaria, A. Phase behavior and effects of microstructure on viscoelastic properties of a series of polylactides and polylactide/poly(ϵ -caprolactone) copolymers. *Rheol. Acta* **53**, 857–868 (2014).
4. Ugartemendia, J. M., Muñoz, M. E., Santamaria, A. & Sarasua, J. R. Supramolecular structure, phase behavior and thermo-rheological properties of a poly (l-lactide-co- ϵ -caprolactone) statistical copolymer. *J. Mech. Behav. Biomed. Mater.* **48**, 153–163 (2015).
5. Fernández, J., Larrañaga, A., Etxeberria, A. & Sarasua, J. R. Effects of chain microstructures and derived crystallization capability on hydrolytic degradation of poly(l-lactide/ ϵ -caprolactone) copolymers. *Polym. Degrad. Stab.* **98**, 481–489 (2013).
6. Yu, X. *et al.* A shape memory stent of poly(ϵ -caprolactone-co-DL-lactide) copolymer for

- potential treatment of esophageal stenosis. *J. Mater. Sci. Mater. Med.* **23**, 581–589 (2012).
7. Chiriac, S., Facca, S., Diaconu, M., Gouzou, S. & Liverneaux, P. Experience of using the bioresorbable copolyester poly(DL-lactide- ϵ -caprolactone) nerve conduit guide Neurolac™ for nerve repair in peripheral nerve defects: Report on a series of 28 lesions. *J. Hand Surg. (European Vol.* **37**, 342–349 (2012).
 8. Sartoneva, R. *et al.* Comparison of a poly-L-lactide-co- ϵ -caprolactone and human amniotic membrane for urothelium tissue engineering applications. *J. R. Soc. Interface* **8**, 671–677 (2011).
 9. Yang, L. Q. *et al.* Potential Biodegradable Implants from ϵ {lunate}-Caprolactone and D, L-Lactide Copolymers: Synthesis, Properties, and In Vivo Degradation. *Int. J. Polym. Anal. Charact.* **19**, 422–440 (2014).
 10. Lämsä, T. *et al.* Biocompatibility of a new bioabsorbable radiopaque stent material (BaSO₄ containing poly-L,D-lactide) in the rat pancreas. *Pancreatology* **6**, 301–305 (2006).
 11. Chan, W. A., Bini, T. B., Venkatraman, S. S. & Boey, F. Y. C. Effect of radio-opaque filler on biodegradable stent properties. *J. Biomed. Mater. Res. Part A* **79A**, 47–52 (2006).
 12. Han, C. M. *et al.* Biodegradable sheath-core biphasic monofilament braided stent for bio-functional treatment of esophageal strictures. *J. Ind. Eng. Chem.* **67**, 396–406 (2018).
 13. Isotalo, T. *et al.* Biocompatibility testing of a new bioabsorbable X-ray positive SR-PLA 96/4 urethral stent. *J. Urol.* **162**, 1764–1767 (1999).
 14. Isotalo, T. *et al.* Biocompatibility and implantation properties of 2 differently braided, biodegradable, self-reinforced polylactic acid urethral stents: An experimental study in the rabbit. *J. Urol.* **174**, 2401–2404 (2005).
 15. Vaajanen, A. *et al.* Expansion and fixation properties of a new braided biodegradable urethral stent: An experimental study in the rabbit. *J. Urol.* **169**, 1171–1174 (2003).
 16. Göpferich, A. Mechanisms of polymer degradation and erosion1. *Biomater. Silver Jubil. Compend.* **17**, 117–128 (1996).
 17. Grizzi, I., Garreau, H., Li, S. & Vert, M. Hydrolytic degradation of devices based on poly(dl-lactic acid) size-dependence. *Biomaterials* **16**, 305–311 (1995).
 18. Kang, E. Y., Lih, E., Kim, I. H., Joung, Y. K. & Han, D. K. Effects of poly(L-lactide- ϵ -caprolactone) and magnesium hydroxide additives on physico-mechanical properties and degradation of poly(L-lactic acid). *Biomater. Res.* **20**, 1–9 (2016).
 19. Burkersroda, F. von, Schedl, L. & Göpferich, A. Why degradable polymers undergo surface erosion or bulk erosion. *Biomaterials* **23**, 4221–4231 (2002).
 20. Hofmann, D., Entrialgo-Castaño, M., Kratz, K. & Lendlein, A. Knowledge-based approach towards hydrolytic degradation of polymer-based biomaterials. *Adv. Mater.* **21**, 3237–3245 (2009).
 21. Lyu, S. P. *et al.* Kinetics and time-temperature equivalence of polymer degradation. *Biomacromolecules* **8**, 2301–2310 (2007).
 22. Tsuji, H. & Ikarashi, K. In vitro hydrolysis of poly(L-lactide) crystalline residues as extended-chain crystallites: III. Effects of pH and enzyme. *Polym. Degrad. Stab.* **85**, 647–656 (2004).
 23. Gleadall, A., Pan, J., Krufft, M. A. & Kellomäki, M. Degradation mechanisms of bioresorbable polyesters. Part 1. Effects of random scission, end scission and

- autocatalysis. *Acta Biomater.* **10**, 2223–2232 (2014).
24. Shih, C. Chain-end scission in acid catalyzed hydrolysis of poly (d,l-lactide) in solution. *J. Control. Release* **34**, 9–15 (1995).
 25. Li, S. & Vert, M. Hydrolytic degradation of coral/poly(DL-lactic acid) bioresorbable material. *J. Biomater. Sci. Polym. Ed.* **7**, 817–827 (1996).
 26. Fernández, J., Larrañaga, A., Etxeberria, A., Wang, W. & Sarasua, J. R. A new generation of poly(lactide/ε-caprolactone) polymeric biomaterials for application in the medical field. *J. Biomed. Mater. Res. - Part A* **102**, 3573–3584 (2014).
 27. Wang, J. L. & Dong, C. M. Synthesis, sequential crystallization and morphological evolution of well-defined star-shaped poly(ε-caprolactone)-b-poly(L-lactide) block copolymer. *Macromol. Chem. Phys.* **207**, 554–562 (2006).
 28. Ang, H. Y. *et al.* Tailoring the mechanical and biodegradable properties of binary blends of biomedical thermoplastic elastomer. *J. Mech. Behav. Biomed. Mater.* **79**, 64–72 (2018).
 29. Sarasua, J. R., Remiro, P. M. & Pouyet, J. The mechanical behaviour of PEEK short fibre composites. *J. Mater. Sci.* **30**, 3501–3508 (1995).
 30. Le Borgne, A., Prud, R. E., Sarasua, J.-R., Spassky, N. & Wisniewski, M. Crystallization and Melting Behavior of Polylactides. *Macromolecules* **31**, 3895 (1998).
 31. Zuza, E. *et al.* Glass transition behavior and dynamic fragility in polylactides containing mobile and rigid amorphous fractions. *Polymer (Guildf)*. **49**, 4427–4432 (2008).
 32. Fernández, J., Etxeberria, A. & Sarasua, J. R. In vitro degradation of poly(lactide/δ-valerolactone) copolymers. *Polym. Degrad. Stab.* **112**, 104–116 (2015).
 33. Lehtonen, T. J., Tuominen, J. U. & Hiekkänen, E. Resorbable composites with bioresorbable glass fibers for load-bearing applications. in vitro degradation and degradation mechanism. *Acta Biomater.* **9**, 4868–4877 (2013).
 34. Wu, J. *et al.* In vitro and in vivo characterization of strontium-containing calcium sulfate/poly(amino acid) composite as a novel bioactive graft for bone regeneration. *RSC Adv.* **7**, 54306–54312 (2017).

**Chapter 3: Optimization of Polydopamine coating
in Poly(ϵ -caprolactone)/multiwalled
carbon nanotubes composites for
improvement of mechanical and
bioactive properties**

Summary

Functionalization of Multiwalled carbon nanotubes (MWCNT) with polidopamine (PDA) has proved to be a suitable technique to obtain poly(ϵ -caprolactone) (PCL) composites with high mechanical properties. It is proved that the good interphase is dependent on the PDA coating thickness and PDA fraction. The optimal results are obtained after 6h of reaction. For longer functionalization times PDA layer is enough thick to promote shear stresses which overpass the interphase limit, ultimately achieving a “plateau” in yield stress values. The bioactivity of the optimal scaffolds, PCL containing 2 wt.% of PDA coated carbon nanotubes is proved by XRD showing the presence of hydroxyapatite crystals.

Introduction

Poly(ϵ -caprolactone) (PCL) is a biodegradable semi-crystalline polymer with a wide range of applications such as biodegradable packaging, drug delivery system and 3D scaffold for tissue engineering¹⁻³. It is especially interesting for long term medical implants due to its low degradation rates in human body conditions^{4,5}.

Since the discovery of carbon nanotubes by Iijima in 1991⁶ they are being proposed as a reinforcement of composites for wide of applications. Within these allotropic forms of carbon, the multi-walled carbon nanotubes (MWCNT) are very good electrical conductors and for this reason they are used in electrical and electronic applications^{7,8}. As reinforcement in polymeric matrices they have shown to increase electrical conductivity, especially if a critical value is reached in which the nanotubes are well dispersed and connected^{9,10}. In addition, they have very high specific mechanical properties with theoretical stiffness values close to 1000 MPa and high mechanical resistance, which makes them very good candidates as mechanical reinforcement¹¹. Moreover, for biomedical applications, it is one of the most studied nano-reinforcement in a variety of applications as a contrast agent in diagnostic applications¹², electromechanical biosensors¹³ or genetic release and drugs^{14,15}.

It is important to highlight their use in tissue engineering together with biodegradable polymers, since it has been reported MWCNT to be a good substrate for cell adhesion

and to promote the signals of neuronal cells^{10,16}. For all these reason the study of PCL and MWCNT composites has achieve great success in developing materials for tissue engineering in application such as nerve conduit¹⁷.

Despite these successes, PCL/MWCNT composites do not achieve sufficient mechanical properties for use in hard tissue regeneration, such bone or cartilage. A common strategy to overcome this drawback is the use of reinforcement functionalization. Polydopamine (PDA) is a mussel-inspired bio-adhesive widely use in biomedical applications, especially due to high adhesion capacity on organic and inorganic surfaces¹⁸⁻²⁰. PDA has been widely used as a coating material for carbon nanotubes^{20,21}, graphene²² and boron nitride nanotubes²³ revealing the capacity to enhance mechanical and thermal properties in composites. Moreover, the most promising attribute of PDA coating is the capacity to provide to the surfaces functional groups that can link other molecules with biological activity. This have been explored grafting to PDA molecules such DNA²⁴, growth factors^{25,26} and metal nanoparticles²⁷. The result of these studies have demonstrated also an improvement in nano-particle dispersion in water, reducing hidrophobicity²⁸ that is a key factor in cytotoxicity of carbon nanotubes²⁹.

Hence, PDA is a good candidate for functionalize MWCNT in PCL matrix composites since can provide a better reinforcement/matrix adhesion and provide the capacity to form hydroxyapatite due to the capacity of attach Ca⁺ cations and acts as a nucleation points. Nevertheless, to the best of the author's knowledge, no study have considered the effect of the PDA coating thickness in mechanical properties of the composites. This is always a key factor for reinforcement coating since thick layers in adhesives are related with an increment of shear stress in the interphase. To overcome this, in the present work a PDA functionalization quantity study in MWCNT and PCL nanocomposites is performed. The aim of the study is to stablish the optimal methodology for coating and dispersing nanotubes in order to obtain high mechanical properties PCL composites.

Several studies have reported that PDA coating of nanotubes could promote the formation of hydroxyapatite in their surface due to interaction of Ca²⁺ ions with functional groups of polydopamine^{30,31}. It would be of special interest to demonstrate that the same result could be achieved using low quantities of nanotubes dispersed in a biodegradable polymer matrix. Hence the possible effect in bioactivity of PDA coating nanotubes is going to be

studied in PCL with MWCNT composite scaffolds. Samples are going to be evaluated by X-ray diffractometry (XRD) to study the possibility of hydroxyapatite formation on the surface after being submerged for 28 days in simulated body fluid (SBF).

Materials and methods

Poly(ϵ -caprolactone) (PCL) CAPA6500, with weight average molecular weight (M_w) of 147.6 kDa and a dispersity (D) of 1.49 was provided by Solvay (Perstorp). Graphistrength C100 Multi Walled Carbon Nano-Tubes (MWCNT) were supplied by ARKEMA (France). These MWCNT have 5 to 15 walls, average diameters of 5 to 20 nm and lengths of 0.5 to 2 μ m. Dopamine hydrochloride, tris(hydroxymethyl)aminomethane (Trizma® base), NaCl, NaHCO₃, KCl, K₂HPO₄·3H₂O, MgCl₂·6H₂O, CaCl₂, Na₂SO₄, hydrochloric acid (HCl, 37%) and formic acid (> 98% assay) were purchased from Sigma-Aldrich (Spain).

Composite preparation

For composite preparation first, 50 ppm of nanotubes were added to formic acid and then were dispersed by ultrasonic homogenizer Q500 at 80% amplitude with 14 mm tip for 10 min. The solution of formic acid/MWCNT was refrigerated under continuous cool water stream. Then PCL was added and solved with magnetic stirring for 1h to obtain the composites having 0, 0.5%, 1% and 2% of MWCNT in weight percentage. Next, the mixing was dispersed by ultrasonic homogenizer again for 20 min at the same conditions and frozen at -24 °C for 24 h. Formic acid was eliminated by sublimation at 0.05 mbar for 4h using liquid nitrogen trap for recovery. Finally 1mm thick plates were prepared by hot press Collin P200E at 150 °C and 25MPa. On none and Composites were named using code "PCLX.X_DY" where X.X is the weight percentage of MWCNT in mass composition and Y time of dopamine functionalization.

Dopamine functionalization

To evaluate the optimal functionalization conditions, samples with 2wt.% of nanotubes with different times of functionalization (0, 3, 6, 12, 18 and 24h) were prepared according to literature procedures²⁶. Firstly, 200 ppm of MWNTs were sonicated in an ultrasonic homogenizer Q500 at 60% amplitude with 14 mm tip for 10 min in Tris-HCl (pH 8.5, 10

mM) buffer solution. Then, DOPA hydrochloride was added in 4:1 (hPDA:MWCNT) mass proportion to the solution, followed by stirring at room temperature for different times (3, 6, 12, 18 and 24h). Next, PDA-coated MWNTs were filtered with large quantity of deionized water several times to remove excessive PDA. At last, the filtered products were dried in vacuum at 50 °C for 2 hours, and the resultant was named as MWCNTD-X, where X is reaction time.

Coated nanotubes were studied with X-ray photoelectron spectroscopy (XPS) to ensure dopamine adhesion. SPECS system was used equipped with Phoibos 150 1D-DLD energy analyzer and monochromatic radiation source Focus 500 with Al anode (1486.6 eV).

Dopamine quantity was determined using thermogravimetric analysis (TGA) model Q50 (TA instruments). 10-15 mg of neat carbon nanotubes, DOPA hydrochloride and nanotubes coated with PDA at different times were heated from room temperature to 500 °C at a constant rate of 10 °C min⁻¹ under a nitrogen atmosphere.

To study the effect of polydopamine layer thickness on mechanical properties of PCL, samples were subjected to uniaxial tensile mode tests in the Instron 5565 testing machine at 10 mm min⁻¹ deformation rate. ISO 37-2 was followed for specimen preparation. Five samples for composition were tested (n=5). The young modulus (E) was calculated using linear fitting at 2% of strain rate.

Composite characterization

Once determined that the best time of functionalization was 6h, composites with different amount of reinforcement (0, 0.5, 1 and 2 wt.%) were prepared with non-functionalized and functionalized nanotubes (MWCNT and MWCNTD-06) according to the method explained previously. Basic mechanical characterization was performed in an Instron 5565 testing machine at the same conditions described before.

Young modulus ($E_{2\%}$) is going to be defined using linear fitting at first 2% of strain and yield stress (S_y) with the first local maximum point.

$$E_{2\%} \text{ improvement } (\%) = \frac{E_{\text{composite}} * 100}{E_{PCL}} \quad (1)$$

$$S_y \text{ improvement (\%)} = \frac{S_{y,composite} * 100}{S_{y,PCL}} \quad (2)$$

Moreover, to compare mechanical properties at different temperatures and viscoelastic properties the Dynamic-Mechanical-Thermal analysis (DMTA) was employed (Mettler Toledo DMA/SDTA861e). Samples of 1x4x10 mm were tested in tension mode from -80 to 20°C at 1Hz frequency. Measurements were carried out in the elastic region by setting the maximum load at 2N and maximum displacement at 3 μm. An offset of 50% was fixed to do test in complete tension-tension mode.

Bioactivity study in scaffolds

Many works in literature reported the bioactivity as the capacity of the material to form hydroxyapatite at simulated human body conditions. In this work, the bioactivity of the samples was studied at 37°C and submerging the samples in simulating body fluid (SBF) to compare the possible activity induced by PDA on nanotubes.

Scaffolds were prepared using solvent casting particulate leaching method for neat PCL, PCL with non-coated 2% wt. carbon nanotubes and 2% wt. functionalized nanotubes (MWCNTD-06). To maximize qualitative results samples with high area-volumen shapes were prepared. Scaffolds were prepared according to literature procedures³². Firstly, PCL was dissolved in dichloromethane in proportion 1:10 mg/ml. Then, NaCl (200-355 μm) was added in a 90:10 volume proportion and mechanically compounded. Next, dichloromethane was evaporated in vacuum at 50mbar for 24h. Finally, NaCl was removed submerging samples in deionized water for 2 days, changing water every 12 h. Scaffolds of ≈ 1.1 mm thickness were obtained.

SBF was prepared according to method described by T. Kobuto et al³³. 10x10 mm samples were submerged in 40 ml SBF and stored at 37 ± 0.5°C for 21 days. SBF was substituted every 3 days. Then, samples were washed with deionized water and dried in vacuum at 50 mbar for 24h. The formation and crystallization of hydroxyapatite was confirmed by means of X-ray diffractometry (XRD). The X-ray powder diffraction patterns were collected by a PHILIPS X'PERT PRO automatic diffractometer operating at 40 kV and 40 mA, in Theta-Theta configuration, secondary monochromator with Cu-K(alpha) radiation (λ = 1.5418 Å) and a PIXcel solid state detector.

Results and discussion

Dopamine coating characterization

The coating of polydopamine (PDA) on carbon nanotubes was confirmed by XPS. Figure 3-1 shows the survey spectra of MWCNT and PDA coated nanotubes. Neat MWCNT spectra shows the presence of C_{1s} (284.6 eV) on the surface as can be expected. After coating, survey spectra shows new peaks at O_{1s} (532.6 eV) and N_{1s} (399.6 eV). The presence of Nitrogen on the surface is related to the amine groups of PDA and confirms the dopamine coating. Unfortunately, as a carbon based nanoparticle, the relation N/C signal ration cannot be used to compare with PDA N/C ratio, but N/O ratio in coated nanotubes is 2.29 near to the theoretical value reported for PDA (N/O \approx 2).

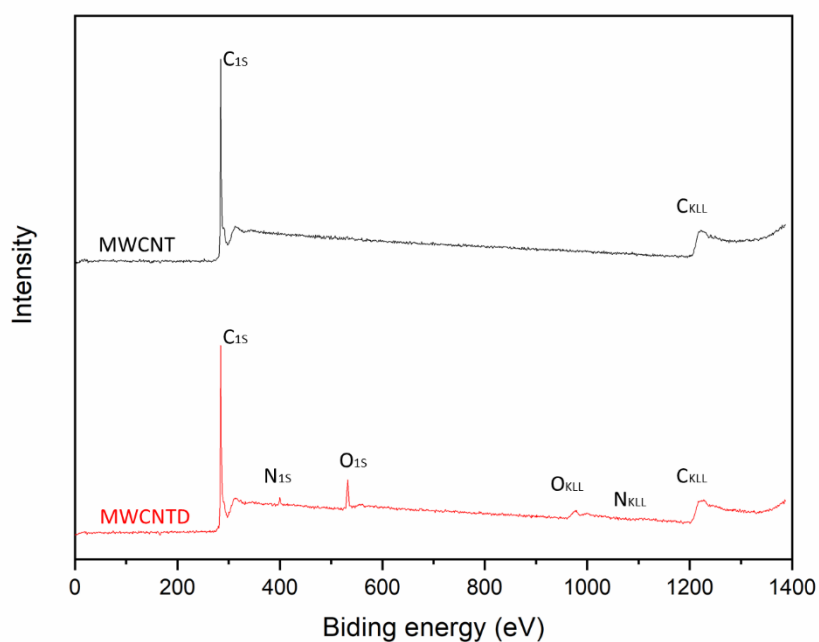


Figure 3-1. XPS survey spectra of MWCNT and poly(dopamine) functionalized MWCNTD.

Optimization of the Functionalization process

The aim of this part of the work is to study the functionalization process conditions to get the optimal coating thickness which eventually will deal to the optimal mechanical properties. For this study the composite of 2% wt. nanotube was employed. In order to

quantify the PDA coating in nanotubes TGA analysis under nitrogen atmosphere were used. As shown in Figure 3-2 neat MWCNT do not show any degradation at 500°C. From this standpoint one can consider that the drop in mass of coated samples is related to PDA. The dopamine fraction was calculated according to equation 3:

$$\text{Dopamine (\%)} = \frac{\Delta\text{CNTD (\%)}}{\Delta\text{PDA(\%)}} \quad (3)$$

Where ΔPDA is the drop in mass (%) for neat PDA at 500°C ($22 \pm 2\%$) and ΔMWCNTD is the drop in mass (%) of coated nanotubes. Table 3-1 resumes TGA results and mechanical properties of PCL/MWCNTD composites at different times of PDA functionalization.

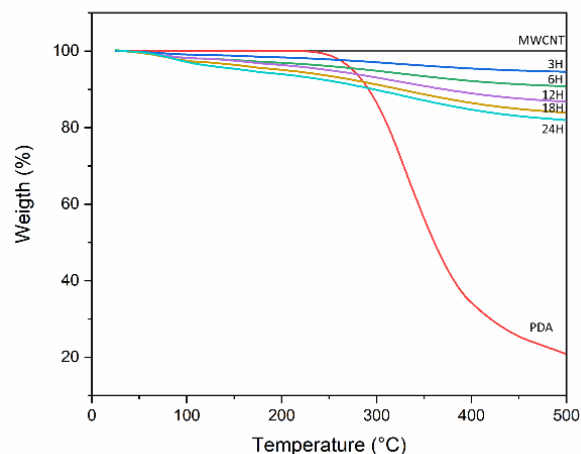
Table 3-1. Summary of functionalization study from TGA and Traction test analysis.

Name	Reaction time (h)	TGA (%)*	Dopamine (%)**	E _{2%} (MPa)	S _y (MPa)
PCL	-	-	-	267 ± 12	11.6 ± 0.9
PCL2.0	0	99.9 ± 0.2	00.0	323 ± 09	14.8 ± 0.3
PCL2.0_D03	3	93.3 ± 0.5	11.8	369 ± 04	16.2 ± 0.2
PCL2.0_D06	6	89.3 ± 0.2	18.7	387 ± 13	17.5 ± 0.3
PCL2.0_D12	12	86.0 ± 0.3	24.6	372 ± 11	16.0 ± 0.1
PCL2.0_D18	18	81.9 ± 0.4	31.7	362 ± 10	16.2 ± 0.3
PCL2.0_D24	24	81.0 ± 0.3	33.4	340 ± 10	15.9 ± 0.2

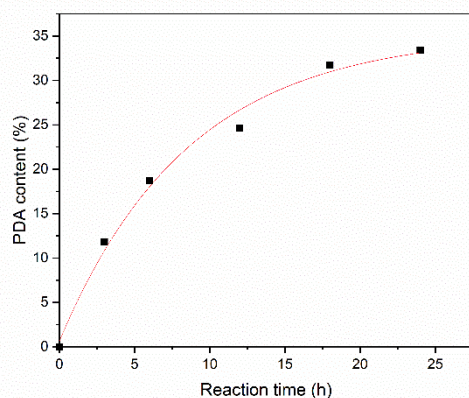
* Values at 500°C.

**Using formula (1).

According to Table 3-1 and Figure 3-2 dopamine fraction shows an exponential decay relation ($R^2 = 0.99$) with functionalization time. No big difference was observed for 18h and 24h reaction times concluding that the reaction reaches its maximum efficiency around 24h.



(a)



(b)

Figure 3-2. (a) TGA curves of PDA, and functionalized nanotubes at different times.(b) PDA fraction with reaction time.

To analyze the effect of the PDA functionalization process on mechanical properties tensile test were performed and compared for neat PCL, PCL with uncoated 2wt.% MWCNT and PCL with coated 2wt.% MWCNT (see Figure 3-3). On one hand stress-strain curves shown a clear improvement in stiffness and strength with composite samples coated with PDA. On the other hand PDA coating is changing the shape of plastic peak reducing the peak width. This behavior is probably related to the effect of interphase adhesion of PDA.

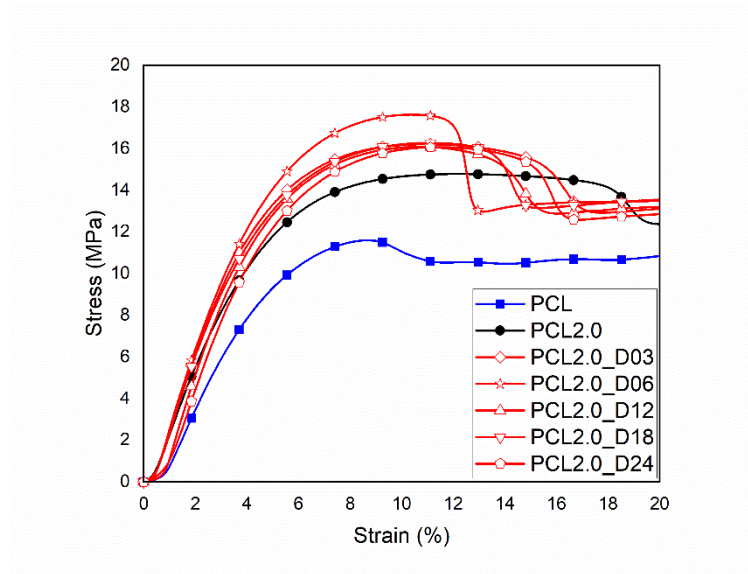
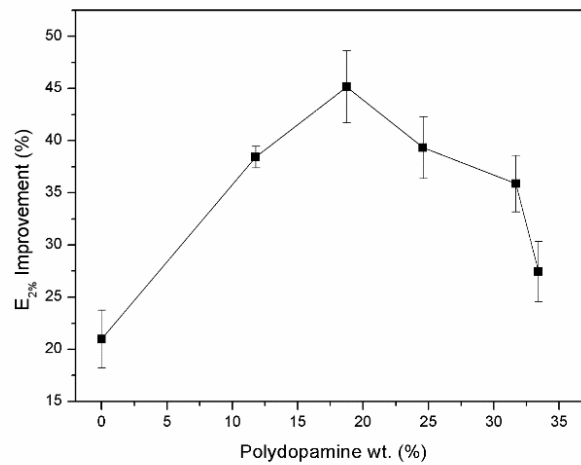
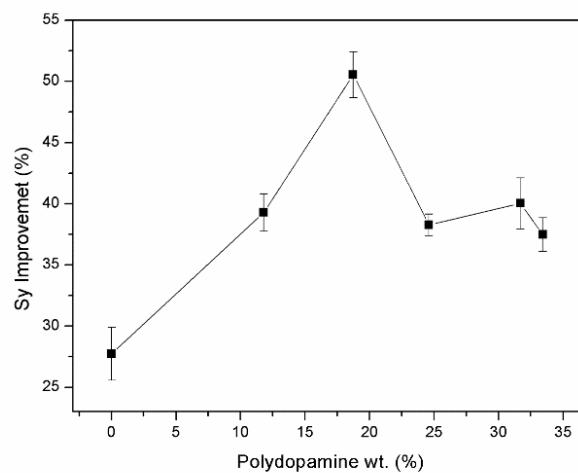


Figure 3-3. Stress-strain curves of PCL and PCL+CNT composites with different times of PDA functionalization.

In order to measure these effects of PDA the improvement ratio of the young's modulus ($E_{2\%}$) and yield stress (S_y) were calculated according to equation 1 and equation 2 and their evolution are graphed in Figure 3-4. Both, stiffness and yield strength increase up to a maximum and then decrease with functionalization time or PDA fraction content. The stiffness is improved in a maximum of 45% comparing to neat PCL after 6h of MWCNT functionalization. In fact, the PDA coating increases de young's modulus value from 267 MPa to 387 MPa. The same behavior is noticed for yield strength reaching the 50% of improvement after 6h of functionalization. In this case, the presence of the PDA coating increases the value from 11.6 MPa to 17.5 MPa.



(a)



(b)

Figure 3-4. (a) Young modulus evolution with PDA content and (b) Yield point evolution with PDA content.

Even though the optimal mechanical properties are obtained for 6h of functionalization, in general PDA coating improves mechanical properties in PCL/MWCNT composites. This suggests a good interaction in the interphases of MWCNT-PDA and PDA-PCL when PDA layer is thin (PDA fraction of 18.7%). For higher fractions of PDA the coating layer seems to be enough thick to promote shear stress increase, overpassing the interphase capacity. This is evident in S_y evolution (Figure 3-4b), where a plateau is found after the

maximum. At the micromechanical level, an increase in adhesive thickness implies an increase in adhesive deformation under load. The failure seems to occur at a critical level of shear strain, so that the ability to transmit the load to the PDA reinforcement is limited.

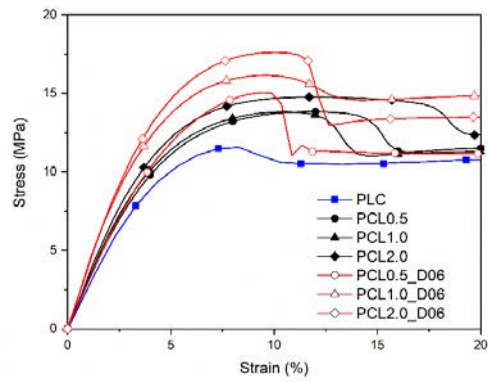
Composite characterization

In the previous section it was demonstrated that the optimal functionalization process is achieved after 6h. In this section the mechanical properties of PCL composites having uncoated and PDA coated 0, 0.5, 1 and 2% of MWCNT are going to present.

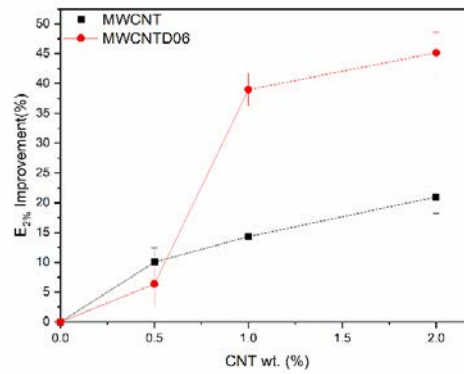
Table 3-2 summarizes the values of the stiffness and yield strength obtained from stress-strain curves shown in Figure 3-5a. For mechanical properties, comparison Young modulus ($E_{2\%}$) and yield strength (S_y) improvement were calculated following equation 1 and equation 2. Mechanical properties improvement is impressive for all composition for two main reasons (1) MWCNT incorporation and the good dispersion and (2) PDA coating. For example, stiffness increases from 267 MPa to 323 MPa barely due to MWCNT presence; and to 387 MPa when coating the nanotubes. In case of yield strength, it increases from 11.6 MPa to 14.8 MPa and to 17.5 MPa. Figure 3-6 B) and C) they show the improvements in mechanical properties of the functionalized and non-functionalized composites. Except for the case of Young's modulus in the composition of 0.5% MWCNT with PDA, the improvement appears linear with the amount of reinforcement for both types, a sign of good dispersion of the nanocomposite. Furthermore, the improvement of PDA incorporation seems to be constant with the amount of nanotubes.

Table 3-2. Mechanical properties of PCL and CNT composites from standard tensile test.

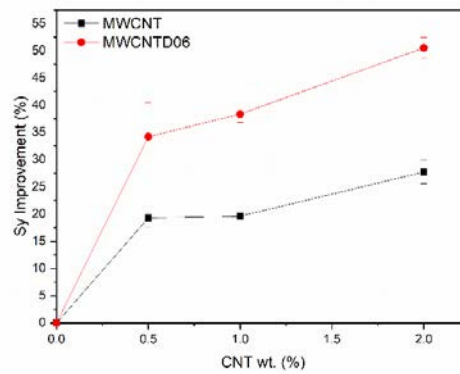
	$E_{2\%}$ (MPa)	S_y (MPa)
PCL	267 ± 12	11.6 ± 0.9
PCL+0.5% CNT	294 ± 07	13.8 ± 0.2
PCL+1.0% CNT	305 ± 01	13.9 ± 0.1
PCL+2.0% CNT	323 ± 09	14.8 ± 0.3
PCL+0.5% CNTD06	284 ± 11	15.6 ± 1.0
PCL+1.0% CNTD06	371 ± 10	16.1 ± 0.3
PCL+2.0% CNTD06	387 ± 13	17.5 ± 0.3



(a)



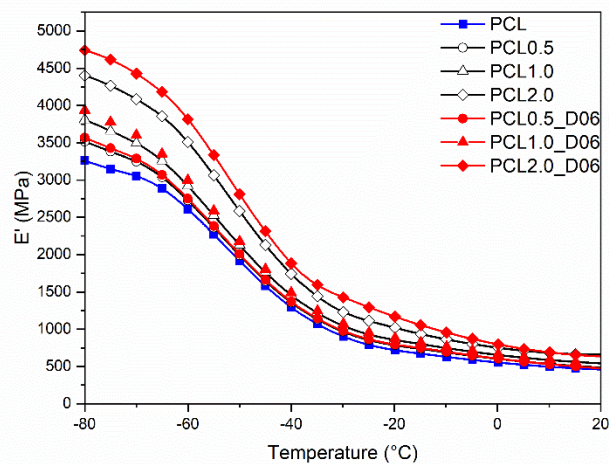
(b)



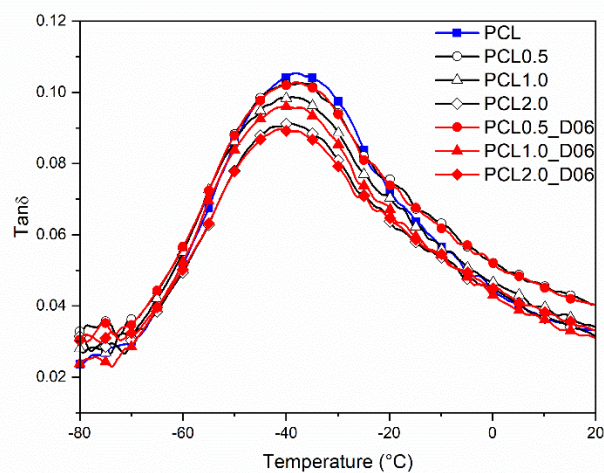
(c)

Figure 3-5. Mechanical properties of PCL and uncoated and coated nanotube composites (a) Stress-strain curves of. (b) Young modulus improvement and (c) Yield strength improvement.

Figure 3-6 shows DMTA curves of PCL and PCL composites. Storage modulus (E') is increased with filler content as expected. The effect of the PDA coating on dynamic stiffness is specially visible for 2% wt.. The value increases from 3320 MPa to 4550 MPa at -80°C . The peak of $\text{Tan}\delta$ at T_g decreases gradually with nanotube content from 0.105 to 0.091 for 2% of CNT composition. This drop in peak is sharper for PDA coated samples suggesting the effect of a high molecular interaction in the composite interphase.



(a)



(b)

Figure 3-6. (a) Storage modulus E' and (b) $\text{tan}\delta$ curves from DMTA for PCL and PCL composites with coated and non-coated nanotubes.

In order to study the interphase behavior the evolution of the height of the $\tan\delta$ peak at T_g in function of the reinforcement particles is analyzed according equation 4:

$$\frac{\text{Tan}\delta_{\text{Composite}}}{\text{Tan}\delta_{\text{PCL}}} = 1 - b * V_r \quad (4)$$

Where V_r is the volume fraction of reinforcement and b the parameter giving account of the interaction/adhesion level. When $b=1$ the $\tan\delta$ reduction is proportional to volume fraction. If $b \geq 1$, damping ($\tan\delta$) is dropping less steeply hence an interaction/adhesion at polymer/particle interfaces can be assumed. If $b \leq 1$ viscoelastic lost in composites is higher than in neat polymer fraction at the fiber/matrix interfaces and therefore bad adhesion level is concluded. Figure 3-7 shows the $\tan\delta$ peak values at T_g for PCL and its composites. The figure includes a linear regression analysis with $R^2=0.91$ and 0.89 for coated and no coated nanotubes respectively.

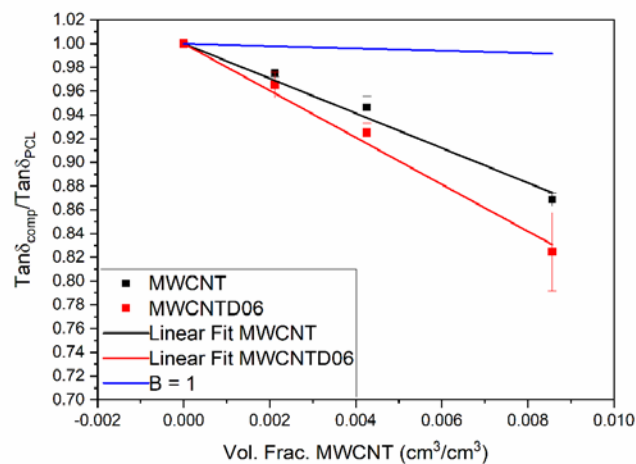


Figure 3-7. $\text{Tan}\delta$ evolution with nanotube volume fraction from DMTA analysis.

Adjusted B parameter for PCL/CNT and PCL/CNTD are 14 and 19, respectively. These values are much higher than the ones presented by traditional fiber reinforcement composites with $B \approx 1-2^{34}$. This might be related to the size effect of nanoparticles. In general, the interaction between the matrix and reinforcement is correlated to the area of the filler. In our case, the PCL is interacting with nanoparticles, MWCNT, having a high area-volume relation. Consequently, the amount of mobile polymeric chains of the matrix

is much restrained than in traditional fiber composites. Therefore, the effect of MWCNT nanoparticles on PCL might be high especially for low quantities of reinforcement. However, DMTA analysis is not sensitive enough for statistically significant results between functionalized and non-functionalized nanotubes.

Bioactivity study

Bioactivity was analyzed by submerging scaffolds of PCL, PCL with uncoated nanotubes and PCL with PDA coated nanotubes in SBF for 28 days. In order to demonstrate the presence of hydroxyapatite formation on the surface of the scaffold XRD analysis was performed. Samples with PDA coated carbon nanotubes show new peaks at 31.59° , 32.02° , 45.38° and 66.23° according to crystalline hydroxyapatite (see Figure 3-8).

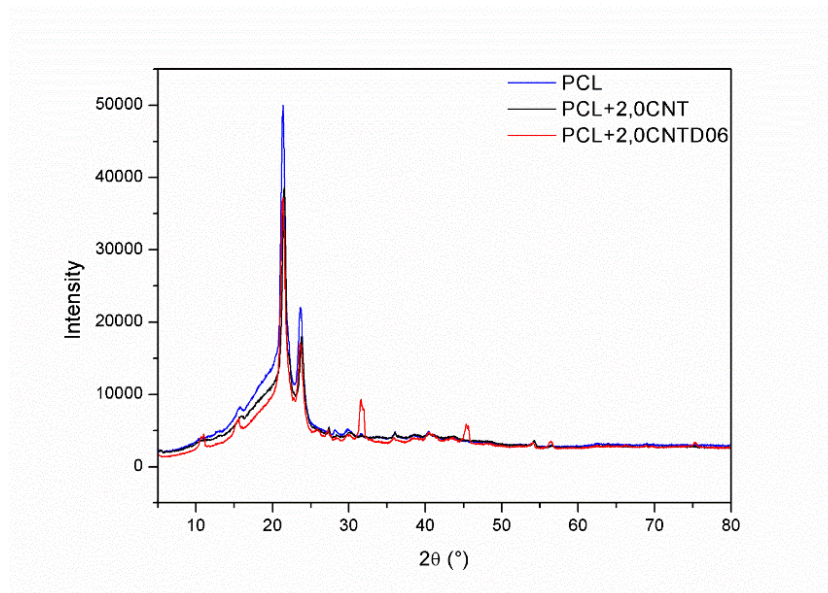


Figure 3-8. XRD patterns of PCL and PCL with coated and no-coated carbon nanotubes after 28 days submerged in SBF.

Several studies have demonstrated that PDA can attach Ca^{2+} cations which could act as a nucleation points for hydroxyapatite formation. In this study XRD results show that this effect can be achieved by coated nanotubes on the surface of PCL. This could be useful in comparison with simple surface functionalization for degradable polymers since polymer surface erosion can expose new coated nanotubes and therefore the bioactivity of these materials is less sensitive to hydrolytic degradation of the surface.

Conclusions

The inclusion of sublimation in MWCNT dispersion process has proved to be a suitable technique to obtain PCL and carbon nanotube composites with high mechanical properties. Moreover, the stiffness and yield strength were improved when the nanotubes were functionalized with polydopamine; a 45% of improvement was observed for E_{young} and 50% of improvement in S_y for 2wt.% coated CNT composites. This enhancement in mechanical properties is related to a good compatibility of PDA with PCL and nanotubes in the interphase. DMTA results have shown a high reduction in viscoelasticity peak $\text{Tan}\delta$ at glass transition temperature for PDA coated and not coated nanotubes confirming the good interaction of nanoparticles in the interphase.

It is proved that the good interphase is dependent on the PDA coating thickness or PDA fraction. The optimal results are obtained after 6h of reaction. For longer functionalization times PDA layer is enough thick to promote shear stresses which overpass the interphase limit, ultimately achieving a plateau in yield stress values.

The bioactivity of the optimal scaffolds, PCL containing 2 wt.% of PDA coated carbon nanotubes, is proved by XRD showing the presence of hydroxyapatite crystals. These results demonstrate the possibility of having continuous bioactive composites less sensitive to the surface hydrolytic erosion in biodegradable polymers.

References

1. Jimenez, G., Ogata, N., Kawai, H. & Ogihara, T. Structure and thermal/mechanical properties of poly(ϵ -caprolactone)-clay blend. *J. Appl. Polym. Sci.* **64**, 2211–2220 (1997).
2. Sanchez-Rexach, E. *et al.* Novel biodegradable and non-fouling systems for controlled-release based on poly(ϵ -caprolactone)/Quercetin blends and biomimetic bacterial S-layer coatings. *RSC Adv.* **9**, 24154–24163 (2019).
3. Sanchez-Rexach, E., Martínez de Arenaza, I., Sarasua, J. R. & Meaurio, E. Antimicrobial poly(ϵ -caprolactone)/thymol blends: Phase behavior, interactions and drug release kinetics. *Eur. Polym. J.* **83**, 288–299 (2016).
4. Woodruff, M. A. & Hutmacher, D. W. The return of a forgotten polymer - Polycaprolactone in the 21st century. *Prog. Polym. Sci.* **35**, 1217–1256 (2010).
5. Larrañaga, A., Aldazabal, P., Martín, F. J. & Sarasua, J. R. Hydrolytic degradation and bioactivity of lactide and caprolactone based sponge-like scaffolds loaded with bioactive glass particles. *Polym. Degrad. Stab.* **110**, 121–128 (2014).
6. Iijima, S. Helical microtubules of graphitic carbon. *Nature* **354**, 56–58 (1991).

7. Monthioux, M. *et al.* Carbon Nanotubes. in *Springer Handbooks* vol. PartF1 193–247 (2017).
8. Belin, T. & Epron, F. Characterization methods of carbon nanotubes: A review. *Mater. Sci. Eng. B Solid-State Mater. Adv. Technol.* **119**, 105–118 (2005).
9. Ribeiro, B., Botelho, E. C., Costa, M. L. & Bandeira, C. F. Carbon nanotube buckypaper reinforced polymer composites: A review. *Polimeros* **27**, 247–255 (2017).
10. Li, J. *et al.* Correlations between percolation threshold, dispersion state, and aspect ratio of carbon nanotubes. *Adv. Funct. Mater.* **17**, 3207–3215 (2007).
11. Yao, N. & Lordi, V. Young's modulus of single-walled carbon nanotubes. *J. Appl. Phys.* **84**, 1939–1943 (1998).
12. Gong, H., Peng, R. & Liu, Z. Carbon nanotubes for biomedical imaging: The recent advances. *Adv. Drug Deliv. Rev.* **65**, 1951–1963 (2013).
13. Ojeda, I. *et al.* Grafted-double walled carbon nanotubes as electrochemical platforms for immobilization of antibodies using a metallic-complex chelating polymer: Application to the determination of adiponectin cytokine in serum. *Biosens. Bioelectron.* **74**, 24–29 (2015).
14. Liu, Z., Sun, X., Nakayama-Ratchford, N. & Dai, H. Supramolecular Chemistry on Water-Soluble Carbon Nanotubes for Drug Loading and Delivery. *ACS Nano* **1**, 50–56 (2007).
15. Liu, Z. *et al.* Supramolecular stacking of doxorubicin on carbon nanotubes for in vivo cancer therapy. *Angew. Chemie - Int. Ed.* **48**, 7668–7672 (2009).
16. Lovat, V. *et al.* Carbon nanotube substrates boost neuronal electrical signaling. *Nano Lett.* **5**, 1107–1110 (2005).
17. Yu, W. *et al.* A novel electrospun nerve conduit enhanced by carbon nanotubes for peripheral nerve regeneration. *Nanotechnology* **25**, (2014).
18. Lyngø, M. E., Van Der Westen, R., Postma, A. & Städler, B. Polydopamine - A nature-inspired polymer coating for biomedical science. *Nanoscale* **3**, 4916–4928 (2011).
19. Ruan, M. *et al.* Improved dielectric properties, mechanical properties, and thermal conductivity properties of polymer composites via controlling interfacial compatibility with bio-inspired method. *Appl. Surf. Sci.* **439**, 186–195 (2018).
20. Ling, Y. *et al.* Epoxy resin reinforced with nanothin polydopamine-coated carbon nanotubes: A study of the interfacial polymer layer thickness. *RSC Adv.* **6**, 31037–31045 (2016).
21. Wang, Y. *et al.* Ultra-stretchable, sensitive and durable strain sensors based on polydopamine encapsulated carbon nanotubes/elastic bands. *J. Mater. Chem. C* **6**, 8160–8170 (2018).
22. Li, W. *et al.* Effectively Exerting the Reinforcement of Dopamine Reduced Graphene Oxide on Epoxy-Based Composites via Strengthened Interfacial Bonding. *ACS Appl. Mater. Interfaces* **8**, 13037–13050 (2016).
23. Thakur, V. K. *et al.* Novel polymer nanocomposites from bioinspired green aqueous functionalization of BNNTs. *Polym. Chem.* **3**, 962–969 (2012).
24. Ham, H. O., Liu, Z., Lau, K. H. A., Lee, H. & Messersmith, P. B. Facile DNA immobilization on surfaces through a catecholamine polymer. *Angew. Chemie - Int. Ed.* **50**, 732–736 (2011).

25. Tao, C., Yang, S., Zhang, J. & Wang, J. Surface modification of diamond-like carbon films with protein via polydopamine inspired coatings. *Appl. Surf. Sci.* **256**, 294–297 (2009).
26. Lee, Y. Bin *et al.* Polydopamine-mediated immobilization of multiple bioactive molecules for the development of functional vascular graft materials. *Biomaterials* **33**, 8343–8352 (2012).
27. De Victoria Rodríguez, M., Brunet, E., Nocchetti, M., Presciutti, F. & Costantino, F. Redox properties of LDH microcrystals coated with a catechol-bearing phosphonate derived from dopamine. *RSC Adv.* **4**, 26912–26917 (2014).
28. Wu, H. & Kessler, M. R. Multifunctional Cyanate Ester Nanocomposites Reinforced by Hexagonal Boron Nitride after Noncovalent Biomimetic Functionalization. *ACS Appl. Mater. Interfaces* **7**, 5915–5926 (2015).
29. Obarzanek-Fojt, M. *et al.* From implantation to degradation - are poly (L-lactide)/multiwall carbon nanotube composite materials really cytocompatible? *Nanomedicine Nanotechnology, Biol. Med.* **10**, e1041–e1051 (2014).
30. Yan, P. *et al.* The in vitro biomineralization and cytocompatibility of polydopamine coated carbon nanotubes. *Appl. Surf. Sci.* **257**, 4849–4855 (2011).
31. Lee, M., Ku, S. H., Ryu, J. & Park, C. B. Mussel-inspired functionalization of carbon nanotubes for hydroxyapatite mineralization. *J. Mater. Chem.* **20**, 8848–8853 (2010).
32. Larrañaga, A. *et al.* A study of the mechanical properties and cytocompatibility of lactide and caprolactone based scaffolds filled with inorganic bioactive particles. *Mater. Sci. Eng. C* **42**, 451–460 (2014).
33. Kokubo, T. & Takadama, H. How useful is SBF in predicting in vivo bone bioactivity? *Biomaterials* **27**, 2907–2915 (2006).
34. Sarasua, J. R. & Pouyet, J. Dynamic Mechanical Behavior and Interphase Adhesion of Thermoplastic (PEEK, PES) Short Fiber Composites. *J. Thermoplast. Compos. Mater.* **11**, 2–21 (1998).

Chapter 4: Viscoelasticity and fatigue behavior of Poly(ϵ -caprolactone) and Poly(ϵ -caprolactone)/multiwalled carbon nanotube composites.

Chapter 4.1: Poly(ϵ -caprolactone)

Summary

Two mechanisms dominate the fatigue behavior: (1) strain-softening and (2) crack growing. Dynamic-creep is promoting micro-plastic deformations that are softening by cavitation and crystal deformation. At high stress levels, the creep behavior dominates and thus the samples fail in a ductile mode. At medium stress, formed cracks follow usual fracture mechanics with crack growth. Cracks grow under cyclic stress causing area reduction of the samples, which ultimately causes the failure by sharp neck instability. The “healing” mechanism helps in recovering the stiffness lost by first strain-softening by chain mobility with cycles. Figure 4-1 is a graphical representation of all the processes involved in viscoelastic polymers fatigue summarizing the mechanical behavior involved and their effect.

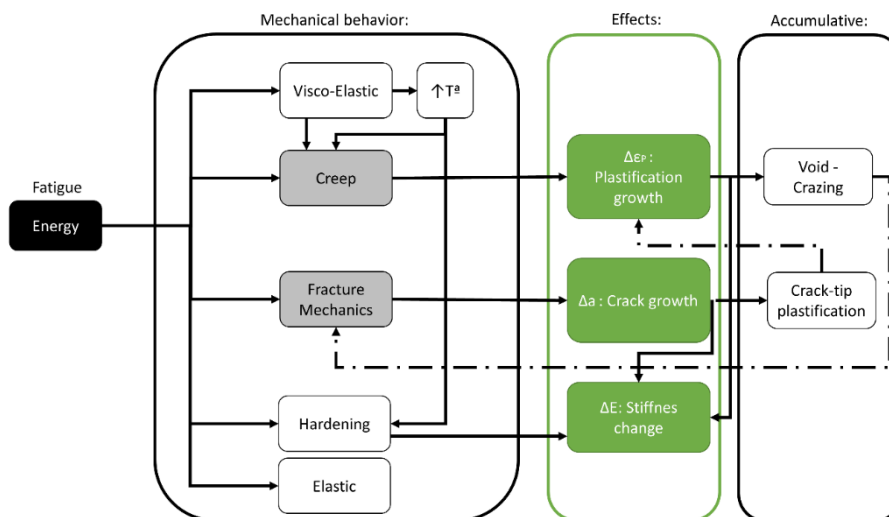


Figure 4-1. Graphical representation of the processes involved in viscoelastic polymers fatigue behavior.

Introduction

Poly(ϵ -caprolactone) (PCL) is a thermoplastic semi-crystalline aliphatic polyester^{1–4}. It exhibits a glass transition temperature of $-60\text{ }^{\circ}\text{C}$ and a melting temperature around $60\text{ }^{\circ}\text{C}$. Therefore, at body temperature ($\approx 37\text{ }^{\circ}\text{C}$) PCL is at the rubbery state and so it presents an excellent ability to deform plastically. Its low melting temperature and its viscoelastic

properties make this polymer easy to process by conventional processing techniques such as, compression-molding, injection or extrusion³.

Moreover, it is a biocompatible and biodegradable polymer approved by the FDA (Food and Drug Administration) showing long hydrolytic degradation time (3-4 years)⁵.

All mentioned physical-mechanical characteristics make PCL a good candidate for using it in the bioengineering or biomedical fields. Not only PCL is reported to be used for stents³, cardiovascular patches and sutures⁶, but also in regenerating peripheral nerves or skin⁷. A great number of research works support the use of PCL and its derivatives also as materials for fabricating scaffolds for their use in soft tissue engineering and drug delivery systems⁸⁻¹⁰.

Despite the fact that the mechanical properties of PCL have been the object of study in several articles using uniaxial static loads such as compression or tensile tests, there is a certain lack in the number of articles on the study of its dynamic properties. And in particular its resistance to fatigue, which is remarkable considering that the behavior of the material may differ and does not have to be the same under mechanical static stress and dynamic stress.

Furthermore, the vast majority of organs and tissues of the human body present a viscoelastic behavior and are subjected to cyclical stresses (and strain) due to the cyclical nature of human activities and/or the different biological rhythms of the human system such as breathing and blood circulation, or the stretching-narrowing of muscles and movement of the joints when walking. Therefore, fatigue is considered one of the most common causes of failure in the different organs/tissues of the human body. Then studying the resistance to fatigue of biomaterials that are introduced into the human body is of vital importance.

Studies on the fatigue behavior of PCL are limited and mostly focused on porous scaffolds^{11,12}. However, fatigue is still insufficiently explored due to the complexity of dynamic properties, enhanced by scaffold inner morphology variability (number of pores, size and interconnection between pores). A new approach is therefore needed to enhance the understanding about cyclic stress in PCL in human body conditions without the problematic introduced in properties by scaffold manufacturing. Moreover, it has been

addressed insufficiently in the literature about PCL scaffold properties simulating human body conditions under fatigue loads.

Therefore, the aim of this study is to perform fatigue tests on PCL film samples simulating human body conditions (37 °C and liquid medium) in order to understand the mechanical behavior of this material under cyclic stress loads. The film-like sample format allows studying in a more controlled and reliable way the causes of failure associated with the material itself and not with morphological factors. The results obtained from this preliminary study can be valuable to understand the differences in the results in case of scaffolds knowing in advance that they are not caused by the material but by the morphology.

Figure 4-2 show the scheme of the complex mechanical behavior of PCL under fatigue loadings. As mentioned before, PCL presents a glass transition temperature $T_g \approx -60$ °C and therefore at human body conditions ($T \approx 37$ °C) has a high mobile amorphous phase³. At these conditions viscoelastic and creep effects (accumulative plasticity, stiffness changes) are notable, changing the usual mechanical behavior especially under dynamic-cyclic loads¹³⁻¹⁵. Furthermore, cracks and fracture mechanics in fatigue and some hardening mechanism related to chain orientations or crystal reorganization may present in PCL^{4,16}. All these phenomena can be explained by carrying out fatigue tests and explaining their correlation by using different models (see Figure 4-2)

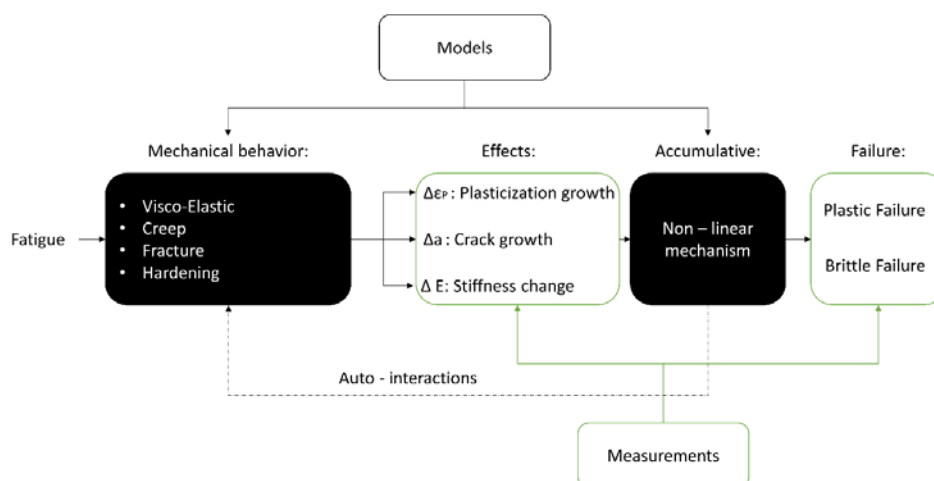


Figure 4-2. Scheme of mechanical behavior of PCL under fatigue loadings.

The mechanical effects (Plasticization and Crack growth) are accumulated during stress/strain cycles by some non-linear mechanism ending up in samples failure. Figure 4-3 shows mentioned accumulative effects and their relationship with failure modes.

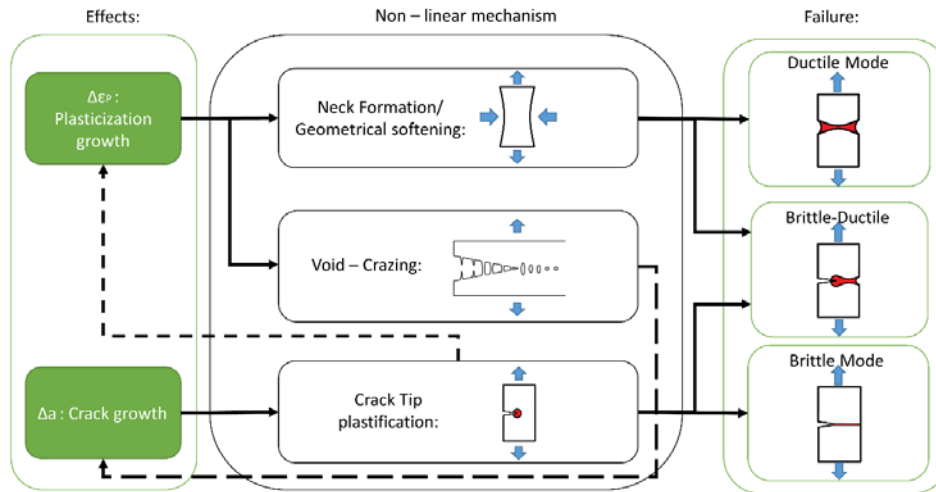


Figure 4-3. Non-linear accumulative mechanism in PCL and their effect in type of failures.

Micro-plasticization is related with cavitation and void formation^{17,18}. The accumulation of voids by stress concentration and coalescence can create eventually defects similar to cracks. This phenomenon is known as crazing. Therefore, this situation approaches fracture mechanics in plastic polymers^{19–21}. The sum of both effects, the creation of crack and stress intensification in the tip, promotes more accumulated plasticization and crazing during cycles²². These mechanisms are synergic and furthers a constant crack growth similar to the metal fatigue mechanics. If the intensity factor in the crack reaches the fracture toughness (K_{IC}) of the material a brittle failure is induced²³.

Plasticization is also related to permanent deformation. Deformation not only occurs in longitudinal direction (applied load direction) but also due to three dimensional elastic-plastic mechanics in a transversal direction. In the latter, area reduction dependent on Poisson constant occurred forming a neck. This is known as necking effect. Necking cause a stress enhancement in its surroundings; this is usually known as “geometrical-softening”^{24,25}. Softening causes strain instabilities and at high loads causes the typical ductile failure. The presence of cracks can also cause an area reduction as they act as

stress concentration points near to the crack tips. The combination of these two mechanisms can lead to a brittle-ductile failure which has similar characteristics of plastic failure but with the presence of a neck in the crack tip.

Figure 4-4 shows how stiffness is affected by different factors in polymers under fatigue loads. Stiffness plays an important role in medical applications, especially in tissue engineering. Some reported studies support that stiffness has a significant effect on cell activity, specifically, on cell proliferation and differentiation²⁶. Therefore, having a material with adequate stiffness over time is essential to achieve adequate regeneration of damaged tissue. However, several studies have reported the softening of PCL under fatigue in scaffolds^{11,27} which could be detrimental for its correct performance unless it is controlled.

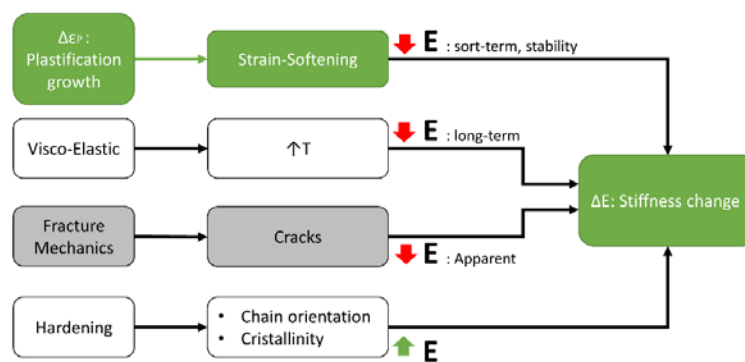


Figure 4-4. Principal factors related to stiffness in polymers under fatigue loads.

The key aspects of stiffness changes are mainly three; plasticization, temperature and crack presence. As mentioned before plasticization promoted by viscoelasticity/creep/high-stress is related to cavitation and void formation. Furthermore, these voids can cause a loss in elastic modulus by some mechanisms usually known as “strain-softening”^{17,19}. Crystal breakage and deformation induced by high strain are included within this mechanism. Another important factor related to viscoelasticity is the temperature rise induced by cyclic chain friction which causes a drop in stiffness due to “thermal fatigue effects”²⁸. Besides, the presence of cracks cause an increase in the compliance of the material and hence a material stiffness reduction²⁹. However, some

other mechanisms can cause an increase in stiffness, known as “hardening”. In general for polymers and specifically for PCL, at high temperatures, over T_g , strain-hardening is not significant but high chain mobility can promote some chain reorientation and crystal rearrangement leading to an increase in the young modulus^{30,31}.

Taking into account all the above mentioned, the aim of this chapter is to study the fatigue properties of PCL including studies of failure analysis at different stress levels, S-N curve characterization and the study of the stiffness evolution under cyclic loads. This work also makes a major contribution to fatigue behavior analysis on polymers by demonstrating the reliability of some specific models to foresee the type of failure.

Material and methods

Materials and sample preparation

The Poly (ϵ -Caprolactone) (PCL) with weight average molecular weight (Mw) of 127 KDa and a polydispersity (D) of 1.49 was supplied by Solvay (Perpstop, England). PCL films with $450 \pm 50 \mu\text{m}$ thickness were obtained by hot pressing in a P 200 E Collin at 85 °C and 25 MPa.

Thermal characterization

The thermal behavior of PCL was carried out using a Q80 (TA instruments) differential scanning calorimeter (DSC). Three samples (n=3). of $7 \pm 1 \text{ mg}$ were heated from -85 °C to 100 °C at $20 \text{ }^\circ\text{C min}^{-1}$ in a nitrogen atmosphere to determine principal thermal characteristic on use conditions after preparation.

Tensile Tests

Mechanical characterization was conducted according to ASTM D822 standard for polymer films. Tensile tests were performed in an Instron 5565 universal testing machine at 500 mm min^{-1} deformation rate and at $37 \pm 0.5 \text{ }^\circ\text{C}$ using a temperature control chamber 3119-600 series. Previous to tensile tests, samples of $100 \text{ mm} \times 10 \text{ mm}$ were punched out from the prepared films and submerged in PBS (pH 7.4) for 48h at $37 \pm 0.5 \text{ }^\circ\text{C}$. This allows a homogenization of the crystallinity of the PCL at the same time that the conditions of

the human body are simulated. At least five samples were tested (n=5). Elastic modulus (E) was obtained using linear fitting at 2% of strain rate and yield stress (σ_y) using maximum stress point.

Fatigue Tests

Fatigue test were performed in liquid medium in a Bose ElectroForce 3200 Series III with a BioDynamic 5100 test instrument according to ASTM D7991 standard for uniaxial polymer fatigue. The testing chamber was maintained at $37\text{ }^{\circ}\text{C} \pm 2\text{ }^{\circ}\text{C}$ by means of pumping water from an external controlled bath at a flowrate of 40mL/min. Fatigue specimens with 55 mm x10 mm dimensions were punched out from the prepared film and were submerged, as in tensile test, in PBS for 48h and at 37°C . Clamp distance was set at 35mm due to chamber size restrictions.

In order to obtain S-N curves, tests were performed under load controlled and followed 3 Hz frequency sinusoidal wave with a stress ratio ($R=\sigma_{\max}-\sigma_{\min}$) of 0.1. Force limits were adjusted individually for sample to test at 10, 8, 6 and 4 MPa and at least 6 samples were tested for each tension level according to ASTM E739-91. Two possible limits were set as stop-criteria: a) when samples reach 10^6 cycles considering this number a limit value that allows to know if the material will present an adequate performance when using it in the human body or b) when the strain value for a sample is over 18%. This second limit present the material failure for excessive plasticization or brittle break.

Result and discussion

Basic characterization

Table 4-1 resumes thermal and mechanical properties of poly (ϵ -caprolactona) (PCL) obtained by DSC and tensile tests. DSC curves show no evidence of thermal properties change after samples being submerged in PBS for 48h at $37\text{ }^{\circ}\text{C}$. Usual glass transition temperature (T_g) of $-60\text{ }^{\circ}\text{C}$ and melting temperature (T_m) of $60\text{ }^{\circ}\text{C}$ were obtained. Crystallinity degree or crystal fraction (χ_c). was assessed by applying equation 1 where $\Delta H_{100\%}$ is the theoretical enthalpy of PCL at 100% of crystallinity (139 J/g^{32}) and ΔH_m is the melting enthalpy.

$$\chi_c = \frac{\Delta H_m}{\Delta H_{100\%}} \quad (1)$$

Crystal fraction was measured to be 46%. This relative high value is the consequence of samples being submerged in PBS for 48h at body temperature where chain mobility is promoted.

Table 4-1. Thermal and Mechanical properties of PCL

T _g (°C)	T _m (°C)	ΔH _m (J/g)	χ _c (%)	E _{2%} (MPa)	σ _y (MPa)	ε _y (%)	ε _b (%)
-60.1 ± 0.4	67.0 ± 0.8	70.5 ± 1.1	46	286 ± 13	13.9 ± 0.3	9.9 ± 0.7	300*

* Strain limit of the temperature control chamber.

Regarding mechanical properties, elastic modulus at 2% of strain (E_{2%}) is obtained by linear fitting (with R ≥ 0.995 for all samples). Yield stress (σ_y) and yield strain (ε_y) values correspond to the first peak point and strain at break (ε_b) to the last point of the graph. Figure 4-5 shows stress-strain curves of PCL samples in tensile test. These curves show classical semicrystalline thermoplastic polymer behavior with and extremely high ductility. All five samples were deformed up to the limit of the tensile machine frame (>300%) despite being tested at high deformation rates (500 mm/min).

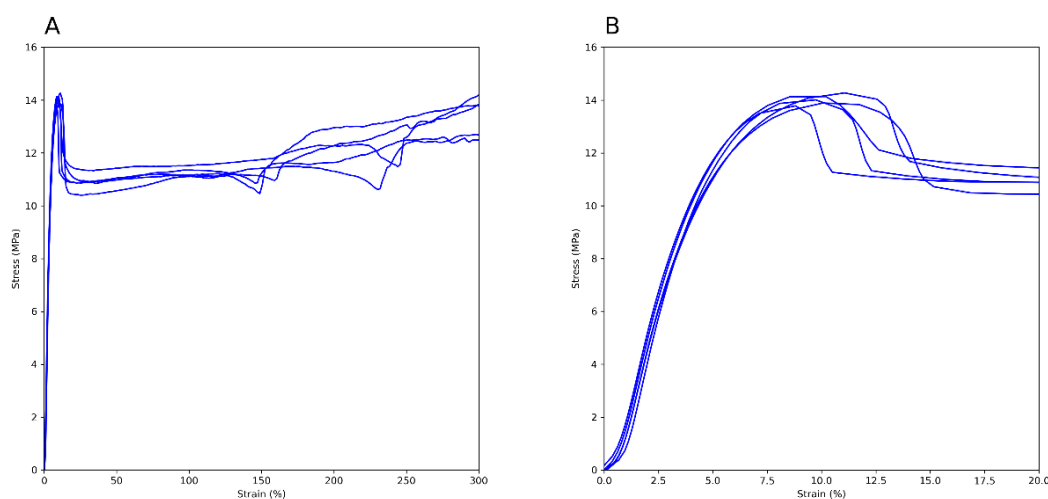


Figure 4-5. A) Stress-Strain curves of five PCL samples and B) zoomed graph of the yield point zone.

Fatigue analysis

As mentioned in the introduction, according to literature PCL shows an extremely complex behavior under fatigue loadings. In order to give an answer to this complex behavior a top-down approach is followed in this section starting from failure analysis and ending with the study of stiffness evolution under cyclic loads.

Failure analysis

Failure of PCL can be classified in four categories: 1) No failure (NF); when samples remain stable during 10^6 cycles. 2) Plastic failure (PF); when an unstable strain deformation occur due to neck formation. 3) Crack-Plastic failure (CPF); when crack growth ends with unstable strain deformation due to area reduction and stress intensity in crack tip. 4) Crack-brittle (CBF); when crack growth ends up in brittle fracture of the sample.

Table 4-2 resume the failure distribution of PCL samples at different fatigue stress loadings. The maximum fatigue value coincides with the value of the yield strength obtained from the tensile test, 14 MPa. This value is considered as the stress at which the sample failures in static mode (1 cycle).

Table 4-2. Failure behavior distribution of PCL samples at different fatigue stress loadings.

Fatigue stress (MPa)	Crack-Brittle failure (%)	Crack-Plastic failure (%)	Plastic failure (%)	No failure (10^6 cycles)
14 *	-	-	100 %	-
10	-	50 %	50 %	-
8	-	100 %	-	-
6	-	100 %	-	-
4	-	25 %	-	75 %

*Value obtained from tensile test

Attending to results PCL shows three different failure behaviors. Transitions to one failure to another are observed close to 10 MPa and 4 MPa.

At low fatigue stresses (4 MPa), no failure (NF) and no cracks were observed for 75% of the PCL samples. This level of stress corresponds to the elastic linear region ($R^2 > 0.995$), close to the stress values corresponding to 2% of strain. At medium fatigue stresses (4-10 MPa), all PCL samples fail by CPF mode. This is related to the loss of linear behavior of

PCL and the “strain-softening” effect due to the high mobile polymer chains in amorphous phase above T_g . It is remarkable that even if samples exhibit large cracks (>50% of the width of the samples) they do not show any brittle fracture and all of them fail due to plastic instability by area reduction.

However, at high fatigue stress (10 MPa), half of the samples show a PF. This region corresponds to the complete loss of linear behavior where stress levels are close to the plateau. At this conditions PCL is under two different softening mechanisms, the previously referred “Strain-softening” and the “Geometrical-softening”. The latter mechanism is the consequence of neck formation under 3D real strain situation which reduces the real area in respect to the engineering area. The stability of plastic deformation will depend on whether the hardening mechanism (for example polymer chain orientation) compensates the area reduction.

The mentioned strain-softening cases can be enhanced by the increase of temperature under cyclic loadings due to the friction of chain mobility. The temperature increase can lead to a decrease in the elastic modulus causing the failure of the material eventually. This type of failure is known as “thermal fatigue failure” and it is the typical failure mode of semi-crystalline polymers at high-stress or high-strain fatigue.

S-N curves

Materials fatigue performance is commonly characterized by an S-N curve. This is often plotted with the cyclic stress (S) against the cycles to failure (N) on a logarithmic scale. The American Society for Testing and Materials defines fatigue life, N_f , as the number of stress cycles of a specified character that a specimen sustains before failure.

Data obtained from fatigue tests at different stress levels were plotted to obtain the S-N curve (see Figure 4-6). The mean values of sustained cycles before failure for each stress level are shown in Table 4-3. From these data one can see that the sustained cycles before failure increases while stress decreases.

Table 4-3. Mean and deviation of sustained cycles for PCL under different fatigue loads.

Stress (MPa)	Cycles
10	13.377 ± 7.982
8	96.566 ± 29.655
6	359.266 ± 123.404
4	966.410 ± 65.211

For further analysis data from Figure 4-6 were fitted using the following linear exponential equation where σ is the stress applied, N number of cycles and “A” and “m” are constants.

$$\sigma = A * N^{-\frac{1}{m}} \quad (2)$$

PCL did not show the usual linear behavior. Therefore, a double linear model was used to fit data from **Figure 4-6** . This behavior is ascribed to the change in failure mode. The inflexion point is observed around 9 MPa. The calculated constant values for this double fitting are summarized in table 4.

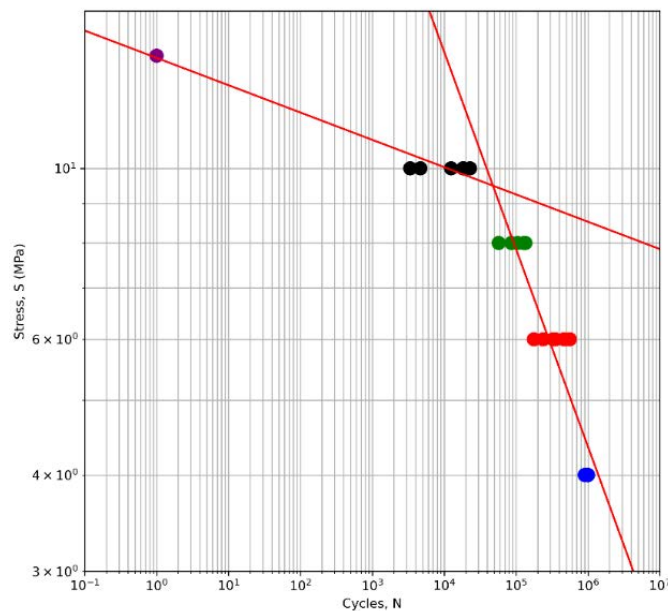


Figure 4-6. S-N curve for PCL in log-log scale for four different stress levels (purple) 10 MPa, (black) 8 MPa, (green) 6MPa, (blue) 4 MPa. Fitting lines in red.

Table 4-4. Exponential parameters (A and m) to fit the S-N curve

Stress levels (MPa)	A (MPa/cycles ^{-1/m})	m
> 9	13.9	28.1
9- 4	149.3	3.9
< 4	> 10E6 Cycles*	> 10E6 Cycles*

* 75% of samples reach the limit of 10⁶ cycles

On one hand the PCL start with an exponential factor m of 28 and after the transition point this exponential starts dropping to a value of 3.9. The drop from 28 to 3.9 in the value of “m” parameters indicates the appearance of a new mechanism in the fatigue behavior of PCL that is shortening the fatigue life at medium stress levels (9-5 MPa). As can be seen from failure analysis this new mechanism is related to crack growing and fracture mechanics. It is important to highlight that this fatigue exponent m in medium stress levels is near to the exponents of usual metals.

Evolution of stiffness under fatigue loadings

In order to understand the role of different mechanical phenomena, such as viscoelasticity, creep and fracture mechanics (crack growth, brittle approach), the evolution or changes in some key mechanical properties (stiffness and crack length) during fatigue test need to be studied. Due to the impossibility of constant crack growth measurements in liquid medium, in this work only the stiffness is going to be studied.

The stiffness is going to be defined by the next formula where E_i is the elastic modulus at i cycle, $\sigma_{max,i}$ and $\sigma_{min,i}$ are the maximum and minimum cycle stresses and $\varepsilon_{max,i}$ and $\varepsilon_{min,i}$ are the maximum and minimum cycle strains

$$E_i = \frac{\sigma_{max,i} - \sigma_{min,i}}{\varepsilon_{max,i} - \varepsilon_{min,i}} \quad (3)$$

Plastic strain at cycle i ($\varepsilon_{p,i}$) is defined by the following formula (4) where $\varepsilon_{min,i}$ is the minimum cycle strain and the $\varepsilon_{min,0}$ is the minimum cycle strain for the first cycle:

$$\varepsilon_{p,i} = \varepsilon_{min,i} - \varepsilon_{min,0} \quad (4)$$

A popular explanation for fatigue modeling is the concept of damage accumulation³³. These models assume that the failure is the consequence of the accumulation of damage

during stress cycles. In the case of PCL damage can derive from two possible mechanisms, the strain-softening and crack growing. Both mechanisms are related to a loss in stiffness. Damage (D_i) is going to be assessed by the following formula (5) where E_i is de young modulus of cycle i and E_0 is the initial young modulus.

$$D_i (\%) = 100 - \frac{E_i \cdot 100}{E_0} \quad (5)$$

Figure 4-7 shows the evolution of damage with cycles in log scale at different fatigue stress levels. At high stress (10 MPa and 8 MPa) the damage grows linearly in log scale until a certain point where it becomes unstable and the growth in damage increases abruptly.

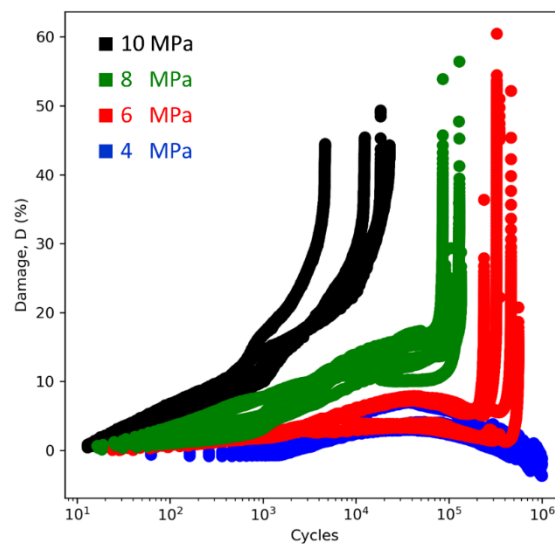


Figure 4-7.The evolution of damage with cycles for different fatigue stress levels

In order to understand this behavior Figure 4-8 shows the relation of damage and accumulated plastic strain in the first 50.000 cycles.

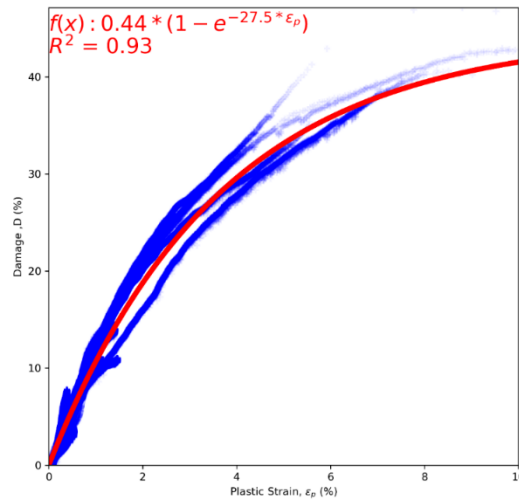


Figure 4-8. Damage-Plastic strain relation at first 50.000 cycles of PCL samples.

This trend is fitted by an exponential decay model employing the next formula (6) where D is the sustained damage, ε_p is the plastic strain and α and β constant parameters.

$$D = \alpha * (1 - e^{-\beta * \varepsilon_p}) \quad (6)$$

The correlation of this model with data have an $R^2 = 0.93$ and is in accordance with the results reported by F. Dtrez et al.³² who applied the same damage-plasticity model in their work. In their study atomic force microscopy (AFM) images of PCL under strain show the deformation of crystals especially in the center, where crystal lamellas are connected. Therefore, the loss of stiffness by strain softening appear to be related to the PCL crystallinity deformation as a principal “strain-softening” mechanism.

For medium stress levels (6MPa), Figure 4-7 show a peak at 50.000 cycles followed by a decrease in damage. According to equation (5) the decrease in damage value is related to the increase in stiffness. This means that samples recover stiffness with cycles. This “healing” effect (in opposite to “damage”) need to be related to structural changes in polymer chains. PCL at 37 °C is 100 °C above its glass transition temperature, so the “strain-hardening” mechanisms is not good candidate due to a high chain mobility. This chain mobility can restore PCL damaged crystals by strain-softening and recover part of

the initial stiffness. Nevertheless near to 200.000 cycles these samples show an exponential increase in damage in the same way of all failed samples. This exponential loss of stiffness is related to the crack growth. The strain-softening creates voids and these voids can merge and form a crack. These cracks then can grow due to usual fracture mechanics. The “healing” effect of crystal reconstruction can recover part of the stiffness of material but cannot repair cracks and therefore the crack growth mechanism continues accumulatively until the crack-plastic failure is reached.

For low stress (4 MPa) the behavior is the same but for some of the samples (75%) the strain softening mechanism is not sufficient to form a critical crack. This finding suggests that for stress bellow 4 MPa the fatigue life of PCL could be extremely large due to the healing effect of crystal reconstruction.

Conclusions

In resume the stiffness analysis supports the notion of two mechanism dominating the fatigue behavior: (1) strain-softening and (2) crack growing. Dynamic-creep is promoting micro-plastic deformations that are softening by cavitation and crystal deformation. At high stress levels, the creep behavior dominates and thus the samples fail in a ductile mode.

At medium stress (from 4 MPa to 9 MPa) creep mechanism is stabilized causing the micro-plasticization process stabilization. However, this micro-plasticization activates the void and crazing mechanism. Formed cracks follow usual fracture mechanics. Cracks grow under cyclic stress causing area reduction of the samples, which ultimately causes the failure by sharp neck instability. The “healing” mechanism helps in recovering the stiffness lost by first strain-softening by chain mobility with cycles. However, when softening reach a critical value of plasticity, cracks form and therefore, this mechanism can not prevent crack growth and ultimate crack-plastic failure.

For samples at low stress (4MPa) creep plasticization come stable at low plastic strain and the material is under the crack growth intensity factor (voids and coalesced voids are under critical lengths at this stress levels). At these levels “healing” mechanism can

prevent crack growth and therefore PCL can be seen as good material for long fatigue life at these stress levels.

References

1. Larrañaga, A. et al. A study of the mechanical properties and cytocompatibility of lactide and caprolactone based scaffolds filled with inorganic bioactive particles. *Mater. Sci. Eng. C* 42, 451–460 (2014).
2. Ugartemendia, J. M., Larrañaga, A., Amestoy, H. & Sarasua, J. R. Supramolecular evolution over an initial period of biodegradation of lactide and caprolactone based medical (co)polyesters. *Polym. Degrad. Stab.* 108, (2014).
3. Woodruff, M. A. & Hutmacher, D. W. The return of a forgotten polymer - Polycaprolactone in the 21st century. *Prog. Polym. Sci.* 35, 1217–1256 (2010).
4. Pires, L. S. O., Fernandes, M. H. F. V. & de Oliveira, J. M. M. Crystallization kinetics of PCL and PCL–glass composites for additive manufacturing. *J. Therm. Anal. Calorim.* 134, 2115–2125 (2018).
5. Dwivedi, R. et al. Polycaprolactone as biomaterial for bone scaffolds: Review of literature. *Journal of Oral Biology and Craniofacial Research* vol. 10 (Craniofacial Research Foundation, 2020).
6. Singh, S., Prakash, C. & Ramakrishna, S. Polymer-Based Additive Manufacturing System. *Additive Manufacturing* (2020). doi:10.1142/9789811224829_0002.
7. Ciardelli, G. & Chiono, V. Materials for peripheral nerve regeneration. *Macromol. Biosci.* 6, 13–26 (2006).
8. Vieira, A. C. et al. Mechanical study of PLA-PCL fibers during in vitro degradation. *J. Mech. Behav. Biomed. Mater.* 4, 451–460 (2011).
9. Sanchez-Rexach, E., Martínez de Arenaza, I., Sarasua, J. R. & Meaurio, E. Antimicrobial poly(ϵ -caprolactone)/thymol blends: Phase behavior, interactions and drug release kinetics. *Eur. Polym. J.* 83, 288–299 (2016).
10. Sanchez-Rexach, E., Meaurio, E. & Sarasua, J. R. Recent developments in drug eluting devices with tailored interfacial properties. *Adv. Colloid Interface Sci.* 249, 181–191 (2017).
11. Panadero, J. A., Vikingsson, L., Gomez Ribelles, J. L., Sencadas, V. & Lanceros-Mendez, S. Fatigue prediction in fibrin poly- ϵ -caprolactone macroporous scaffolds. *J. Mech. Behav. Biomed. Mater.* 28, 55–61 (2013).
12. Fernández, J., Auzmendi, O., Amestoy, H., Diez-Torre, A. & Sarasua, J. R. Mechanical properties and fatigue analysis on poly(ϵ -caprolactone)-polydopamine-coated nanofibers and poly(ϵ -caprolactone)-carbon nanotube composite scaffolds. *Eur. Polym. J.* 94, 208–221 (2017).
13. Martins, C., Pinto, V., Guedes, R. M. & Marques, A. T. Creep and Stress Relaxation Behaviour of PLA-PCL Fibres - A Linear Modelling Approach. *Procedia Eng.* 114, 768–775 (2015).
14. Guedes, R. M., Singh, A. & Pinto, V. Viscoelastic modelling of creep and stress relaxation behaviour in PLA-PCL fibres. *Fibers Polym.* 18, 2443–2453 (2017).

15. Leung, L. H. & Naguib, H. E. Viscoelastic properties of poly(ϵ -caprolactone) - hydroxyapatite micro- and nano-composites. *Polym. Adv. Technol.* 24, 144–150 (2013).
16. Yang, Z., Peng, H., Wang, W. & Liu, T. Crystallization behavior of poly(ϵ -caprolactone)/layered double hydroxide nanocomposites. *J. Appl. Polym. Sci.* 116, 2658–2667 (2010).
17. Lesser, A. J. Changes in mechanical behavior during fatigue of semicrystalline thermoplastics. *J. Appl. Polym. Sci.* 58, 869–879 (1995).
18. Science, M. Microscopic and Molecular Fundamentals of Crazing. *Kobunshi* 42, 389–393 (1993).
19. Estevez, R., Tijssens, M. G. A. & Van Der Giessen, E. Modeling of the competition between shear yielding and crazing in glassy polymers. *J. Mech. Phys. Solids* 48, 2585–2617 (2000).
20. Argon, A. S. Craze initiation in glassy polymers - Revisited. *Polymer (Guildf)*. 52, 2319–2327 (2011).
21. Sauer, J. A. & Hara, M. Effect of molecular variables on crazing and fatigue of polymers. *Adv. Polym. Sci.* 91, 69–118 (1990).
22. Passaglia, E. Crazes and Fracture. *J. Phys. Chem. Solids* 48, 1075–1100 (1987).
23. Sauer, J. A. & Richardson, G. C. Fatigue of polymers. *Int. J. Fract.* 16, 499–532 (1980).
24. Rozanski, A. & Galeski, A. Plastic yielding of semicrystalline polymers affected by amorphous phase. *Int. J. Plast.* 41, 14–29 (2013).
25. Sedighiamiri, A., Govaert, L. E., Kanters, M. J. W. & Van Dommelen, J. A. W. Micromechanics of semicrystalline polymers: Yield kinetics and long-term failure. *J. Polym. Sci. Part B Polym. Phys.* 50, 1664–1679 (2012).
26. De Croos, J. N. A., Dhaliwal, S. S., Grynepas, M. D., Pilliar, R. M. & Kandel, R. A. Cyclic compressive mechanical stimulation induces sequential catabolic and anabolic gene changes in chondrocytes resulting in increased extracellular matrix accumulation. *Matrix Biol.* 25, 323–331 (2006).
27. Fernández, J., Auzmendi, O., Amestoy, H., Diez-Torre, A. & Sarasua, J.-R. Mechanical properties and fatigue analysis on poly(ϵ -caprolactone)-polydopamine-coated nanofibers and poly(ϵ -caprolactone)-carbon nanotube composite scaffolds. *Eur. Polym. J.* 94, (2017).
28. Katunin, A. Thermal fatigue of polymeric composites under repeated loading. *J. Reinf. Plast. Compos.* 31, 1037–1044 (2012).
29. Ramsteiner, F., Schuster, W. & Forster, S. Concepts of Fracture Mechanics for Polymers. 27–50 (2001) doi:10.1007/978-3-662-04556-5_2.
30. Zhao, Y., Keroack, D. & Prud'homme, R. Crystallization under Strain and Resultant Orientation of Poly(ϵ -caprolactone) in Miscible Blends. *Macromolecules* 32, 1218–1225 (1999).
31. Dolynchuk, O. et al. Reversible Shape-Memory Effect in Cross-Linked Linear Poly(ϵ -caprolactone) under Stress and Stress-Free Conditions. *Macromolecules* 50, 3841–3854 (2017).
32. Pitt, C. G., Chasalow, F. I., Hibionada, Y. M., Klimas, D. M. & Schindler, A. Aliphatic polyesters. I. The degradation of poly(ϵ -caprolactone) in vivo. *J. Appl. Polym. Sci.* 26, 3779–3787 (1981).

33. Detrez, F., Cantournet, S. & Seguela, R. Plasticity/damage coupling in semi-crystalline polymers prior to yielding: Micromechanisms and damage law identification. *Polymer (Guildf)*. 52, 1998–2008 (2011).

Chapter 4.2: Fatigue analysis of Poly(ϵ -caprolactone) (PCL) and multiwall carbon nanotubes (MWCNT) composites

Summary

Mutiwalled carbon nanotubes have proof to be a good way to improve fatigue life of PCL at high stress levels (9MPa) triplicating the design life of PCL from 26,487 to 87,622 cycles for 1 wt. % of nanotube content. This fatigue life enhancement appear to be related to a reduction in strain-softening in the first stage of viscoelastic evolution for PCL and a crack growth reduction by crack biding and deboning mechanism.

Polyvinylpyrrolidone coating of nanotubes have shown improve results for 0.5 wt.% MWCNT composite increasing the fatigue life to 98,481 cycles but decreasing for 1 wt.% MWCNT composite. These results suggest that the good interaction in the interphase between PVP and PCL might reduce the chain mobility, but also reduce the benefits of plastification in stopping crack growth mechanism obtaining lower fatigue life values.

Introduction

In chapter 4.1 it was shown that the viscoelastic effect related to high chain mobility could cause accumulative micro-plastification and “strain-softening” by void formation in PCL films under cyclic loadings and human body conditions (fluid medium and 37°C). The coalescence of the voids lead to crack formation which under cyclic stress will grow until plastic-crack failure is reached. A reasonable strategy to minimize this fatigue failure could be the incorporation of a filler with the capacity of reducing polymeric chain mobility by physical-chemical interactions in the interphase.

In Chapter 3, it was proved by Dynamic Mechanical Thermal Analysis (DMTA) analysis that multiwall carbon nanotubes (MWCNT) have a great effect reducing viscoelasticity of the material. Moreover, it is reported in literature that reinforcements such as MWCNTs enhance the fracture toughness of the polymer through so-called composite mechanisms¹⁻³. These composite mechanisms dissipate part of the crack-opening energy and thus reduce the crack propagation rate by increasing the fracture toughness of the composite.

However, there is great difficulty in preparing well-dispersed MWCNT composites due to their specific surface area and strong Van der Walls interactions⁴⁻⁶. This is important, since good dispersion is a key factor in achieving large improvements in mechanical

properties. Many studies of nanoparticle dispersion have largely focused on aqueous solutions, where surfactant molecules are used to achieve stable dispersions^{7,8}. However, this is not practical for composite materials, which require organic solvents and where the use of surfactants can be detrimental⁹. Amphiphilic molecules such as polyvinylpyrrolidone (PVP), which can bind to the hydrophobic surface of MWCNTs, have been tested to solve these problems¹⁰. In addition PVP is non-toxic and biocompatible^{11,12} which makes it an ideal candidate for nanocomposites focused on medical applications.

For these reasons in this work a high stress fatigue testing of PCL and PCL/MWCNT composite films is presented. The effect of different quantities of nanotubes in fatigue life is going to be studied and the effect of PVP as a functionalization material.

Material and methods

The poly (ϵ -Caprolactone) with weight average molecular weight (M_w) of 127 KDa and a dispersity index (D) of 1.49 was supplied by Solvay (Perpstop, England). Graphistrength C100 Multiwalled Carbon Nano-Tubes (MWCNT) were supplied by ARKEMA (France). These MWCNT have 5 to 15 walls, average diameter of 5 nm to 20 nm and lengths of 0.5 μ m to 2 μ m. Polyvinylpyrrolidone (PVP) with weight average molecular weight of 10 KDa was supplied by Sigma Aldrich (Spain). Methanol, dichloromethane and phosphate buffer solution (PBS, pH = 7.4) was supplied by Sigma Aldrich (Spain).

Polyvinylpyrrolidone functionalization

Functionalization of MWCNT with PVP was carried out by simple coating method. First, 200 ppm of nanotubes were added to methanol. Then, MWCNTs were dispersed following the method described in **Figure 4-9**: (1) pre-dispersion with ULTRA-TURRAX T25 homogenizer at 25.000 rpm for 2 min (2) ultrasonic homogenization using the Ultrasonicator UP400st with a flow chamber having 14mm tip sonotrode for 30 min and 300W; where the solution flows in a closed loop from the chamber to the 3-neck flask at 50 ml/min thanks to a peristaltic pump; the temperature of the flask is monitored and adjusted not to exceed 30 °C.

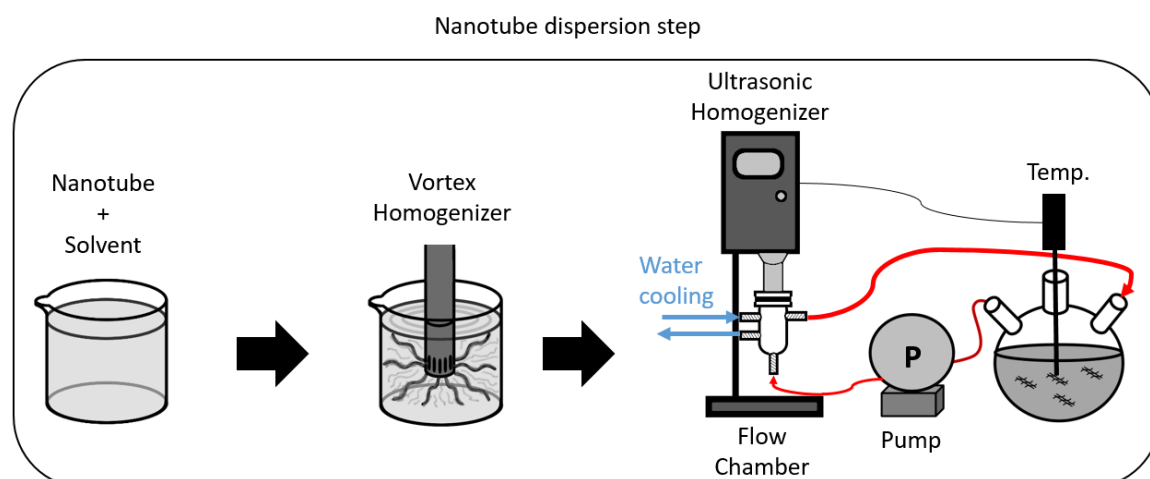


Figure 4-9. Scheme of Multiwalled carbon nanotubes dispersion steps.

After nanotube dispersion PVP was added in a 8:1 (PVP:CNT) mass proportion in 3-neck flask and the ultrasonic dispersion was repeated again for 10 min at the same conditions. The dispersed solution was then filtered using a nylon filter with porosity of 200 nm assisted by vacuum pump. Finally, functionalized nanotubes were recovered by first washing the filter with ethanol and subsequently evaporating it under magnetic stirring.

Sample preparation

For this study composites of PCL with PVP functionalized and non-functionalized MWCNT were prepared according to proportions resumed in **Table 4-5**.

Table 4-5. Sample compositions

Label	CNT content (%)	Functionalized
PCL	0	No
0.5 MWCNT	0.5	No
1.0 MWCNT	1	No
0.5 MWCNT-PVP	0.5	Yes
1.0 MWCNT-PVP	1	Yes

Four steps have to be followed to prepare PCL with MWCNT composites: (1st step) 200 ppm and 400 ppm MWCNT were dispersed in dichloromethane (DCM) for composites having 0.5% and 1.0% of MWCNT, respectively. PCL is added to dispersed MWCNT solution in a proportion to ensure the desire wt.%, then the polymeric solution is again subjected to the ultra-sonication process for 10 min at the same conditions; in this way it

is ensured the good dispersion of MWCNT within the polymer. (3rd Step) The evaporation of DCM is carried out in a fume hood under magnetic stirring for 24h. Then to ensure complete DCM evaporation, the resulting film was hot press in Colling P200 at 85 °C and 25 MPa resulting in 250 µm sheet. Hot press sheets were placed in a chamber at 150°C for 10 min under vacuum of 50 mbar and then 2 h more in vacuum without temperature. (4th Step) Sheets of 450 µm thickness of PCL and PCL/MWCNT composites were obtained finally by hot pressing the films obtained in the previous step at 150 °C and 25 MPa.

Basic characterization

The thermal behavior of PCL and composites was carried out on a Q80 differential scanning calorimeter (DSC) model Q80 (TA instruments). Samples of 7 ± 1 mg were heated from -85 °C to 100 °C at 20 °C min⁻¹ on a nitrogen atmosphere to determine principal thermal characteristic on use conditions after preparation (n=3).

Mechanical characterization was conducted following standard ASTM D822 for polymer films. Standard tension test was performed in an Instron 5565 testing machine at 500 mm min⁻¹ deformation rate using a temperature control chamber 3119-600 series to perform test at 37 ± 0.5 °C. Samples of 100 x10 mm were obtained from the 450 µm sheets and submerged for 48 h in PBS (pH 7.4) at 37 ± 0.5 °C in order to simulate human body conditions. Five samples for composition were tested (n=5). Young modulus (E) was obtained using linear fitting at 2% of strain rate and yield stress (σ_y) using first local maximum stress point.

Fatigue characterization

Fatigue test were performed in a Bose ElectroForce 3200 following standard ASTM D7991 for fatigue test of polymers under uniaxial stress. Samples of 55x10 mm and 450 µm thickness were submerged 48h in PBS and 37 °C. Fatigue test were carried out by using BioDynamic chamber (see Figure 4-10) in order to simulate human body conditions with liquid medium flowing continuously from thermal controlled bath with a peristaltic pump at 37 ± 1 °C. Clamp distance was set at 35 mm due to chamber size restrictions.

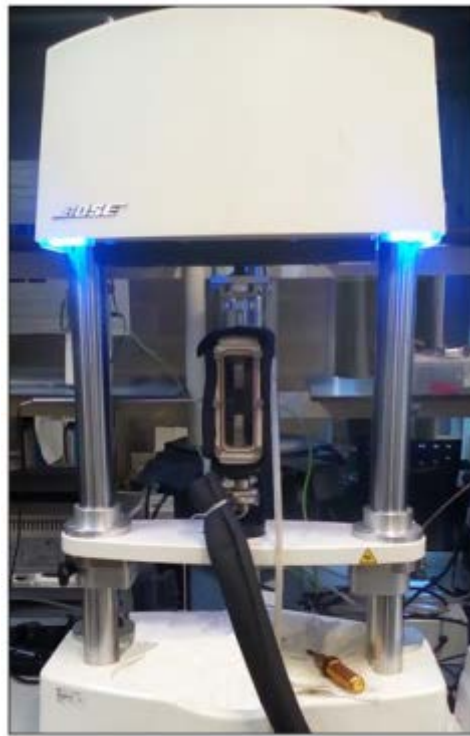


Figure 4-10. Bose ElectroForce 3200 with BioDynamic chamber for liquid medium fatigue testing.

Test were performed using force controlled method, in tension-tension mode ($R=0.1$) under sinusoidal stimulus at 3Hz. Force limits were adjusted individually for sample to test samples at 9 MPa. Tests were stopped under two limits: a) sample stay for 10^6 cycles or b) sample strain exceed 18%. This second limit present the material failure for excessive plastification or brittle break. At least six samples ($n=6$) were tested for each tension level.

Results and discussion

Uniaxial Mechanical Properties

Mechanical properties are going to discuss in terms of stiffness (Young's Modulus , E) and yield strength (σ_y). Young modulus is calculated with linear fitting at first 2% of strain and yield stress as the first maximum local stress of the curve. The results obtained from the stress-strain curves of Figure 4-11 are summarized in Table 4-6.

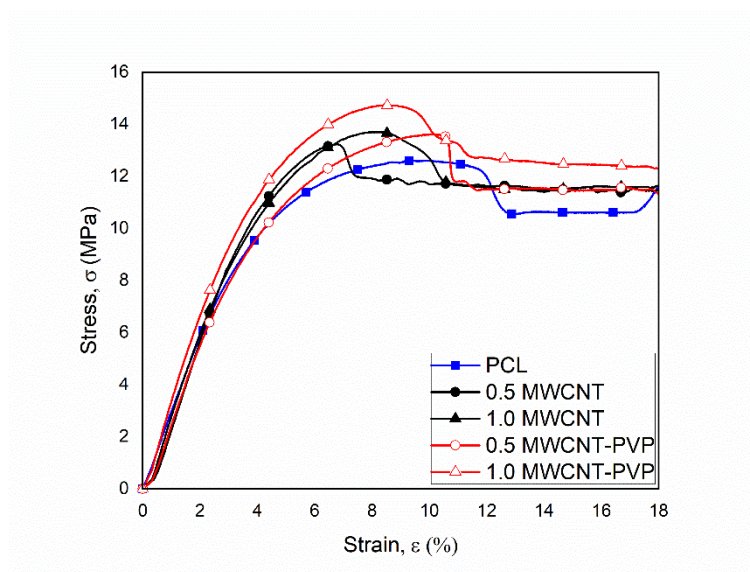


Figure 4-11. Stress-Strain curves of PCL and its MWCNT composites.

Table 4-6. Mechanical properties of PCL and its MWCNT composites.

Sample	E (MPa)	σ_y (MPa)
PCL	270.4 ± 17.6	12.75 ± 0.72
0.5 MWCNT	261.3 ± 14.2	13.19 ± 0.21
1.0 MWCNT	296.4 ± 8.2	13.57 ± 0.98
0.5 MWCNT-PVP	284.2 ± 16.3	13.57 ± 0.63
1.0 MWCNT-PVP	308.3 ± 15.8	14.6 ± 0.14

Results reveal a slight drop from 270.4 to 261.3 MPa in stiffness when incorporating 0.5 wt.% MWCNT to PCL. Although this result is not statistically significant ($p=0.4$), it could suggest that the dispersion method was not completely effective at low MWCNT concentrations. However, for 1 wt.% MWCNT composite the young's modulus increases up to 296.4 MPa ($p=0.02$) indicating that at higher carbon nanotube content the dispersion method is suitable. Regarding the yield strength values, the presence of MWCNT increases the yield stress in both cases, from 12.75 MPa to 13.19 MPa when incorporating 0.5 wt.% and to 13.57 MPa when incorporating 1 wt.% ($p = 0.04, 0.06$).

In order to improve the mechanical properties, MWCNT were coated with polyvinylpyrrolidone (PVP). Composites with coated nanotubes show improve mechanical properties comparing with non-coated ones. Stiffness increases from 270.4 MPa to 284.2 MPa and to 308.3 MPa ($p = 0.23, 0.01$) for 0.5 wt.% and 1 wt.% CNT-PVP composites. Moreover, yield stress increases from 12.75 MPa to 13.57 MPa and to 14.6 MPa ($p = 0.02, 0.00$) for 0.5 wt.% and 1 wt.% CNT-PVP composites. These findings can

be attributed to two main reasons: (1) PVP coating promote better dispersion of MWCNT in polar solvents, as DCM; and (2) PVP coating promote better adhesion in the interphases of PCL matrix and MWCNT.

Fatigue

A common strategy to study fatigue life when working at single stress level is the survival analysis. These survival curves indicate the probability that a sample would survive a specific number of cycles. In other words, they allow us to calculate the survival cycles (time) of the samples for a given probability. Each step of the curve represents the failure moment of one of the samples of the same material. Therefore, the final step of each curve corresponds to the life of the more resistant sample in each system or material. The survival curves obtained for this work are represented in **Figure 4-12**.

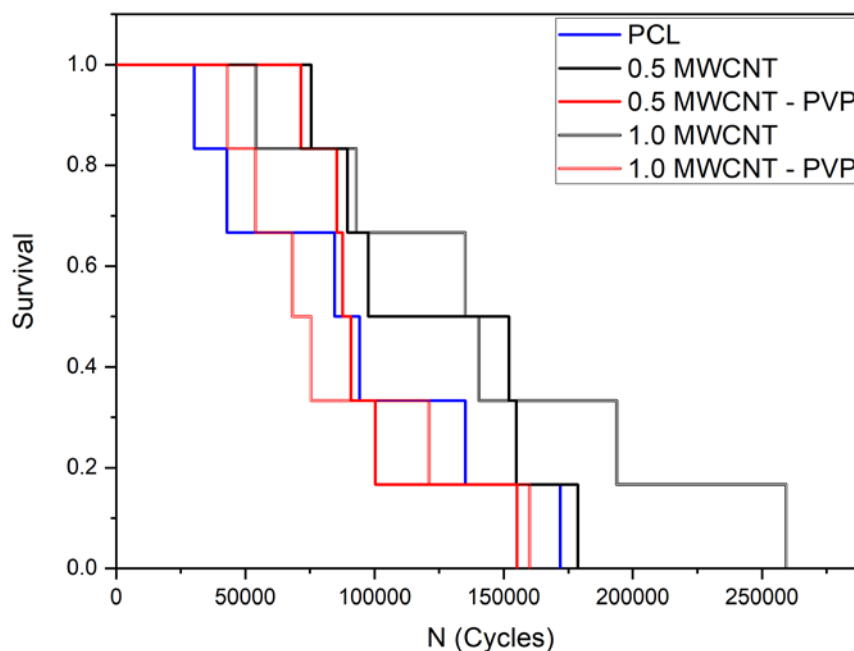


Figure 4-12. Survival curves of PCL an PCL with MWCNT composites for 9MPa of fatigue loading.

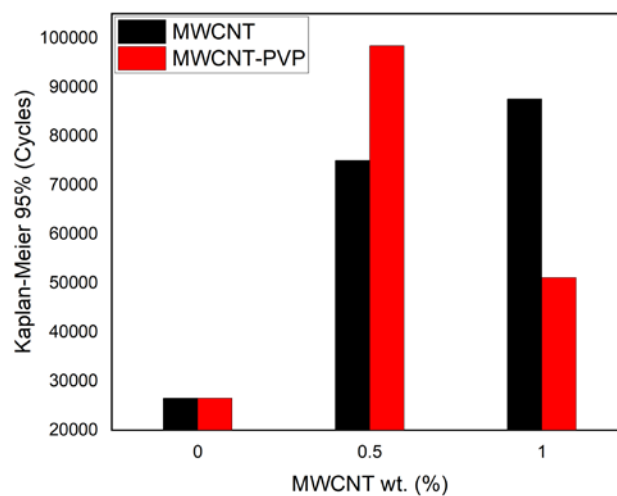
From Figure 4-12 the number of survival cycles for a 95 % of confidence level, known as Kaplan-Meier estimator can be obtained. Table 4-7 resumes the mean fatigue life and Kapla-Meier cycles (KM95%).

Table 4-7. Fatigue life and Kapla-Meier cyles for PCL and its MWCNT composite at 9MPa.

Sample	Mean fatigue life (Cycles)	Kapla-Meier (KM95%)
PCL	77,997 ± 26,281	26,487
0.5 MWCNT	98,481 ± 11,955	75,050
1.0 MWCNT	145,917 ± 29,743	87,622
0.5 MWCNT-PVP	124,677 ± 17,274	98,481
1.0 MWCNT-PVP	86,922 ± 18,262	51,130

The obtained results demonstrate that the incorporation of MWCNT to PCL improve considerably its fatigue life. The KM95% values of composites are tripled comparing to PCL. This value increases from 26,487 cycles to 75,050 and 87,622 cycles for 0.5wt% and 1 wt.% MWCNT composites, respectively.

Composites having PVP-coated nanotubes show a different trend (see Figure 4-13). The composition having 0.5 wt.% of coated MWCNT quadruplets the fatigue life comparing to PCL (KM95% = 98,481 cycles). However, the incorporation of 1 wt.% of coated MWCNT decreases the fatigue life to 51,130 cycles.

**Figure 4-13.** Kaplan-Meier estimator (95% of confidence level) evolution with nanotube content for coated and no coated MWCNT.

From these results two conclusions could be reached: (1) MWCNT have the potential to increase the fatigue life of PCL; (2) Fatigue life does not increase linearly with MWCNT content when coating with PVP. A critical value exists which is state around 0.5 wt.%.

Our previous studies (See Chapter 4.1 Fatigue life of PCL films simulating human body conditions) suggest that the fatigue behavior of these samples could also be studied analyzing the evolution of the plastic deformation or strain during fatigue loads.

Fatigue plastic strain (ε_p) is defined according to equation X where $\varepsilon_{min,i}$ is the minimum strain at cycle i and $\varepsilon_{min,0}$ the minimum strain in the first cycle

$$\varepsilon_{p,i} = \varepsilon_{min,i} - \varepsilon_{min,0}$$

Figure 4-14 shows the evolution of plastic strain ($\varepsilon_{p,i}$) with cycles for PCL and its MWCNT composites under fatigue loads of 9MPa. The curves of the samples reinforced with MWCNT present an identical shape. This curves consist of three different stages (see Figure 4-14a): (Stage I) High initial plastic strain (Stage II) Stabilization of the plastic strain (Stage III) Uncontrolled increase of plastification

Unlike composites, two of the samples of neat PCL show pure plastic failure with and extremely fast increase of plastic strain (see arrows in Figure 4-14b). The other four samples of PCL show a previously described three stage behavior. In the first stage strain-softening phenomenon predominates with a loss in stiffness due to cavitation. Then, at critical point P_i the plastic strain is stabilized showing a constant growth rate (ΔP) up to critical point where the plastic strain growth become instable (P_f). This second stage is related to crack opening mechanism and thus, controls or dominates the fatigue life; cracks increase in size, reducing the useful area of the sample and causing a fast plastification and a failure ultimately.

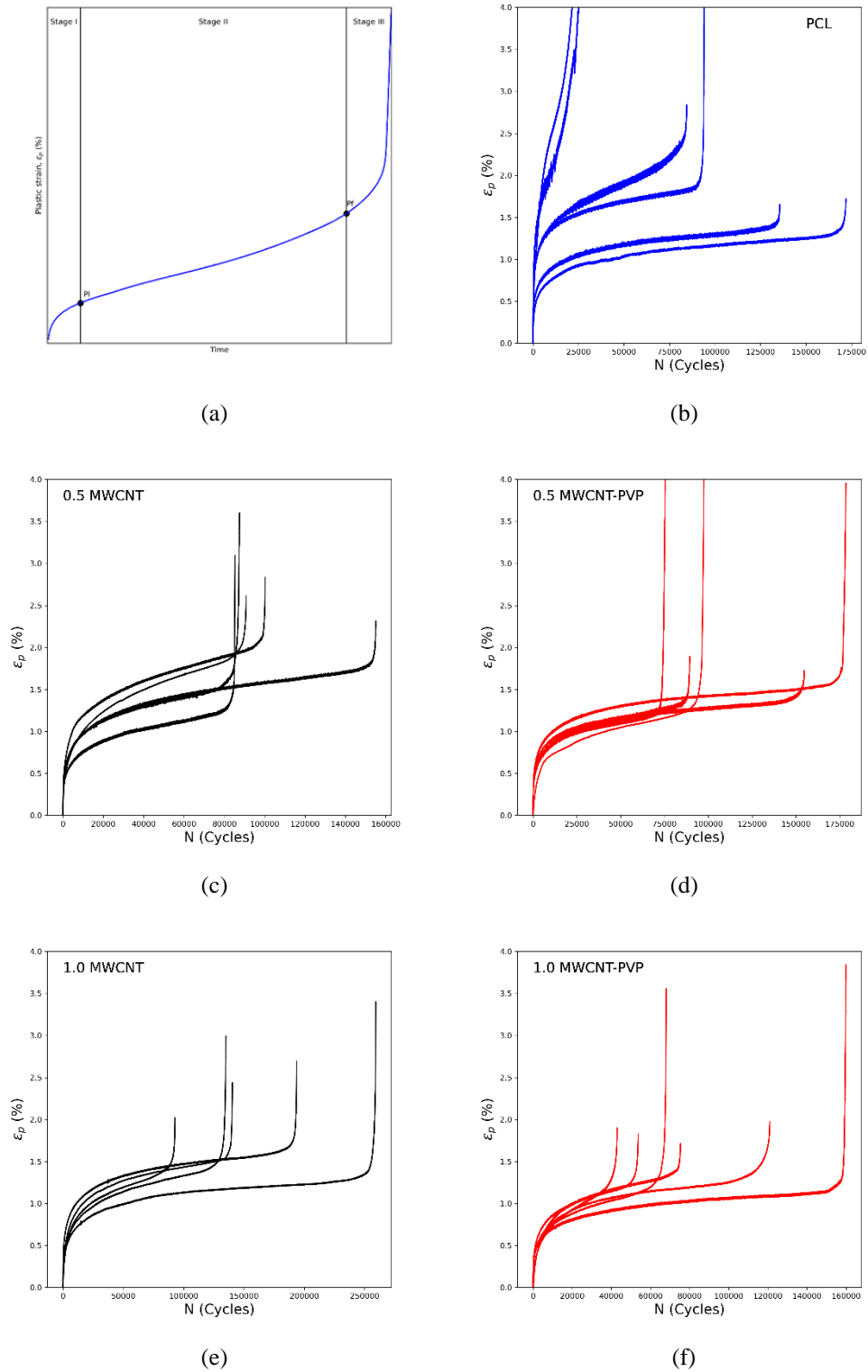


Figure 4-14. Plastic strain evolution under fatigue loads of 9 MPa for PCL and its MWCNT composites: (a) Phase changes in plastification (b) PCL (c) 0.5 CNT (d) 0.5 CNT-PVP (e) 1.0 CNT (f) 1.0 CNT-PVP.

The value of the critical parameters P_i , P_f and ΔP could be used to study the changes induced by nanotube fillers in fatigue properties of PCL (see Table 4-8). The incorporation of MWCNT decreases the value of P_i from 1.1 to 0.7 and to 0.6 for uncoated and coted-MWCNT, respectively. The drop in P_i means that the first strain-softening phenomenon is reduced due to the MWCNT presence, it is to say, the composites have a higher capacity for hardening avoiding a pure plastic failure. Moreover, it seems that MWCNT content has no any significant effect in this first stage. Therefore, if the nano-filler is good dispersed, extreme low quantity of MWCNT, i.e. 0.5 wt.%, is enough to immobilized the polymeric chains of the matrix leading to a hardening of the material. The enhance in the reinforcement interface provided by PVP functionalization is the responsible of P_i reduction from 0.7 to 0.6 due to a better capacity to immobilize PCL polymeric chains.

Table 4-8. Critical parameters for fatigue analysis of PCL and its MWCNT composites. P_i : Plastic strain stabilization start point; P_f : Plastic strain stabilization end point and ΔP : the plastic strain growth rate.

Sample	P_i (%)	P_f (%)	$\Delta P \times 1E6$ (% cycles ⁻¹)
PCL	1.1	1.9	52.7
0.5 CNT	0.7	1.7	11.8
1.0 CNT	0.7	1.7	8.5
0.5 CNT-PVP	0.6	1.4	7.3
1.0 CNT-PVP	0.6	1.4	13.2

Moreover, the value of P_f decreases also with nanotubes. This drop is attributed to the change in failure mode. The addition of MWCNT makes the failure mode to change from crack-ductile failure to crack-brittle failure. Failure in PCL samples is the consequence of the area reduction caused by crack growth combined with the increase of the stress intensity K_I in crack tip. In the case of composite, carbon nanotubes constrains the mobility of the PCL chains preventing plastic deformation and therefore samples are more brittle, and reach the critical intensity factor, K_{IC} , ending in a brittle fracture. Furthermore, composites having PVP coated MWCNT reach lower P_f values. This indicates that functionalized composites show more brittle behavior during failure.

Regarding plastic growth rate (ΔP) significant changes are observed. This parameter is the most relevant attribute in fatigue life which describes how fast samples reach the P_f

critical value, and failure ultimately. Therefore, low ΔP values indicate longer fatigue life. According to Table 4-8, PCL shows the highest ΔP values indicating that non-reinforced samples fail sooner than reinforced ones. The reduction in ΔP when incorporating MWCNT is obvious. The value of ΔP is reduced from $52.7E^{-6}$ to $11.8E^{-6}$ and $8.5E^{-6}$ % cycle⁻¹ for 0.5 wt.% and 1 wt.% MWCNT composites, respectively. This means that carbon nanotubes are reducing significantly the plastic strain growth rate related to crack growth. In contrast to P_i and P_f values, ΔP values seems to be more affected by carbon nanotube content. This indicates that the filler contributes in delaying the crack opening mechanism.

Moreover, the functionalization of 0.5 wt.% of MWCNT with PVP increase the fatigue life of the composite reducing the ΔP value to $7.3E^{-6}$ % cycle⁻¹, which is the lowest value obtained for this polymeric composite system. However, for 1 wt.% of functionalized carbon nanotubes ΔP value increases to $13.2E^{-6}$ % cycle⁻¹, indicating a lower fatigue life. These findings highlight the complexity in fracture mechanics behavior when trying to enhance fatigue life with composites. The presence of PVP in MWCNT helps to improve the interphase between filler and matrix causing a greater reduction in PCL chain mobility. This have a positive effect in reducing viscoelasticity and micro-plastification. However, the chain mobility reduction also reduces the benefits of the plastification in fracture mechanics. This is the case of the composite having 1 wt.% of PVP coated nanotubes. In this composite, the stress in the crack tip is higher and as the ability of the material to deformed plastically is less effective, it gives rise to a faster crack growth rate and a lower critical crack size to cause the fracture.

Conclusions

Porrivinilpirrolidone functionalization has proved to be a suitable technique to enhance static mechanical properties in poly(ϵ -caprolactone) and Multiwalled carbon nanotube composites.

The study of strain evolution with cycles in fatigue test simulating human body conditions (liquid medium and 37 °C) have been proved a good method to understand de viscoelastic and fracture mechanics of PCL and PCL with MWCNT composites. Using three key parameters (P_i : strain-softening plastification, P_f : final plastification and ΔP :

plastification constant rate) the differences in fatigue behavior between PCL and composites samples can be explained.

Mutiwalled carbon nanotubes have proof to be a good way to improve fatigue life of PCL at high stress levels (9MPa). From survival analysis using Kaplan-Meier estimator to predict fatigue life at confidence level or 95% nanotubes have triplicate the design life of PCL from 26,487 to 87,622 cycles for 1 wt. % of nanotube content. This fatigue life enhancement appear to be related to a reduction in strain-softening in the first stage of viscoelastic evolution for PCL ($P_i \downarrow$) and a crack growth reduction by crack biding and deboning mechanism ($\Delta P \downarrow$).

Polyvinylpyrrolidone coating of nanotubes have shown improve results for 0.5 wt.% MWCNT composite increasing the fatigue life to 98,481 cycles but decreasing for 1 wt.% MWCNT composite. These results suggest that the good interaction in the interphase between PVP and PCL might reduce the chain mobility ($P_i \downarrow$), but also reduce the benefits of plastification in stopping crack growth mechanism obtaining lower fatigue life values ($P_f \downarrow\downarrow$).

References

1. Liu, Y. *et al.* Research on the interface properties and strengthening-toughening mechanism of nanocarbon-toughened ceramic matrix composites. *Nanotechnol. Rev.* **9**, 190–208 (2020).
2. Ovid'ko, I. A. Micromechanics of fracturing in nanoceramics. *Philos. Trans. R. Soc. A Math. Phys. Eng. Sci.* **373**, (2015).
3. Zhang, W., Picu, R. C. & Koratkar, N. Suppression of fatigue crack growth in carbon nanotube composites. *Appl. Phys. Lett.* **91**, 1–4 (2007).
4. Qiu, J. & Wang, G. J. Comparative study on modification of multi-walled carbon nanotubes by a hydrophilic polymer with different approaches. *Appl. Surf. Sci.* **254**, 5691–5694 (2008).
5. Al-Saleh, M. H. & Sundararaj, U. Microstructure, electrical, and electromagnetic interference shielding properties of carbon nanotube/acrylonitrile-butadiene-styrene nanocomposites. *J. Polym. Sci. Part B Polym. Phys.* **50**, 1356–1362 (2012).
6. Salimbeygi, G., Nasouri, K. & Shoushtari, A. M. Fabrication of homogeneous multi-walled carbon nanotube/poly (vinyl alcohol) composite films using for microwave absorption application. *Fibers Polym.* **15**, 583–588 (2014).
7. Green, A. A. & Hersam, M. C. Solution phase production of graphene with controlled thickness via density differentiation. *Nano Lett.* **9**, 4031–4036 (2009).
8. Das, S., Wajid, A. S., Shelburne, J. L., Liao, Y. C. & Green, M. J. Localized in situ

- polymerization on graphene surfaces for stabilized graphene dispersions. *ACS Appl. Mater. Interfaces* **3**, 1844–1851 (2011).
9. Moniruzzaman, M. & Winey, K. I. Polymer nanocomposites containing carbon nanotubes. *Macromolecules* **39**, 5194–5205 (2006).
 10. O’Connell, M. J. *et al.* Reversible water-solubilization of single-walled carbon nanotubes by polymer wrapping. *Chem. Phys. Lett.* **342**, 265–271 (2001).
 11. Yang, Q. *et al.* Influence of solvents on the formation of ultrathin uniform poly(vinyl pyrrolidone) nanofibers with electrospinning. *J. Polym. Sci. Part B Polym. Phys.* **42**, 3721–3726 (2004).
 12. Ignatova, M., Manolova, N. & Rashkov, I. Novel antibacterial fibers of quaternized chitosan and poly(vinyl pyrrolidone) prepared by electrospinning. *Eur. Polym. J.* **43**, 1112–1122 (2007).

General conclusion

In the current PhD thesis a study of different biodegradable composites has been carried out in order to obtain materials with new functionalities. Two matrix have been used, poly(ϵ -caprolactone) (PCL) and terpolymer poly(D,L-L-lactide-co- ϵ -caprolactone) (PDLCL) mixed with barium sulphate (BaSO_4) and multiwall carbon nanotubes (MWCNT).

Although conclusions are displayed at the end of each chapter, here the general and most relevant conclusions derived from the results of the research carried out are compiled:

1. Composites with BaSO_4 sub-micron particles:

- Blended with a long-term biodegradable semi-crystalline polymer PCL:
 - Barium sulphate reveals a nucleating effect that change crystallization kinetic and crystal shape of the polymer. These changes result in a statistically significant grow in PCL crystallinity.
 - 15 wt. % is sufficient to present radiopacity for devices to be visible for use in medical imaging techniques according to X-ray images.
 - BaSO_4 enhance mechanical properties at low quantities (< 15%) despite signs of poor adhesion of the reinforcement and matrix. This enhancement might be related to the effect in crystallinity.
- Blended with short-term biodegradable terpolymer PDLCL:
 - DMTA analysis show a good matrix/reinforcement adhesion and therefore mechanical properties are improved.
 - Polymer chains attached to the filler form a new rigid amorphous phase (RAP). This RAP changes the biodegradation kinetics since the chains immobilized by the reinforcement are less sensitive to hydrolytic degradation.
 - We can control the biodegradation rate of PDLCL with the barium sulfate content since the effect is proportional to the amount of reinforcement.

2. Composites with MWCNT functionalized with polydopamine:

- Mixed with PCL:

- MWCNT show a high capacity of interaction with PCL chains reducing their viscoelasticity. This is further enhanced by the PDA coating.
- The amount of functionalization of PDA can be controlled by the number of functionalization hours.
- The PDA coating improves mechanical properties as it has better matrix/reinforcement adhesion. But the effect is dependent on the amount of PDA, as large amounts end up giving worse results. The best properties were obtained for a functionalization of 6 hours.
- Using PDA-modified MWCNTs to make scaffolds, they show a bioactive ability to generate hydroxyapatite from media that simulates the human body (SBF), even though the nanotubes are integrated into the PCL matrix. This opens the possibility of not losing the bioactive capacity of PDA during PCL surface.

3. Fatigue of PCL:

➤ Neat PCL:

- PCL has a complex fatigue behavior where viscoelasticity, fracture mechanics, recrystallization and thermal effects are mixed.
- Depending on the stress level, PCL films can fail in different ways. Ductile failure, brittle/ductile failure or no failure.
- At high stresses the specimens usually fail by ductile failure. Due to the viscoelastic effect, micro deformations accumulate and damage the crystalline structure, resulting in a drop in stiffness.
- At medium stresses the viscoelastic deformation damage effect stabilizes, but is high enough to form the initiation of a crack. These cracks propagate by the usual fracture mechanics behavior until they reduce the area so much that the specimen fails in ductile mode at the created neck.
- As mentioned above deformation damage effect stabilizes with cycles. With time, as the polymer chains are well above the T_g , the material can rearrange

its crystals and recover part of the stiffness lost by the viscoelasticity in a "healing" effect. This means that at low stresses, where crack formation does not occur, the fatigue life is very high, since the damage produced at the beginning is gradually reversing.

- With MWCNT and MWCNT coated with polyvinylpyrrolidone (PVP):
 - MWCNT have demonstrated the ability to improve the fatigue life of PCL at both 0.5 and 1 wt.% at high stresses (9MPa). This improvement is related to the reduction of viscoelasticity provided by MWCNTs.
 - When MWCNTs are modified with PVP, fatigue life improves at lower amounts (0.5 wt.%) but not so much at higher amounts (1 wt.%). Modification by PVP seems to further reduce the viscoelastic effects of PCL which is positive at low quantities. But with large quantities it is reduced so much that the fracture behavior changes, making it more brittle and therefore the failure by cracking appears earlier.

Appendix

A1. List of Figures

Figura I. Efectos de los refuerzos para obtener materiales médicos multifuncionales...	15
Figura II. Imágenes SEM de <i>scaffolds</i> de Poli(Lactida) con porosidades del B) 70 y C) 90%.....	18
Figura III. Ejemplos de aplicaciones biomédicas del polímero poli(ϵ -caprolactona) (PCL) y copolímero poli(D,L-lactida-co-epsilon-caprolactona) (PDLCL).....	20
Figura IV. Reacción por apertura de anillo de ϵ -caprolactona para obtener poli(ϵ -caprolactona).	20
Figura V. Reacción por apertura de anillo de ϵ -caprolactona y lactona para obtener poli(L-lactida-co- ϵ -caprolactona).....	21
Figura VI .Uso de composites multifuncionales en aplicaciones médicas.....	23
Figura VII. Tomografía computarizada de implantes de polilactida con y sin nanopartículas de Fe ₃ O ₄	24
Figura VIII. Estructura de los nanotubos (izquierda) monocapa o SWCNT y (derecha) multicapa o MWCNT.	25
Figura IX. Ejemplos de funcionalización en nanotubos de carbono.	26
Figura X Curva S-N para materiales dividida en 4 zonas en función de la duración en ciclos: LCF (low cycle fatigue), HCF (high cycle fatigue) vHCF (very high cycle fatigue) y GCF (giga cycle fatigue).	28
Figura XI. Curva de “Creep” de un polímero sometido a tensión constante.....	29
Figura XII. Curva característica de propagación de grieta en materiales. Ley de Paris. 30	
Figure 1-1. (a) Melting temperature and (b) Degree of crystallinity of neat PCL and its barium sulphate (BaSO ₄) composites.	47
Figure 1-2. Crystal morphology for neat PCL and its composites having 5 and 35 wt.% of BaSO ₄ after non-isothermal crystallization at cooling rates of (left column) 1 °C min ⁻¹	

and (right column) 10 °C min ⁻¹ . Black holes in micrographs correspond to air bubbles formed during <i>in-situ</i> crystallization treatments.....	49
Figure 1-3. Cooling curves obtained by Differential Scanning Calorimetry (DSC) for neat PCL and its BaSO ₄ composites at different cooling rates. (solid line) 1 °C min ⁻¹ (dash line) 5 °C min ⁻¹ (dot line) 10 °C min ⁻¹	50
Figure 1-4. The increase of crystallization enthalpies of PCL and its BaSO ₄ composites obtained at (■) 1 °C min ⁻¹ (●) 5 °C min ⁻¹ (▲) 10 °C min ⁻¹ cooling rates from melt.	51
Figure 1-5. Degree of crystallinity versus time of PCL and its BaSO ₄ composites at different cooling rates.(a) 1 °C min ⁻¹ (b) 5 °C min ⁻¹ (c) 10 °C min ⁻¹	52
Figure 1-6. log(-ln(1-X _t)) versus log(t) of PCL and its BaSO ₄ composites at different cooling rates to adjust the Avrami-Ozawa-Jeziorny model. (a) 1 °C min ⁻¹ (b) 5 °C min ⁻¹ (c) 10 °C min ⁻¹	54
Figure 1-7. Example of simple (blue) and double linear (red) fitting model of experimental results of crystallization kinetics for PCL and its composites. Black arrows indicate the double- fitting area corresponding to the secondary crystallization. Data shown correspond to neat PCL at 1 °C min ⁻¹ cooling rate	55
Figure 1-8. Mechanical behavior of PCL and its BaSO ₄ composites (a)Stress-Strain curves (b) Zoom of the plastification peak at yield point. Evolution of the mechanical properties (c) Young´s modulus (d) Yield Stress (e) Yield Plateau (f) Elongation at break.	58
Figure 1-9. X-ray images of Aluminum, PCL and its barium sulphate composites.....	60
Figure 2-1. Biodegradable polyesters degradation scheme.....	69
Figure 2-2. DMTA curves for PDLCL and PDLCL with barium sulphate composites. a) Storage modulus (E'); b) Tangent delta (tanδ).....	77
Figure 2-3. Evolution of Tanδ according to equation (5) with barium sulphate volume fraction.....	79

Figure 2-4. Variation of rigid amorphous phase fraction (RAP) of PDLCL composites with barium sulphate content.....	81
Figure 2-5. Storage modulus curves by DMTA of PDLCL composites at day 0 and 21 of hydrolytic degradation. Neat PDLCL samples were impossible to test due to brittleness induced by hydrolytic degradation at day 21.....	82
Figure 2-6. DMTA curves of PDLCL+35BaSO ₄ composition at different days of degradation.	83
Figure 2-7. Remaining weight (RW%) and water absorption (WA%) evolution during days of degradation.....	84
Figure 2-8. Molecular weight evolution with days of degradation of PDLCL and PDLCL with barium sulphate composites.	85
Figure 2-9. Evolution of GPC curves at different days of degradation: a) PDLCLD; b) PDLCL+35BaSO ₄	88
Figure 2-10. Illustration of the interphase between PDLCL macromolecules and BaSO ₄ explaining the double phase degradation behavior phase in PDLCL composites.....	89
Figure 2-11. Photos of hydrolytic study of PDLCL and PDLCL with barium sulphate composites at different day of degradation.....	91
Figure 2-12. X-ray images of Aluminum and composite samples at different days of hydrolytic degradation.....	91
Figure 3-1. XPS survey spectra of MWCNT and poly(dopamine) functionalized MWCNTD.....	104
Figure 3-2. (a) TGA curves of PDA, and functionalized nanotubes at different times.(b) PDA fraction with reaction time.....	106
Figure 3-3. Stress-strain curves of PCL and PCL+CNT composites with different times of PDA functionalization.....	107
Figure 3-4. (a) Young modulus evolution with PDA content and (b) Yield point evolution with PDA content.	108

Figure 3-5. Mechanical properties of PCL and uncoated and coated nanotube composites (a) Stress-strain curves of. (b) Young modulus improvement and (c) Yield strength improvement..... 110

Figure 3-6. (a) Storage modulus E' and (b) $\tan\delta$ curves from DMTA for PCL and PCL composites with coated and non-coated nanotubes..... 111

Figure 3-7. $\tan\delta$ evolution with nanotube volume fraction from DMTA analysis..... 112

Figure 3-8. XRD patterns of PCL and PCL with coated and no-coated carbon nanotubes after 28 days submerged in SBF..... 113

Figure 4-1. Graphical representation of the processes involved in viscoelastic polymers fatigue behavior. 121

Figure 4-2. Scheme of mechanical behavior of PCL under fatigue loadings..... 123

Figure 4-3. Non-linear accumulative mechanism in PCL and their effect in type of failures. 124

Figure 4-4. Principal factors related to stiffness in polymers under fatigue loads. 125

Figure 4-5. A) Stress-Strain curves of five PCL samples and B) zoomed graph of the yield point zone. 128

Figure 4-6. S-N curve for PCL in log-log scale for four different stress levels (purple) 10 MPa, (black) 8 MPa, (green) 6MPa, (blue) 4 MPa. Fitting lines in red. 131

Figure 4-7. The evolution of damage with cycles for different fatigue stress levels 133

Figure 4-8. Damage-Plastic strain relation at first 50.000 cycles of PCL samples. 134

Figure 4-9. Scheme of Multiwalled carbon nanotubes dispersion steps. 143

Figure 4-10. Bose ElectroForce 3200 with BioDynamic chamber for liquid medium fatigue testing. 145

Figure 4-11. Stress-Strain curves of PCL and its MWCNT composites..... 146

Figure 4-12. Survival curves of PCL an PCL with MWCNT composites for 9MPa of fatigue loading..... 147

Figure 4-13. Kaplan-Meier estimator (95% of confidence level) evolution with nanotube content for coated a no coated MWCNT..... 148

Figure 4-14. Plastic strain evolution under fatigue loads of 9 MPa for PCL and its MWCNT composites: (a) Phase changes in plastification (b) PCL (c) 0.5 CNT (d) 0.5 CNT-PVP (e) 1.0 CNT (f) 1.0 CNT-PVP. 150

A2. List of Tables

Table 1-1 Name-Code of composite samples showing real barium sulphate content after processing calculated by TGA analysis.....	45
Table 1-2. Thermal properties and degree of crystallinity of poly(ϵ -caprolactone) (PCL) and its BaSO ₄ composites. T _m : Melting temperature, ΔH_m : Melting enthalpy, X _c : Degree of crystallinity.....	48
Table 1-3. Crystallization temperature and crystallization enthalpy of PCL and its BaSO ₄ composites at different cooling rates.	50
Table 1-4. The parameters of the double linear Avrami-Ozama-Jeziorny model for PCL and its BaSO ₄ composites at different cooling rates.....	56
Table 1-5. Values of the mechanical properties measured by tensile test for neat PCL and its BaSO ₄ composites. Young modulus (E), Yield stress and yield strain (σ_y , ϵ_y), yield plateau stress (σ_{yp}) and elongation at break (ϵ_b)	59
Table 2-1 Principal characterization parameters of PDLCL by proton NMR and GPC.	71
Table 2-2. BaSO ₄ content measured with TGA.....	72
Table 2-3 Glass transition temperature and molecular mass properties by DSC and GPC of PDLCL and its barium sulphate composites.	75
Table 2-4 . Mechanical properties of PDLCL and barium sulphate composites from standard tension test and DMTA analysis.	76
Table 2-5 Results of thermal analysis for PDLCL and its barium sulphate composites.	80
Table 2-6. Results of logarithmic fitting for first 28 days of degradation.....	86
Table 3-1. Summary of functionalization study from TGA and Traction test analysis.	105

Table 3-2. Mechanical properties of PCL and CNT composites from standard tensile test.	109
Table 4-1. Thermal an Mechanical properties of PCL	128
Table 4-2. Failure behavior distribution of PCL samples at different fatigue stress loadings.....	129
Table 4-3. Mean and deviation of sustained cycles for PCL under different fatigue loads.	131
Table 4-4. Exponential parameters (A and m) to fit the S-N curve.....	132
Table 4-5. Sample compositions	143
Table 4-6. Mechanical properties of PCL and its MWCNT composites.....	146
Table 4-7. Fatigue life and Kapla-Meier cyles for PCL and its MWCNT composite at 9MPa.....	148
Table 4-8. Critical parameters for fatigue analysis of PCL and its MWCNT composites. Pi: Plastic strain stabilization start point; Pf: Plastic strain stabilization end point and ΔP : the plastic strain growth rate.....	151

A3. Symbols and Abbreviations

ΔC_p	change in heat capacity
ΔH_m	melting enthalpy
ΔH_m^0	melting enthalpy (infinite crystal thickness)
ΔH_c	crystallization enthalpy
ΔT	supercooling
δ	phase angle
ε	elongation
ε_r	strain recovery
ε_u	ultimate elongation
ρ	density
σ	tensile strength
σ_{max}	tensile strength
σ_u	ultimate tensile strength
σ_y	yield stress
χ	weight fraction
ω	frequency
D	dispersity index
E	elastic modulus
E'	storage modulus
E _a	activation energy

E_{young}	young's modulus
E_{sec}	secant modulus
G	crystal growth rate
H	enthalpy
K_{Mw}	apparent degradation rate
l_{CL}	average sequence length of caprolactone
l_i	number-average sequence lengths
l_{LA}	average sequence length of lactide
l_0	average length of the main chain bonds
m_0	molecular weight per main chain bond
M	molecular weight
M_n	number average molecular weight
M_w	weight average molecular weight
M_{w0}	initial weight average molecular weight
MWCNT	multiwalled carbon nanotubes
R	randomness character
$t_{1/2}$	half degradation time
t_a	aging time
T_p	peak temperature
T_c	crystallization temperature
T_g	glass transition temperature
T_m	melting temperature
T_{ref}	reference temperature

tan δ	damping factor
V	volume
wt. %	weight percent
X_c	crystallinity degree
CL	ϵ -caprolactone
ϵ -CL	ϵ -caprolactone
DMTA	dynamic mechanical thermal analysis
DSC	differential scanning calorimetry
GPC	gel permeation chromatography
NMR	nuclear magnetic resonance
LA	lactide
L-LA	L-lactide
MAF	mobile amorphous phase
PBS	phosphate buffered saline
PCL	poly(caprolactone)
PDLCL	poly(D,L-L-lactide-co- ϵ -caprolactone)
PLOM	polarized light optical microscopy
PDA	polydopamine
PVP	polyvinylpyrrolidone
RAF	rigid amorphous fraction
TGA	thermogravimetric analysis
WAXD	wide angle X-ray diffraction

A4. List of Publications and Congresses

As a result of this work, one paper have been submitted to international indexed scientific journals:

- Amestoy, H.; Diego, P.; Meaurio, E.; Muñoz, J.; Sarasua, J.-R. Crystallization Behavior and Mechanical Properties of Poly(ϵ -caprolactone) Reinforced with Barium Sulfate Submicron Particles. *Materials* **2021**, *14*, 2368. <https://doi.org/10.3390/ma14092368>

A5. Curriculum Vitae

Nombre y Apellidos: Hegoi Amestoy Muñoz

DNI: 72746915-P

Fecha de Nacimiento: 03/06/1983

Sexo: M

Dirección de contacto:

Email: hegoi.amestoy@ehu.es

Líneas de investigación

Polímeros biodegradables y biorreabsorbibles, nano-composites, caracterización estructura-propiedades, Fatiga de materiales.

Formación académica

Máster en Ingeniería de Materiales Avanzados: 2008-2009 (E.T.S.I. Bilbao)

Ingeniería de Materiales: 2006-2008 (E.T.S.I. Bilbao)

Ingeniería técnica en mecánica industrial: 2002-2006 (Universidad Politécnica de Donostia-San Sebastian)

Experiencia laboral y disfrute becas

Docencia universitaria:

- Profesor Laboral Interino. Tiempo parcial. Departamento Ingeniería Minera y Metalúrgica y Ciencia de los Materiales. E.T.S. de Ingeniería de Bilbao. 02/2018-08/2018

Becas de convocatoria oficial del MEC, Gobierno Vasco y UPV/ EHU postdoctorales:

- Convocatoria de contratación para formación de personal investigador en la universidad del País Vasco. 04/2014- 08/2018.
-

Publicaciones o documentos científico-técnicos

- De Arenaza, I. M. et al. Polylactide stereocomplex crystallization prompted by multiwall carbon nanotubes. *J. Appl. Polym. Sci.* 130, 4327–4337 (2013).
- Larrañaga, A., Ramos, D., Amestoy, H., Zuza, E. & Sarasua, J. R. Coating of bioactive glass particles with mussel-inspired polydopamine as a strategy to improve the thermal stability of poly(l-lactide)/bioactive glass composites. *RSC Adv.* 5, 65618–65626 (2015).
- Fernández, J. et al. Effect of molecular weight on the physical properties of poly(ethylene brassylate) homopolymers. *J. Mech. Behav. Biomed. Mater.* 64, 209–219 (2016).
- Fernández, J., Auzmendi, O., Amestoy, H., Diez-Torre, A. & Sarasua, J. R. Mechanical properties and fatigue analysis on poly(ϵ -caprolactone)-polydopamine-coated nanofibers and poly(ϵ -caprolactone)-carbon nanotube composite scaffolds. *Eur. Polym. J.* 94, 208–221 (2017).
- Ugartemendia, J. M., Larrañaga, A., Amestoy, H., Etxeberria, A. & Sarasua, J. R. Tougher biodegradable polylactide system for bone fracture fixations: Miscibility study, phase morphology and mechanical properties. *Eur. Polym. J.* 98, (2018).

“Nos hacemos a la mar en este nuevo océano porque existen nuevos conocimientos que obtener y nuevos derechos que ganar, que deben ganarse y utilizarse para el progreso de todos los pueblos.”

John F. Kennedy